SIDEROPHORE CYCLING IN THE NORTH PACIFIC SUBTROPICAL GYRE

By

Jingxuan (Jay) Li
B.A. Xiamen University (2014)
M.A. University of British Columbia (2017)

Submitted in partial fulfillment of the requirements for the degree of
Doctor of Philosophy
at the
MASSACHUSETTS INSTITUTE OF TECHNOLOGY
and the
WOODS HOLE OCEANOGRAPHIC INSTITUTION

June 2023

Signature of Author:

_____

Joint Program in Oceanography
Massachusetts Institute of Technology
and Woods Hole Oceanographic Institution
(May 19, 2023)

Certified by:

_____

Daniel J. Repeta
Thesis Supervisor

Accepted by:

_____

Benjamin A. S. Van Mooy
Chair, Joint Committee for Chemical Oceanography
Woods Hole Oceanographic Institution

Abstract

Across large regions of the surface ocean, the essential micronutrient iron (Fe) limits the growth of microbes, including phytoplankton and heterotrophic bacteria. In order to adapt to chronic low Fe conditions, some heterotrophic bacteria are able to produce siderophores, which are small organic ligands with extraordinarily high stability constant for Fe(III), to facilitate Fe uptake. The recently developed mass spectrometry based techniques allow for the characterization and quantification of siderophores in seawater for the first time, and the use of siderophores as biomarker of Fe limitation on heterotrophic bacteria. However, there has been no depth resolved transect data on siderophores distribution, and the prevalence, turnover, and of controlling factor of siderophores in the ocean remain unknown.

In this thesis, I report the distribution of siderophores in the upper 1000 m of the US GEOTRACES GP15 Pacific Meridional Transect. Siderophore concentration ranges from 0-70 pM, and there is no correlation between the concentration of siderophores and dissolved Fe (dFe, <0.2 μm). In contrast, most siderophore hotspots, defined by concentration that is higher than 20 pM, are associated with a dFe:NO_3^- ratio that is lower than 50 μmol/mol, suggesting that the distribution of siderophores which are N rich molecules might be controlled by dFe:NO_3^- ratio. In the North Pacific Subtropical Gyre, hotspots of siderophores are found at 200-400 m. In the upwelling regions where nitracline is lifted to shallower depths, the hotspots are also lifted, to up to 20 m. The transect is dominated by marinobactins, a suite of non polar siderophores with a peptidic head group for Fe binding and a fatty acid chain. In addition, we found that the same siderophore could bind either Fe or Al, which is the first time Al-siderophores are reported in seawater samples.

The hotspots of siderophore could be explained by either a dynamic turnover, or slow turnover and accumulation. To investigate the turnover of siderophores, I report the measurement of ^{57}Fe uptake from siderophores by heterotrophic bacteria at Station ALOHA, which is representative for the North Pacific Subtropical Gyre - using enclosed bottle incubations. Between 200 and 400 m, we found almost complete consumption of

^{57}Fe-siderophores for all of the siderophores over a period of 5 days. At the end of the incubation, approximately 60% of the added siderophores were present as non-metallated apo siderophores. The presence of apo siderophores demonstrates that the drawdown of ^{57}Fe-siderophore was largely due to Fe uptake from siderophores. Therefore, heterotrophic bacteria are Fe limited at 200-400 m, which is in accordance with the high concentration of siderophores in the North Pacific Subtropical Gyre. Our results reveal that the zone of potential Fe limitation in the ocean extends well below the euphotic zone and includes oligotrophic gyres that are not classically Fe limited.

Acknowledgement
I would first like to thank my scientific mentors over the past six years, especially my advisor, Dan Repeta. Throughout my research, Dan always explains things in a way I could understand, and suggests experiments that are purposeful, practical and elegant. This thesis benefits a lot from his knowledge, experience and scientific taste. Another inspiring aspect is his passion for science. He could recall the details of my research six months ago, which I don't necessarily remember. In addition, Dan creates a positive environment in the lab, which makes it a pleasure to be a part of the Repeta lab. Many thanks to my thesis committee members, Penny Chisholm and Mak Saito for the constructive comments and encouragement, for the support on my talk and poster, and for sending me samples and allowing me to use the instruments.

Special thanks go to Lydia Babcock-Adams, for showing me everything about the LC-MS technique multiple times. Every step in the methods section was either taught by her, or inspired by her work. In addition, for a long time, I presented my progress to her before going to Dan, so the discussion section also benefited from her. I would like to thank Matt McIlvin for helping me troubleshoot the instrument and explaining the process step by step. Every time there is an error on the instrument that I don't recognize or recall, Matt is always willing to have a look, which means fix the instrument.

I would also like to thank Marianne Acker, for helping me with the culturing, sharing the ProSB sample, and being flexible for the iCap schedule. Thanks to Ben Granzow for the help in PARAGON 1, for allowing me to use the SpeedVac whenever the samples are ready, and for the Gilson rack. Thanks to Iulia Madalina-Streanga for helping me with the sampling in PARAGON 1, which was a lot of work on a busy cruise. Thanks to Rene Boiteau and Randie Bundy, who have been helping me, and looking after me since my application to the Joint Program.

Thanks to the faculty at WHOI who were always willing to help and collaborate, and keep an open door, especially Jeff Seewald, Ben Van Mooy, Tristan Horner, Amy Apprill, Konrad Hughen for steering the generals exam, participating and chairing my thesis proposal defense, and for the support during the department seminar. Thanks to Allison Coe, Tyler O'Keefe and Eli Salcedo in the Chisholm lab for the help with *Prochlorococcus*. Thanks to Freddy Valois for the help with *Pseudomonas*. Thanks to Julia Westwater, Christine Charette, Lea Fraser and Meg Tivey, Mary Zawoysky and Sheila Clifford for the administrative support.

I am grateful to have participated in the field work three times, and a lot of people have helped me to collect the samples. I would like to thank Phoebe Lam and Karen Casciotti

for their help in GP15, and Greg Cutter for organizing the cruise. Thanks to Brent Summers and Laramie Jensen for sampling in the van. Thanks to Tim Conway for sharing the dFe data. I would also like to thank Matt Church for leading the PARAGON 2 cruise, and for accommodating my request on the last cast, which was made possible by the efficient work of Tim Burrell, Ryan Tabata, Brandon Brenes and all technicians onboard. Thanks to Phil Kong for the help with the trace metal cast and sampling. Many thanks to Lauren Manck and Miranda Seixas for the help with the incubation. Thanks to Rhea Foreman for the nutrients data. Thanks to Dave Karl and Angel White for maximizing the science after the A frame issue. Thanks to everyone onboard Kilo Moana for maintaining high morale during the cruise. I would also like to thank the Seth John lab for hosting me during PARAFIX, and helping me with the sample collection.

Thanks to many friends that provided tremendous support, Tianyi Huang, Jule Middleton, Shavonna Bent, Jen Karolewski, Kaline Grabb, Riss Kellogg, Becca Chmiel, Ellen Lalk, Jen Kenyon. Thanks to Sebastian Essink for driving me to soccer, and Tylor Nelson for being a great teammate. Thanks to Zhongchang Song for the algorithm, thanks to Peigen Lin for looking after me, and thanks to Zhiyuan Gao and Shuai Gu for sharing the experience of graduate school in chemical oceanography.

Finally, I would like to thank my funding sources. Thanks to the National Science Foundation Chemical Oceanography Program (NSF awards OCE-1736280 and OCE-2045223) for providing research and instrumentation funding that made this work possible. Additional support was provided the Simons Collaboration on Ocean Processes and Ecology (SCOPE).

To my mother, father, thank you for your continuous support.

Table of contents

List of Figures

Chapter 5

Appendix 5.1

List of Tables

Chapter 1 Introduction

1.1 Dissolved Iron in seawater

In 1970s, Bruland et al (1979) developed clean sampling techniques to measure copper, cadmium, zinc, and nickel in the ocean, which are low in concentration and easily contaminated by sampling and sample handling. Then, this technique was adopted for Fe by Gordon et al (1982), Landing and Bruland (1987), and Martin and Gordon (1988), which reported the first depth profiles of dissolved Fe (dFe) in the open Ocean. These first profiles showed similar features, including low dFe in surface waters (< 0.1 nmol/L), increasing amounts with depth, and maxima in association with the oxygen minimum.

This concentration was two orders of magnitude lower than previous studies in the surface water of the Indian Ocean (25 nmol/L, Chester and Stoner 1974), the average of the water column of Atlantic Ocean (16 nmol/L, Kremling and Petersen 1977) and the average of the water column of Indian Ocean (8 nmol/L, Danielsson 1980).

The low dFe concentration allowed Martin (1992) to compare the dFe:NO_3^- ratio in the surface ocean to the Fe:N stoichiometry in phytoplankton culture, and hypothesize that phytoplankton in some regions of the surface ocean are Fe limited, which was then confirmed by Fe addition experiments, that resulted in an increase of chlorophyll and a drawdown of nitrate (Martin and Fitzwater, 1988; de Baar et al 1990; Martin et al 1994; Price et al 1994; de Baar et al 2005; Boyd et al 2007).

For example, Boyd et al (2007) summarized the results of 12 mesoscale Fe addition experiments from 1993-2005, which were performed in surface HNLC waters, including Subarctic Pacific, Equatorial Pacific and Southern Ocean. In these regions, the nitrate concentration is 19.2±6.7 μmol/L (1SD, n=9). The Fe addition resulted in an increase in chlorophyll concentration from 0.4±0.3 μg/L (1SD, n=12) on T0 to a chlorophyll maximum of 4.1±6.1 μg/L (1SD, n=12). In addition, the Fe addition resulted in an uptake

of nitrate that accounted for 42±25% (1SD, n=6) of the nitrate inventory in the mixed layer.

1.2 Organic Fe ligands in seawater

Although the dFe concentration measurements using clean techniques yielded lower concentrations than found in previous studies, values were still higher than the solubility of inorganic Fe in artificial seawater (~10 pM at 25 °C, pH 8.1, Liu and Millero 2002). Furthermore, Fe solubility in natural seawater has been shown to decrease under UV irradiation (Wu and Luther 1995, Kuma et al 1996). Therefore, the high Fe solubility in natural seawater was attributed to the complexation of Fe by organic ligands, which were oxidized under UV irradiation.

The presence of organic ligands in seawater was then confirmed by electrochemical technique (van den Berg 1995), which concluded that 99% of dFe was complexed to organic ligands throughout the water column of the Western Mediterranean. Since then, this technique has been broadly used to study the concentrations and stability constants of organic Fe ligands in seawater (Gledhill and van den Berg 1994; Rue and Bruland 1995; Wu and Luther 1995; Croot and Johanson 2000).

The results support the presence of a class of strong ligands (L1) occurring throughout the upper water column, at concentrations on the order of nM, rivaling the concentration of dFe. In addition to strong L1 ligands, a weaker class of ligands (L2) is also present throughout the entire water column at concentrations of ~1-2 nM. The distribution of organic ligands uncovered by electrochemical measurements allowed ligands to be incorporated into biogeochemistry models (13 models compiled in Tagliabue et al 2016) that simulated the distribution of Fe, and ultimately help project the impact of climate change on marine resources.

It was postulated that strong L1 ligands were composed largely of siderophores (Boyd and Ellwood 2010). Siderophores are strong organic ligands synthesized by microbes to

sequester Fe and facilitate Fe uptake. The biosynthesis of siderophores is typically regulated by the Fe levels in the growth environment (Hider and Kong 2010). Therefore, siderophores represent a subset of natural Fe ligands that are strong, small and intentionally produced. Siderophores are well studied for terrestrial bacteria (Crosa 1989) and fungi (Neilands 1984) and siderophore production has been shown in the culture of marine bacteria (Simpson and Oliver 1983; Trick 1989).

L1 ligands are attributed to siderophores because they show: 1) similar stability constants as siderophores (Gledhill and Buck 2012); 2) high concentration near chlorophyll maximum (van den Berg 1995); and 3) predominant partition into the soluble size fraction (< 0.02 μm, in which siderophores are expected due to their low molecular weight) at surface ocean (Cullen et al 2006).

1.3 Siderophore as model ligands for Fe cycling and Fe uptake

These similarities allow siderophores to be used as model ligands to represent natural Fe ligands. There are three major directions in siderophore research, including manipulation of Fe bioavailability in natural seawater, investigations on the bioavailability of different siderophores, and investigations of Fe uptake mechanisms from siderophores.

Some studies use siderophores to manipulate Fe bioavailability, by adding metal free (apo) siderophores into seawater, and comparing the Fe uptake rates, cell abundance, and nutrient concentration with the control where no siderophore is added.

For example, Wells et al (1994) added 10 nM desferrioxamine B (DFB) to seawater collected at the surface of the Equatorial Pacific Ocean, and found lower Fe uptake rates in the DFB treatment than in the control, in all size fractions that are larger than 0.2 μm. Furthermore, addition of 10 pM of DFB would result in lower cell counts of *Synechococcus* in the Equatorial Pacific Ocean over the course of 8 days (Wells et al 1994).

When 200 pM Fe was added to coastal seawater, further addition of 100 nM DFB could quench Fe uptake by both natural phytoplankton and heterotrophic bacteria over a 6 h period and allowed only marginal Fe uptake over 5 d of incubation (Wells 1999). Similar results were found in Hutchins et al (1999), where addition of 100 nM DFB eliminated the Fe uptake by all size fractions of microbes that were larger than 0.2 μm.

Indeed, the threshold of DFB addition that eliminates Fe uptake by natural microbial communities (> 0.2 μm) in Monterey Bay was later refined from 100 nM to 3 nM (Wells and Trick 2004). However, the Fe uptake was not influenced by the addition of two other unknown siderophores isolated from marine prokaryotes (Wells and Trick 2004).

According to these results, the addition of DFB would result in an overall lower Fe bioavailability to phytoplankton and heterotrophic bacteria. It seems that this is due to the conversion from Fe bound to natural ligands, which have a relatively lower stability constant and presumably higher bioavailability, to ferrioxamine B, which has a high stability constant and a lower bioavailability.

Some studies directly measure the bioavailability of different siderophores by adding radiolabeled ^{55}Fe-siderophores or ^{59}Fe-siderophores to cultures or natural microbial communities, and comparing the Fe uptake rates among siderophores or to inorganic Fe. For example, in the presence of 2 nM Fe and 10 nM DFB or desferrioxamine E (DFE), iron uptake is found in both phytoplankton and heterotrophic bacteria, in both coastal waters and oceanic waters of the NE subarctic Pacific (Maldonado and Price 1999). Furthermore, Fe-Ferrioxamine and Fe-Alterobactin seem to be more bioavailable than inorganic Fe to cyanobacteria cultured presumably in Fe sufficient media, but less bioavailable than inorganic Fe to cultured eukaryotic phytoplankton cultured presumably in Fe sufficient media (Hutchins et al 1999). In contrast, diatom *Phaeodactylum tricornutum* grown under Fe limiting conditions took up iron faster from DFE and DFB than from Fe-EDTA and $FeCl_3$ at the same Fe concentration (Soria-Dengg and Horstmann 1995).

In these studies, both Fe and siderophores were added at different concentrations, complicating the direct comparison of the bioavailability of siderophores among studies, suggesting the importance of a proxy for siderophore bioavailability. In the Michaelis-Menten equation, which is presumably the pattern for Fe uptake from Fe-siderophores, the uptake rate is proportional to the concentration of Fe-siderophores, when the concentration is much lower than the half saturation constant. Therefore, in a pure culture of a particular microbe, normalization of uptake rate to Fe-siderophore concentration yields a parameter that is only related to the bioavailability of Fe-siderophore to the microbe. This parameter was used by Lis et al (2015) to compare the bioavailability of siderophores to phytoplankton, which showed that the bioavailability of Fe-siderophores are lower than inorganic Fe, iron bound to humic substances, and Fe bound to natural organic ligands.

The Fe uptake mechanism from siderophores have been well studied. In the ocean, siderophores are produced by heterotrophic bacteria and cyanobacteria. After binding to Fe, the Fe-siderophore complex is transported across the cell membrane by TonB dependent transporters (Moeck and Coulton 1998), which show high affinity and high specificity to siderophores.

In eukaryotic phytoplankton, siderophore synthesis has not been demonstrated (Hopkinson and Morel 2009). However, eukaryotic phytoplankton are able to take Fe bound to exogenous siderophores by different approaches. For example, biological reduction of Fe is well known in microbial systems, and confirmed in *Thalassiosira oceanica* culture by inhibiting the activity of plasma membrane Fe reductases, which decreased the Fe uptake rate from Fe-DFB (Maldonado and Price 2001). Results from similar experiments (Keshtacher-Liebson et al 1999; Maldonado and Price 1999) suggested a non specific Fe reduction prior to Fe uptake from both inorganic Fe and Fe-siderophores (Shaked et al 2005). The affinity of siderophore is much higher for Fe (III) than Fe(II), and the reduction of Fe would result in the dissociation from siderophores.

Kazamia et al (2018) labeled DFB with a fluorophore, and by tracking the fluorescence during an uptake experiment, was able to show that Fe-limited cultures of the diatom *Phaeodactylum tricornutum* were able to take up Ga-DFB by endocytosis. In this study, Fe-DFB was not used, because Fe would quench the fluorescence. However, they also performed Fe uptake experiment using Fe bound to fluorescently labeled DFB, and found fast increase of fluorescence in vesicles near the chloroplast, suggesting that Fe was released from the siderophores after uptake, and reduction was not involved in the uptake of Fe-DFB.

In summary, siderophores have been used to represent natural Fe ligands to study Fe cycling in seawater. For example, the bioavailability of Fe-siderophore could be measured and incorporated into models to simulate the Fe uptake rate. The mechanism of Fe uptake from siderophore has been well studied, which largely promoted our understanding on how microbes acquire Fe from seawater.

1.4 Measurement of siderophores by LC-MS

Although siderophores have been used as proxies for naturally occurring Fe ligands, it remains unclear how representative siderophores are for natural Fe ligands, because the presence of siderophores in seawater was not easily confirmed, and the identity of natural Fe ligands was not widely been investigated on a molecular level. As a result, the source and bioavailability of natural Fe ligands, as well as the microbial Fe uptake mechanism from natural Fe ligands were largely unknown.

To address these issues, McCormack et al (2003) developed a liquid chromatography-mass spectrometry (LC-MS) based method that aimed to characterize natural Fe ligands on a molecular level. Siderophores are concentrated from spent culture media or seawater using solid phase extraction. This step removes salts which is not compatible with MS, and concentrates the siderophores by more than 1000 times. Then, ligands are separated by LC and identified by electrospray ionization mass spectrometry (ESIMS).

For each siderophores in any samples, there is presumably a ^{56}Fe-siderophore:^{54}Fe-siderophore ratio of 15.7, according to the natural abundance of the two isotopes. If there is a pair of co-eluting ions in LC-ESIMS with mass difference of 1.995 and a concentration ratio of 15.7, this pair of ions potentially represent isotopologue of Fe-siderophore, and is further investigated.

However, for some siderophores, the ^{54}Fe-siderophore might not be detected by ESIMS, or might not be recognized in the mass spectra, due to co-eluting compounds that are high in concentration but irrelevant to the Fe-siderophore. In this untargeted approach which aimed at assigning a mass to an unknown ligand, the absence of ^{54}Fe-siderophore would complicate the mass assignment for a potential Fe-siderophore complex. To address this issue, McCormack et al (2003) add gallium (Ga) to their samples to exchange Fe in siderophores by Ga. Gallium has two major isotopes, ^{69}Ga and ^{71}Ga which occur in a 3:2 ratio. Therefore, isotopologues of Ga-siderophores are more likely to be recognized in environmental samples than Fe-siderophores in manual curation.

This method was applied to the detection of the Fe-Rhodotoluric Acid, ferrioxamine-B and ferrichrome from spent culture media (McCormack et al 2003), ferrioxamines and amphibactins from nutrient amended seawater (Gledhill et al 2004), and ferrioxamines in seawater (Mawji et al 2008). However, quantification of Fe-siderophores remains an issue, because the sensitivity Fe-siderophore (or Ga-siderophore) in LC-ESIMS is siderophore specific, and therefore limited by the commercial availability of standards.

To improve the quantification of Fe-siderophores, LC coupled to inductively coupled plasma mass spectrometry (ICPMS) was proposed. Because ICPMS measures the metal ion, the sensitivity of Fe-siderophores is not dependent on siderophores. However, the organic solvent of LC is not compatible with the high temperature plasma used in ICPMS, which could result in the formation of reduced carbon species and carbon deposits in the instrument, and decrease the sensitivity and instrument performance. In addition, there was a high baseline for ^{56}Fe, due to contamination from

the LC instrument, solvents, and the interference of $^{40}Ar^{16}O$, which is formed in the Ar plasma.

Boiteau et al (2013) first addressed these issues, by introducing an oxygen gas stream to the sample carrier gas (Hutton 1986; Hausler 1987), which helps the conversion from organic solvent to CO_2. The high ^{56}Fe baseline was addressed by using bioinert titanium/peek LC, clean LC solvents, and a hexapole collision cell in ICPMS, which minimizes $^{40}Ar^{16}O$ interference by kinetic energy discrimination (Szpunar 2004). In addition, Boiteau and Repeta (2015) developed a mass search algorithm to identify isotopologues representing ^{56}Fe-siderophore and ^{54}Fe-siderophore, without Ga replacement. Although this algorithm does not increase the sensitivity of ^{54}Fe-siderophore by ESIMS, the automated search could find the pair of isotopologues when ^{54}Fe-siderophore is low in concentration, which might not be possible in manual curation.

With these developments, siderophores could be quickly screened from spent culture media and seawater by LC-ICPMS, and identified by LC-ESIMS. Two major classes of siderophores have been found in seawater, including the polar ferrioxamines, which have a peptidic Fe binding group, and the non polar amphibactins, marinobactins and synechobactins, which have a peptidic Fe binding group and a fatty acid chain (Mawij et al 2008; Boiteau et al 2016; Bundy et al 2018; Boiteau et al 2019; Gledhill et al 2022; Park et al 2022). Ferrioxamines seem to be prevalent in surface (0-20 m) waters (Mawij et al 2008; Boiteau et al 2016; Bundy et al 2018). Amphibactins are found in both surface and upper mesopelagic (300-400 m) waters. (Boiteau et al 2016; Bundy et al 2018). Marinobactins and synechobactins have been found in coastal regions, but not in the open ocean (Boiteau et al 2019; Gledhill et al 2022).

1.5 Outline

Although these results largely promoted our understanding on siderophores, there are a few outstanding questions on siderophore cycling in the ocean. To date, siderophore

samples for LC-MS measurement have only been collected from a few depth profiles and surface transects, generating a dataset of less than 100 samples. Therefore, the prevalence of siderophores in the ocean remains unclear. In addition, the relationship between siderophore and dFe concentrations is unknown, because many samples collected in prior studies do not have a paired sample for dFe.

Furthermore, high concentration of siderophores in these samples could be explained by either fast production or slow consumption of siderophores. Because transect data represent only a snapshot of concentrations at the time of sampling, it does not allow us to distinguish these two possibilities, suggesting the importance of Fe uptake rate measurement.

This thesis aims to address these questions. Chapter 2 describes an improved LC-ICPMS/ESIMS method that incorporates a number of changes, including the configuration of instrument hardware and the development of an internal standard, that improves sensitivity of the method by a factor of 5, and allows for more accurate quantitation of siderophores. We also describe a new suite of mass search algorithms that do not rely on the presence or detection of the pair of isotopologues for ^{56}Fe-siderophore and ^{54}Fe-siderophore. Therefore, the new algorithms can find and characterize siderophores at lower concentration, or siderophores with unknown extent of isotope fractionation from natural abundances.

Chapter 3 reports the distribution of siderophores in a section of the Pacific Ocean sampled by the US GEOTRACES GP15 Pacific Meridional Transect. The transect crosses several biogeochemical provinces, including coastal waters along the South Alaskan Shelf, two high nutrient low chlorophyll (HNLC, North Pacific Subarctic Gyre and East Pacific Equatorial upwelling) regions, and two oligotrophic. subtropical (North and South Pacific) gyres. Overall, this transect offered an opportunity to directly compare siderophore concentration, production and consumption at sample sites with different nutrient conditions, thereby providing a window into microbial responses to nutrient stress.

In Chapter 4, we introduce an Fe uptake measurement based on LC-ICPMS, using ^{57}Fe as a stable isotope tracer. At Station ALOHA, we performed Fe uptake experiments by incubating whole seawater collected between 75-500 m in the dark to measure the Fe uptake by heterotrophic bacteria, aiming to investigate the turnover of siderophores and evaluate Fe limitation on heterotrophic bacteria at different depths.

In Chapter 5, we investigate the limitation on siderophore production by heterotrophic bacteria, by dark incubation with nutrient amended seawater collected at 150 m of Station ALOHA. C or N limitation on siderophore production was investigated by 3 types of experiments, including one with no nutrient addition, one with glucose addition, and one with addition of sinking POM. In each experiment, there is a Fe treatment and a no Fe treatment, for the investigation of the influence of Fe on siderophore production.

1.6 References

Bruland, K. W., Franks, R. P., Knauer, G. A., & Martin, J. H. (1979). Sampling and analytical methods for the determination of copper, cadmium, zinc, and nickel at the nanogram per liter level in sea water. Analytica chimica acta, 105, 233-245.

Gordon, R. M., Martin, J. H., & Knauer, G. A. (1982). Iron in north-east Pacific waters. Nature, 299, 611-612.

Landing, W. M., & Bruland, K. W. (1987). The contrasting biogeochemistry of iron and manganese in the Pacific Ocean. *Geochimica et Cosmochimica Acta*, *51*(1), 29-43.

Martin, J. H., & Gordon, R. M. (1988). Northeast Pacific iron distributions in relation to phytoplankton productivity. Deep Sea Research Part A. Oceanographic Research Papers, 35(2), 177-196.

Chester, R., & Stoner, J. H. (1974). The distribution of zinc, nickel, manganese, cadmium, copper, and iron in some surface waters from the world ocean. Marine Chemistry, 2(1), 17-32.

Kremling, K., & Petersen, H. (1977). The distribution of zinc, copper and iron in seawater of the Iceland-Faroe Ridge area. Meteor Forschungsergebnisse: Reihe A, Allgemeines, Physik und Chemie des Meeres, 19, 10-17.

Danielsson, L. G. (1980). Cadmium, cobalt, copper, iron, lead, nickel and zinc in Indian Ocean water. Marine Chemistry, 8(3), 199-215.

Martin, J. H. (1992). Iron as a limiting factor in oceanic productivity. *Primary productivity and biogeochemical cycles in the sea*, 123-137.

Martin, J. H., & Fitzwater, S. E. (1988). Iron deficiency limits phytoplankton growth in the north-east Pacific subarctic. *Nature*, *331*, 341-343.

de Baar, H. J., Buma, A. G., Nolting, R. F., Cadée, G. C., Jacques, G., & Tréguer, P. J. (1990). On iron limitation of the Southern Ocean: experimental observations in the Weddell and Scotia Seas. *Marine ecology progress series*, 105-122.

Martin, J. H., Coale, K. H., Johnson, K. S., Fitzwater, S. E., Gordon, R. M., Tanner, S. J., ... & Tindale, N. W. (1994). Testing the iron hypothesis in ecosystems of the equatorial Pacific Ocean. Nature, 371(6493), 123-129.

Price, N. M., Ahner, B. A., & Morel, F. M. (1994). The equatorial Pacific Ocean: Grazer-controlled phytoplankton populations in an iron-limited ecosystem 1. *Limnology and Oceanography*, *39*(3), 520-534.

De Baar, H. J., Boyd, P. W., Coale, K. H., Landry, M. R., Tsuda, A., Assmy, P., ... & Wong, C. S. (2005). Synthesis of iron fertilization experiments: from the iron age in the age of enlightenment. Journal of Geophysical Research: Oceans, 110(C9).

Boyd, P. W., Jickells, T., Law, C. S., Blain, S., Boyle, E. A., Buesseler, K. O., ... & Watson, A. J. (2007). Mesoscale iron enrichment experiments 1993-2005: synthesis and future directions. *science*, *315*(5812), 612-617.

Liu, X., & Millero, F. J. (2002). The solubility of iron in seawater. Marine Chemistry, 77(1), 43-54.

Wu, J., & Luther III, G. W. (1995). Complexation of Fe (III) by natural organic ligands in the Northwest Atlantic Ocean by a competitive ligand equilibration method and a kinetic approach. Marine Chemistry, 50(1-4), 159-177.

Kuma, K., Nishioka, J., & Matsunaga, K. (1996). Controls on iron (III) hydroxide solubility in seawater: the influence of pH and natural organic chelators. Limnology and Oceanography, 41(3), 396-407.

van den Berg, C. M. (1995). Evidence for organic complexation of iron in seawater. Marine Chemistry, 50(1-4), 139-157.

Gledhill, M., & van den Berg, C. M. (1994). Determination of complexation of iron (III) with natural organic complexing ligands in seawater using cathodic stripping voltammetry. Marine Chemistry, 47(1), 41-54.

Rue, E. L., & Bruland, K. W. (1995). Complexation of iron (III) by natural organic ligands in the Central North Pacific as determined by a new competitive ligand equilibration/adsorptive cathodic stripping voltammetric method. Marine chemistry, 50(1-4), 117-138.

Wu, J., & Luther III, G. W. (1995). Complexation of Fe (III) by natural organic ligands in the Northwest Atlantic Ocean by a competitive ligand equilibration method and a kinetic approach. Marine Chemistry, 50(1-4), 159-177.

Croot, P. L., & Johansson, M. (2000). Determination of iron speciation by cathodic stripping voltammetry in seawater using the competing ligand 2-(2-Thiazolylazo)-p-cresol (TAC). Electroanalysis: An International Journal Devoted to Fundamental and Practical Aspects of Electroanalysis, 12(8), 565-576.

Tagliabue, A., Aumont, O., DeAth, R., Dunne, J. P., Dutkiewicz, S., Galbraith, E., ... & Yool, A. (2016). How well do global ocean biogeochemistry models simulate dissolved iron distributions?. Global Biogeochemical Cycles, 30(2), 149-174.

Boyd, P. W., & Ellwood, M. J. (2010). The biogeochemical cycle of iron in the ocean. Nature Geoscience, 3(10), 675-682.

Hider, R. C., & Kong, X. (2010). Chemistry and biology of siderophores. *Natural product reports*, *27*(5), 637-657.

Crosa, J. H. (1989). Genetics and molecular biology of siderophore-mediated iron transport in bacteria. Microbiological reviews, 53(4), 517-530.

Neilands, J. B. (1984). Siderophores of bacteria and fungi. Microbiological sciences, 1(1), 9-14.

Simpson, L. M., & Oliver, J. D. (1983). Siderophore production by Vibrio vulnificus. Infection and immunity, 41(2), 644-649.

Trick, C. G. (1989). Hydroxamate-siderophore production and utilization by marine eubacteria. Current microbiology, 18, 375-378.

Gledhill, M., & Buck, K. N. (2012). The organic complexation of iron in the marine environment: a review. Frontiers in microbiology, 3, 69.

Cullen, J. T., Bergquist, B. A., & Moffett, J. W. (2006). Thermodynamic characterization of the partitioning of iron between soluble and colloidal species in the Atlantic Ocean. Marine Chemistry, 98(2-4), 295-303.

Wells, M. L., Price, N. M., & Bruland, K. W. (1994). Iron limitation and the cyanobacterium Synechococcus in equatorial Pacific waters. Limnology and oceanography, 39(6), 1481-1486.

Wells, M. L. (1999). Manipulating iron availability in nearshore waters. Limnology and oceanography, 44(4), 1002-1008.

Hutchins, D. A., Franck, V. M., Brzezinski, M. A., & Bruland, K. W. (1999). Inducing phytoplankton iron limitation in iron-replete coastal waters with a strong chelating ligand. Limnology and Oceanography, 44(4), 1009-1018.

Wells, M. L., & Trick, C. G. (2004). Controlling iron availability to phytoplankton in iron-replete coastal waters. Marine chemistry, 86(1-2), 1-13.

Maldonado, M. T., & Price, N. M. (1999). Utilization of iron bound to strong organic ligands by plankton communities in the subarctic Pacific Ocean. Deep Sea Research Part II: Topical Studies in Oceanography, 46(11-12), 2447-2473.

Soria-Dengg, S., & Horstmann, U. (1995). Ferrioxamines B and E as iron sources for the marine diatom Phaeodactylum tricornutum. Marine Ecology Progress Series, 127, 269-277.

Lis, H., Shaked, Y., Kranzler, C., Keren, N., & Morel, F. M. (2015). Iron bioavailability to phytoplankton: an empirical approach. The ISME journal, 9(4), 1003-1013.

Moeck, G. S., & Coulton, J. W. (1998). TonB-dependent iron acquisition: mechanisms of siderophore-mediated active transport. Molecular microbiology, 28(4), 675-681.
Hopkinson, B. M., & Morel, F. M. (2009). The role of siderophores in iron acquisition by photosynthetic marine microorganisms. Biometals, 22, 659-669.

Maldonado, M. T., & Price, N. M. (2001). Reduction and transport of organically bound iron by Thalassiosira oceanica (Bacillariophyceae). Journal of Phycology, 37(2), 298-310.

Keshtacher-Liebson, E., Hadar, Y., & Chen, Y. (1999). Fe nutrition demand and utilization by the green alga Dunaliella bardawil. Plant and soil, 215, 175-182.

Shaked, Y., Kustka, A. B., & Morel, F. M. (2005). A general kinetic model for iron acquisition by eukaryotic phytoplankton. Limnology and Oceanography, 50(3), 872-882.

Kazamia, E., Sutak, R., Paz-Yepes, J., Dorrell, R. G., Vieira, F. R. J., Mach, J., ... & Lesuisse, E. (2018). Endocytosis-mediated siderophore uptake as a strategy for Fe acquisition in diatoms. Science Advances, 4(5), eaar4536.

McCormack, P., Worsfold, P. J., & Gledhill, M. (2003). Separation and detection of siderophores produced by marine bacterioplankton using high-performance liquid chromatography with electrospray ionization mass spectrometry. Analytical Chemistry, 75(11), 2647-2652.

Gledhill, M., McCormack, P., Ussher, S., Achterberg, E. P., Mantoura, R. F. C., & Worsfold, P. J. (2004). Production of siderophore type chelates by mixed bacterioplankton populations in nutrient enriched seawater incubations. Marine Chemistry, 88(1-2), 75-83.

Mawji, E., Gledhill, M., Milton, J. A., Tarran, G. A., Ussher, S., Thompson, A., ... & Achterberg, E. P. (2008). Hydroxamate siderophores: occurrence and importance in the Atlantic Ocean. *Environmental science & technology*, *42*(23), 8675-8680.

Boiteau, R. M., Fitzsimmons, J. N., Repeta, D. J., & Boyle, E. A. (2013). Detection of iron ligands in seawater and marine cyanobacteria cultures by high-performance liquid chromatography–inductively coupled plasma-mass spectrometry. *Analytical chemistry*, *85*(9), 4357-4362.

Hutton, R. C. (1986). Application of inductively coupled plasma source mass spectrometry (ICP-MS) to the determination of trace metals in organics. Journal of Analytical Atomic Spectrometry, 1(4), 259-263.

Hausler, D. (1987). Trace element analysis of organic solutions using inductively coupled plasma-mass spectrometry. Spectrochimica Acta Part B: Atomic Spectroscopy, 42(1-2), 63-73.

Szpunar, J. (2004). Metallomics: a new frontier in analytical chemistry. Analytical and Bioanalytical Chemistry, 378(1), 54-56.
Boiteau, R. M., & Repeta, D. J. (2015). An extended siderophore suite from Synechococcus sp. PCC 7002 revealed by LC-ICPMS-ESIMS. Metallomics, 7(5), 877-884.

Boiteau, R. M., Mende, D. R., Hawco, N. J., McIlvin, M. R., Fitzsimmons, J. N., Saito, M. A., ... & Repeta, D. J. (2016). Siderophore-based microbial adaptations to iron scarcity across the eastern Pacific Ocean. *Proceedings of the National Academy of Sciences*, *113*(50), 14237-14242.

Bundy, R. M., Boiteau, R. M., McLean, C., Turk-Kubo, K. A., McIlvin, M. R., Saito, M. A., ... & Repeta, D. J. (2018). Distinct siderophores contribute to iron cycling in the mesopelagic at station ALOHA. *Frontiers in Marine Science*, *5*, 61.

Boiteau, R. M., Till, C. P., Coale, T. H., Fitzsimmons, J. N., Bruland, K. W., & Repeta, D. J. (2019). Patterns of iron and siderophore distributions across the California Current System. *Limnology and Oceanography*, *64*(1), 376-389.

Gledhill, M., Zhu, K., Rusiecka, D., & Achterberg, E. P. (2022). Competitive interactions between microbial siderophores and humic-like binding sites in european shelf sea waters. *Frontiers in Marine Science*, *9*, Art-Nr.

Park, J., Durham, B. P., Key, R. S., Groussman, R. D., Pinedo-Gonzalez, P., Hawco, N. J., ... & Bundy, R. M. (2022). Siderophore production and utilization by microbes in the North Pacific Ocean. *bioRxiv*, 2022-02.

Chapter 2 Element-selective targeting of nutrient metabolites in environmental samples by inductively coupled plasma mass spectrometry and electrospray ionization mass spectrometry

Jingxuan Li, Rene M. Boiteau, Lydia Babcock-Adams, Marianne Acker, Zhongchang Song, Matthew R. McIlvin, Daniel J. Repeta

Keywords: LC-MS, algorithm, environmental metabolomics, trace metal, siderophores

Citation: Li J, Boiteau RM, Babcock-Adams L, Acker M, Song Z, McIlvin MR and Repeta DJ (2021) Element-Selective Targeting of Nutrient Metabolites in Environmental Samples by Inductively Coupled Plasma Mass Spectrometry and Electrospray Ionization Mass Spectrometry. Front. Mar. Sci. 8:630494. doi: 10.3389/fmars.2021.630494

Abstract

Metabolites that incorporate elements other than carbon, nitrogen, hydrogen and oxygen can be selectively detected by inductively coupled mass spectrometry (ICPMS). When used in parallel with chromatographic separations and conventional electrospray ionization mass spectrometry (ESIMS), ICPMS allows the analyst to quickly find, characterize and identify target metabolites that carry nutrient elements (P, S, trace metals; “nutrient metabolites”), which are of particular interest to investigations of microbial biogeochemical cycles. This approach has been applied to the study of siderophores and other trace metal organic ligands in the ocean. The original method used mass search algorithms that relied on the ratio of stable isotopologues of iron, copper and nickel to assign mass spectra collected by ESIMS to metabolites carrying these elements detected by ICPMS. However, while isotopologue-based mass assignment algorithms were highly successful in characterizing metabolites that incorporate some trace metals, they do not realize the whole potential of the ICPMS/ESIMS approach as they cannot be used to assign the molecular ions of metabolites with monoisotopic elements or elements for which the ratio of stable

isotopes is not known. Here we report a revised ICPMS/ESIMS method that incorporates a number of changes to the configuration of instrument hardware that improves sensitivity of the method by a factor of 4-5, and allows for more accurate quantitation of metabolites. We also describe a new suite of mass search algorithms that can find and characterize metabolites that carry monoisotopic elements. We used the new method to identify siderophores in a laboratory culture of *Vibrio cyclitrophicus* and a seawater sample collected in the North Pacific Ocean, and to assign molecular ions to monoisotopic cobalt and iodine nutrient metabolites in extracts of a laboratory culture of the marine cyanobacterium *Prochorococcus* MIT9215.

2.1 Introduction

Advances in the chromatographic separation and mass spectral analyses of metabolites have opened new avenues for understanding microbial dynamics and organic matter cycling in the ocean (Petras et al 2017; Patriarca et al 2018). Marine environmental metabolomics, the comparative analysis of metabolites expressed in particulate or dissolved organic matter sampled under different conditions, is typically approached in one of two ways: through targeted metabolomics in which metabolites of interest are measured through an experiment or suite of samples, and untargeted metabolomics in which the response of unidentified metabolites are correlated against experimental or environmental variables (reviewed by Soule et al 2015; Cajka and Fiehn, 2016). Each approach comes with trade-offs between the confidence in metabolite identity or amount with the breath of metabolites that are measured. The targeted approach allows for high confidence in metabolite identity and concentration, but is limited to select and spectrally characterized compounds. Untargeted approaches survey a much broader suite of metabolites, but in doing so a detailed knowledge of metabolite identity and quantity is sacrificed. These two approaches bookend other avenues for investigating marine metabolomics that share features with both targeted and untargeted analyses. Here we discuss an approach that combines multi-modal liquid chromatography mass spectrometry data sets to target metabolites containing specific elements. However, the

approach can easily be adapted and applied to metabolites that share other chemical properties such as UV/Vis light absorption or fluorescence.

Nutrient availability drives many microbial biogeochemical cycles, and investigations of how nutrient dynamics impact marine genomes, proteomes, and metabolomes are becoming increasingly common. Methods that target metabolites carrying nutrient elements such as nitrogen, phosphorus, sulfur and bioactive trace metals (Fe, Cu, Zn, Ni, Mn, Co), are therefore of interest. Metabolites incorporating nutrient elements (nutrient metabolites) can be separated in extracts of microbial biomass, dissolved and particulate organic matter by liquid chromatography (LC) and selectively detected by inductively coupled plasma mass spectrometry (ICPMS), enabling a nutrient or element-targeted approach to marine metabolomics. ICPMS is highly sensitive, with femtomole detection limits. However, other than the presence and amount of the nutrient element, LC-ICPMS only characterizes metabolites by their chromatographic retention time. This shortcoming can be addressed by combining LC-ICPMS data with companion mass spectral data obtained from high-resolution electrospray ionization mass spectrometry (LC-ESIMS). LC-ESIMS can be used to identify metabolites, or for unknown compounds, determine their molecular weight, elemental composition, and major ions after MS/MS fragmentation. As an application of this element-targeted metabolomics approach, we have used LC-ICPMS and LC-ESIMS to characterize trace metal organic complexes in laboratory cultures of marine cyanobacteria (Boiteau and Repeta, 2015) and marine dissolved organic matter (Boiteau et al 2016; Bundy et al 2018, Boiteau et al 2019).

In seawater, most bioactive trace metals (Fe, Cu, Zn, Co, Ni, etc.) are complexed to dissolved organic ligands (>99.9% of Fe, reviewed in Gledhill and Buck, 2012; >98% of Cu, Buckley and van den Berg, 1986, Coale and Bruland, 1988, 1990; >98% of Zn, Bruland, 1989; >99% of Co, Saito and Moffett 2001; 10-20% of Ni, Acherberg and van den Berg, 1997). Organic ligands elevate the solubility of trace metals (Kuma et al 1998; Millero, 1998), but also play a crucial role in their bioavailability (Hutchins et al 1999; Wells and Trick, 2004; Hassler et al 2011; Aristilde et al 2012; Lis et al 2015). Some

trace metal organic complexes are readily available to microbes, while others are not. For example, microbial production in approximately one third of the surface ocean is limited by the bioavailability of iron (Boyd et al 2007; Moore et al 2013). Microbes inhabiting these iron-limited regions produce siderophores, organic compounds synthesized to bind iron and facilitate iron uptake (Reid et al 1993; Martinez et al 2000, 2001). Microbes expressing appropriate cross-membrane siderophore transport systems are able to take up siderophore-bound iron to help satisfy their iron requirements (Hopkinson and Barbeau 2012; Tang et al 2012). Cataloguing where siderophores are made in the ocean, and under what conditions, contributes to our understanding of how marine microbes respond to iron bioavailability. However, hundreds of different siderophores, most likely representing only a fraction of the siderophores produced in nature, have been identified in laboratory cultures (Hider and Kong, 2010; Baars et al 2014). Compounding this, marine dissolved organic matter is an extraordinarily complex mixture of 10^5 to 10^6 different compounds. Ideally, methods for analyzing siderophores or other nutrient metabolites should therefore allow the analyst to quickly find and identify known siderophores or characterize new siderophores, at low concentrations and within the very complex mixture of organic compounds that is typical of most environmental samples.

Boiteau and colleagues (2013, 2016) described a method whereby siderophores and other nutrient element metabolites were concentrated from seawater or spent culture media by solid phase extraction (SPE), then separated by LC and detected by ICPMS. An example of the results from an analysis of siderophores in a seawater sample collected in the North Pacific Ocean is provided in Figure 2.1A. Siderophores appear in the iron chromatogram as a series of well-defined peaks at different retention times, which can be quantified after appropriate calibration with iron standards. The sample was then analyzed a second time using the same chromatographic conditions, but with detection by high resolution ESIMS (Fig. 2.1B). The LC-ICPMS data and LC-ESIMS data were then integrated using mass alignment and filtering algorithms to identify the major peaks in the sample as a suite of marinobactins, amphiphilic siderophores synthesized by heterotrophic bacteria.

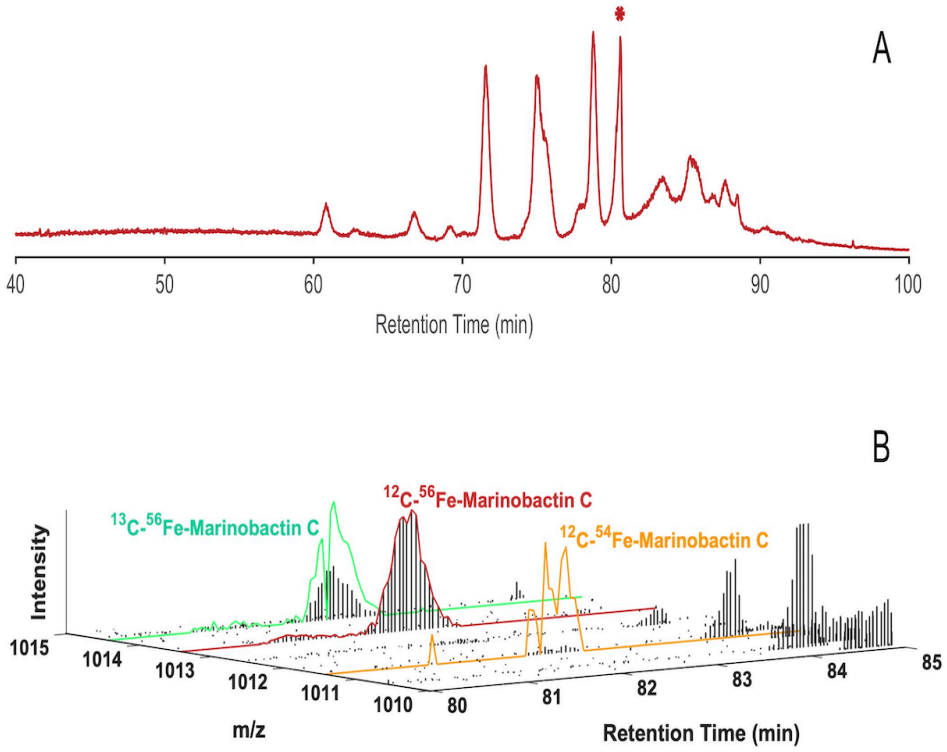

Figure 2.1. A) LC-ICPMS ^{56}Fe-chromatogram of dissolved organic matter collected by SPE from the North Pacific Ocean. Each discrete peak represents one (or a combination of multiple) Fe-containing organic compounds. The starred peak at 80.6 min was selected as our target for characterization, and B) LC-ESIMS data between 80-85 min and 1010.00 D-1015.00 D for the same sample. Using the isotope ratio search algorithm with Δm = 1.995 D and R = 15.7 for ^{54}Fe and ^{56}Fe the mass at 1013.44 D, retention time 80.6 min was identified as marinobactin-C (EIC outlined in red) by comparison of the exact mass with a catalogue of known siderophores. The scaled plots for ^{54}Fe-1011.45 D, and ^{13}C-^{56}Fe-1014.44 D of marinobactin C are outlined in orange and green respectively. Each vertical black bar represents the ion intensity at each mass in a scan at a given retention time.

We have used LC-ICPMS/ESIMS method to identify and quantify pM concentrations of iron, copper, and nickel ligands in a variety of seawater and laboratory culture samples. However, the coupling of a reverse-phase LC method designed to separate relatively nonpolar mixtures of organic compounds, to ICPMS presented several analytical

challenges that were not fully resolved in our original method. First, the ICPMS plasma is sensitive to solvent composition and contamination, which change through the analysis. As the concentration of methanol or acetonitrile increases in the mobile phase, the spectrometer response to iron (for example) decreased by a factor of 2-3, complicating quantitative analysis (Boiteau et al 2013). Second, the LC eluent delivered to the ICPMS interface led to cooling or quenching of the plasma. Therefore, the method incorporated a post column split which directed a majority of a sample to waste. Finally, the mass search algorithms that combined ICPMS and ESIMS data relied on the exact mass difference (Δm) and crustal relative abundance ratio (R) of an element's major isotopologues (Δm = 1.995 D and R = 15.7 for ^{54}Fe and ^{56}Fe, for example). For elements with low abundance isotopologues, the detection and resolution of minor isotopic forms of metabolites that occur at very low concentrations was often difficult to achieve (Fig. 2.1B). Further, many elements of interest (Mn, Co, P, I) do not have stable isotopes pairs, and algorithms that rely on isotopic fine structure analysis are not able to assign masses to a many nutrient metabolites of interest.

Over the past few years we have made a number of improvements to the original method to increase sensitivity and accuracy, and to expand its scope to include monoisotopic elements. The entire sample is now introduced into the mass spectrometer improving sensitivity by 4 to 5-fold. Solvent effects on detector sensitivity have been mitigated and quantified. New mass search algorithms have been coded that allow the molecular ions of metabolites incorporating monoisotopic elements, or isotope pairs for which the isotopic ratio is not known, to be assigned. Here we describe the details of the method, and provide some examples of its application to environmental metabolomics.

2.2 Methods

2.2.1 Reagents and Standards

High purity solvents and reagents were used throughout, including ultrapure water (18.2 MΩ; qH_2O), LCMS grade methanol (MeOH, Optima, Fisher Scientific) redistilled in a

Polytetrafluoroethylene still, and LCMS grade ammonium formate (Optima, Fisher Scientific).

For reference standards, desferrichrome (as metal-free (apo) form), ferrioxamine-E and cyanocobalamin (vitamin B_{12}) were purchased from Sigma Aldrich. Amphibactins siderophores were produced by culturing the marine bacterium*, Vibrio cyclitrophicus* strain 1F-53. The media consisted of 10 g casamino acids, 1 g NH_4Cl, 1.03 g Na_2HPO_4, 3 mL glycerol, and 5 mL vitamin stock solution in 1 L of 0.2 µm filtered Sargasso Sea seawater. The vitamin stock solution consisted of 40 mg biotin, 4 mg niacin, 2 mg thiamin, 4 mg 4-aminobenzoic acid, 2 mg calcium pantothenic acid, 20 mg pyridoxine HCl, 4 mg riboflavin, 4 mg folic acid, and 2 mg cyanocobalamine in 50 mL qH_2O. All vitamins are purchased from Sigma-Aldrich. We induced Fe limitation by adding 10 nM desferrioxmaine B (as desferrioxamine mesylate salt, Sigma Aldrich). The media was sterilized by 0.2 µm filtration (Fisher Scientific), then transferred into an autoclaved glass flask using axenic protocols. An incoulum of *V. cyclitrophicus 1F-53* was added, the culture flask wrapped with aluminum foil and shaken at 150 rpm at room temperature until the culture became turbid and foamy (30-40 hrs). The culture was filtered through 0.2-µm Pall Acropak Supor cartridges, and extracted as discussed below. Equimolar amounts of ferric chloride ($FeCl_3$*$6H_2O$, Fisher Scientific) were added to apo ferrichrome or amphibactins to synthesize ^{56}Fe-siderophore complexes.

2.2.2 Sample collection and extraction

Seawater samples were collected from the North Pacific Ocean during the US GEOTRACES Pacific Meridional Transect (GP15, October 2018) expedition, using a trace metal clean GTC rosette/Go-Flo bottle sampler. Each sample was filtered directly from the Go-Flo bottle a through 0.2 µm Pall Acropak-200 Supor cartridge (Cutter et al 2018) into an acid-cleaned polycarbonate bottle. Trace metal organic complexes were extracted from 4 L of filtered seawater pumped at 20 mL/min through Bond-Elut ENV cartridges (1 g, 6 mL, Agilent Technologies) that had been activated with ~6 mL each of distilled MeOH, pH 2 (Optima HCl, Fisher Scientific) qH_2O, and qH_2O. SPE columns

were frozen (-20°C) immediately after sample collection and returned to the laboratory for processing. To recover samples from the ENV cartridge, columns were thawed, washed with 6 mL qH_2O, and eluted with 6 mL distilled MeOH into acid-cleaned 10 mL falcon tubes. The eluent was concentrated to 500 µL by vacuum centrifugation (SpeedVac, Thermo Scientific).

2.2.3 High pressure liquid chromatography-mass spectrometry

Chromatographic analyses were performed on a bioinert Dionex Ultimate 3000 LC system fitted with a loading pump, a nano pump, and a 10-port switching valve, the schematic of which is shown in Fig 2.2. During the loading phase, 200 µL of sample were withdrawn into the sample loop, then pushed onto a C18 trap column (3.5 µm, 0.5 mm x 35 mm, Agilent PN 5064-8260) by the loading pump at 25 µL/min for 10 min (95% qH_2O, 5% MeOH, 5 mM ammonium formate). Solvent delivery was then switched to the nanopump, the flow rate reduced to 10 µL/min, and the trap column outflow directed onto two C18 columns (3.5 µm, 0.5 mm x 150 mm, Agilent PN 5064-8262) connected in series. Samples were separated with an 80 min gradient from 95% solvent A (5 mM aqueous ammonium formate) and 5% solvent B (5 mM methanolic ammonium formate) to 95% solvent B, followed by isocratic elution at 95% solvent B for 10 minutes. Meanwhile, the loading pump solvent was switched to 100% qH_2O, increased to 35 µL/min and directed as a make-up flow (qH_2O), which was infused with the column eluant (10 µL/min) into the ICPMS. Although ICPMS and ESIMS data can be collected in parallel by splitting the outflow of the LC system between the two spectrometers, in practice we found it easier to perform two separate analyses of a sample and align the data using an internal standard.

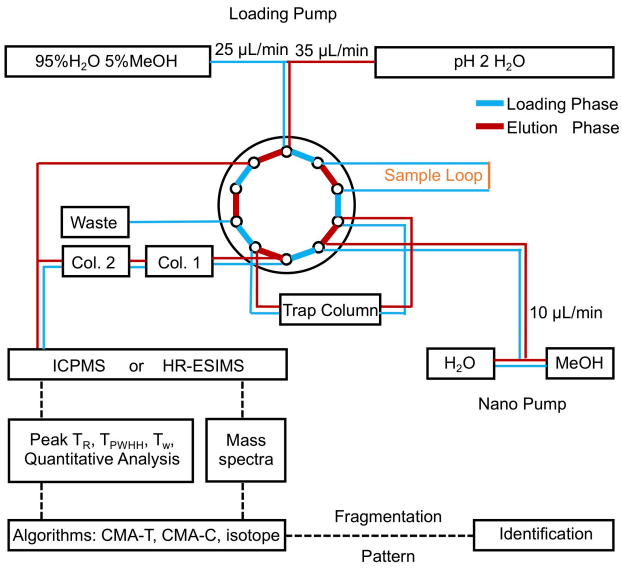

Figure 2.2. Schematic of the low-flow/make-up flow LC-MS instrumentation. Samples are picked up by the injector and loaded onto the trap column by the loading pump. Once loading is complete, the 10 port-valve switches to the nano-pump, which pushes the sample onto the columns, and elutes it using a gradient of aqueous methanol. During the elution phase, the loading pump flow is redirected to deliver a make-up flow that is post column infused, before entering ICPMS. The LC-ICPMS data are used to target nutrient metabolites by retention time and peak width. Companion ESIMS data are then queried by algorithms to assign masses, elemental formula, and MS^2 spectra of nutrient metabolites.

As described in the discussion, for the *Prochlorococcus* sample, the liquid chromatography separation before ICPMS and ESIMS was performed in two modes, resulting in four LC-MS runs for one sample. For the first separation we used a C18 column (3 µm, 2.1 x 150 mm, Hamilton PN 79641), and directed the effluent to ICPMS and ESIMS. Then, for the second separation we used an RP-Amide column (2.7 µm, 2.1 x 150 mm, Supelco PN 53914-U) and directed the effluent to ICPMS and ESIMS. With each column, samples were separated with a 60 min gradient from 95% solvent A (5 mM aqueous ammonium formate) and 5% solvent B (5 mM methanolic ammonium formate) to 95% solvent B, with 120 µL/min flow rate delivered by the loading pump.

2.2.4 Inductively coupled plasma mass spectrometry

The combined flow from LC was analyzed using a Thermo Scientific iCAP Q quadrupole mass spectrometer fitted with a perfluoroalkoxy micronebulizer (PFA-ST, Elemental Scientific), and a cyclonic spray chamber cooled to 4 °C (Boiteau and Repeta, 2016). Measurements were made in kinetic energy discrimination (KED) mode, with a helium collision gas flow of 4-4.5 mL/min to minimize isobaric $^{40}Ar^{16}O+$ interferences on ^{56}Fe. Oxygen was introduced into the sample carrier gas at 25 mL/min to prevent the formation of reduced organic deposits onto the ICPMS skimmer and sampling cones. Isotopes monitored included ^{56}Fe (at an integration time of 0.05 s), ^{57}Fe (0.02 s) and ^{59}Co (0.02 s).

2.2.5 Electrospray ionization mass spectrometry

For LC-ESIMS analysis, the eluant from the LC, without qH_2O infusion, was coupled to a Thermo Scientific Orbitrap Fusion mass spectrometer equipped with a heated electrospray ionization source. ESI source parameters were set to a capillary voltage of 3500 V, sheath, auxiliary and sweep gas flow rates of 5, 2, and 0 (arbitrary units), and ion transfer tube and vaporizer temperatures of 275°C and 20°C. MS^1 scans were collected in high resolution (450K) positive mode. The MS^2 scans were collected, but will not be discussed in the present study. LC-ESIMS data are available as a MassIVE dataset (https://massive.ucsd.edu, accession MSV000086964)

2.2.6 Data Analysis and workflow

The LC-ESIMS data was converted from raw file format to mzXML (MSconvert, ProteoWizard). The mzXML is imported to Matlab, where m/z and intensity from each scan are extracted, and ordered by scan number into a scan number/m/z/intensity matrix, which is then interrogated by mass search algorithms. In the first algorithm, the 3D matrix is cut to discard data beyond the time window defined by the retention time of peaks of interest targeted by LC-ICPMS. The matrix is then binned to generate thousands of extracted ion chromatograms (EIC). Each of the EIC is classified as either a target ion that shows a well-shaped peak, or noise with no defined peak. In the

second algorithm, the matrix is binned, and pairs of EICs are registered as ^{12}C-^{13}C isotopologues if their m/z differ by 1.003 D, and their abundances differ by R, where R is defined by their m/z. Collectively, these two algorithms detect features, either as targeted ions, or as pairs of EICs.

2.3 Results and Discussion

2.3.1 Improvements in LC-ICPMS detection of metabolites

Nutrient metabolites often occur at nano- to femto-molar concentrations in marine samples, making sensitivity and detection limits key concerns in method design. There are several avenues through which analyte detection limits can be increased. First, samples can be concentrated before LC-MS analysis. However, most SPE protocols used to extract metabolites from seawater trap organic matter with a wide range of polarities. This poses a problem for the next step of sample processing in which the volume of the extract is reduced for chromatographic analysis. When SPE extracts (typically ~5-6 mL) are concentrated to < 500 µL (≥ 10x concentration factor), we often observe the formation of precipitates. Further concentration does not yield a homogeneous extract, limiting the extent to which a reduction in sample extract volume can be used to increase sensitivity. A second approach is to increase injection volumes, chromatographic resolution, and signal sensitivity. In our original method, injection volumes were ~20 µL for standards and ~50 µL (~ 10% of total sample extract) for samples, and we used a conventional analytical flow column with a 2.1 mm inner diameter eluted at a flow rate of 200 µL/min. Injection volumes >50 µL increased dispersion in the column and decreased chromatographic resolution and reproducibility. However, we found 200 µL/min of high organic solvent content flow into the ICPMS destabilized and often quenched the plasma. We investigated the relationship between the flow rate of high organic solvent content and plasma stability and found a stable plasma could be achieved at 40-50 µL/min of 95% aqueous methanol. We provisionally addressed this problem by adding a post-column splitter to our system to direct 80% of the 200 µL/min eluent to waste and 20% to the ICPMS. This gave a reliably stable plasma, but resulted in substantial loss of sample.

When samples are directly injected into the ICPMS, a significant 2-3 fold decrease in the counts of iron and cobalt (and presumably other elements) was observed, for the same compound dissolved in methanol versus water (Boiteau et al 2013). For metabolites such as siderophores, which display a wide range of polarities and elute across the entire chromatogram, these solvent effects bias quantitative analyses. In the revised method we therefore reduced the size of our chromatographic system further, incorporated an on-line sample trap column to maintain high injection volumes, and added a post-column make-up flow to reduce solvent effects. We use a loading pump to push ~100-200 µL of sample onto a trap column. The flow into the trap is then switched to a nano pump that elutes the sample at 10 µL/min onto two 0.5 mm ID x 150 mm analytical columns connected in series. Collectively, these columns provide high separation efficiency and resolution. For example, a suite of closely related marinobactins extracted from seawater were efficiently separated from one another by the trap-column/low-flow method (Fig. 2.1). At 10 µL/min, the entire LC eluant can be directed into the ICPMS. We also introduced a post-column make-up flow of 35 µL/min pH 2 qH_2O delivered by the loading pump (Fig. 2.2). The make-up flow improved plasma stability and reduced the change in the organic solvent content of the flow into the ICPMS from 5-95% to 1-21% across the chromatographic run. This smaller fractional change in organic content reduced solvent effects across the analyses. Figure 2.3 compares the separation and detection of two siderophores using the high-flow and low-flow methods, demonstrating the five-fold greater ICPMS response, and the significantly reduced solvent effects with the low-flow method. In this example the ratio of ^{56}Fe peak areas for a 1:1 solution of ferrichrome and ferrioxamine-E applied to the column changed from 1:0.5 without the make-up flow to 1:0.9 with the make-up flow (Fig. 2.3). Particularly for studies where sample amount is limited, the low-flow method offers clear advantages. For the analysis of siderophores in seawater, we were able to reduce the seawater sample size from 20 L to 4 L by adopting the low-flow method.

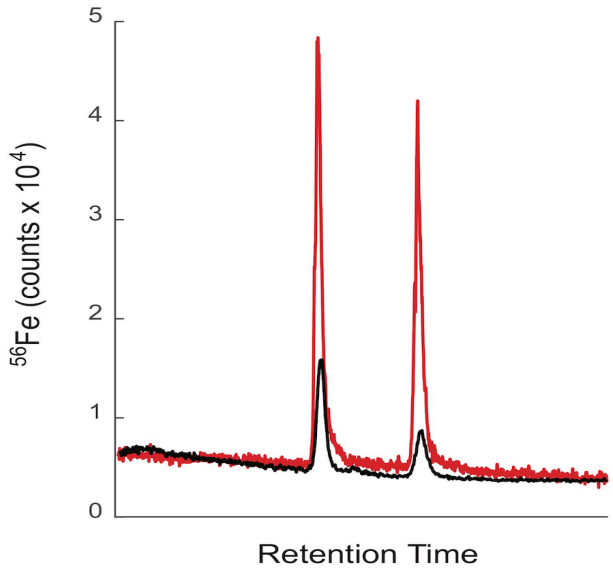

Figure 2.3. LC-ICPMS Fe chromatograms of ferrichrome and ferrioxamine E (2 nmol each) showing the better sensitivity and decreased solvent effects of the low-flow/make-up flow system (red trace) compared to the high-flow/split system (black trace). The low flow/make-up flow system was eluted with a flow rate of 10 µl/min with a make-up flow of 35 µl/min pH 2 qH_2O. The high-flow/split system was eluted with a flow rate of 200 µl/min, which was split post-column with 20% entering the ICPMS, 80% going to waste.

Nevertheless, even with the low-flow method, we noted a significant drop in the baseline detection of iron with increasing percentage of solvent B (Fig. 2.3). We attributed the decrease in baseline ^{56}Fe counts to either: 1) a direct decrease in ICPMS sensitivity due to less efficient atomization and ionization by cooling of the central channel of the ICPMS plasma (Hu et al 2004) when organic solvents are sprayed into the plasma chamber, or 2) a decrease in the amount of Fe contamination delivered to the ICPMS from either a lower level of contamination in, or a lower level of Fe leaching from the stainless steel LC column jacket by, the organic solvent (here LC-MS grade methanol redistilled in Teflon to reduce trace metal contamination) compared to qH_2O (solvent A). In the original method of Boiteau et al (2013), siderophores were quantified by multiplying the baseline-corrected peak area by an ICPMS response factor for Fe derived from a plot of peak area *vs* amount for ferrichrome and ferrioxamine-E standards. If the drop in baseline Fe counts results from less Fe contamination in

solvent B, it would be fully accounted for by baseline correction, and the quantification of siderophores would be accurate. In contrast, if the sensitivity of the ICPMS for Fe decreases due to direct solvent effects on the plasma, baseline correction alone would underestimate the concentration of siderophores eluting later than the calibrations standards. To distinguish and quantify these two effects, we added 10 ppb ^{56}Fe in pH 2 qH_2O to the make-up flow. This is 50 times higher than the amount of iron represented in the baseline of a typical analysis, so changes in iron contamination from the LC solvents or from contamination from the LC column were negligible. In this experiment, the ^{56}Fe delivered to the ICPMS was effectively constant over the course of the experiment. Changes in baseline ^{56}Fe detection were therefore attributed only to change in ^{56}Fe detection by the ICPMS. We chose 40 min, which lies between the retention times of ferrichrome and ferrioxamine-E (the siderophores used to calibrate our measurements) as a reference point for our comparison.

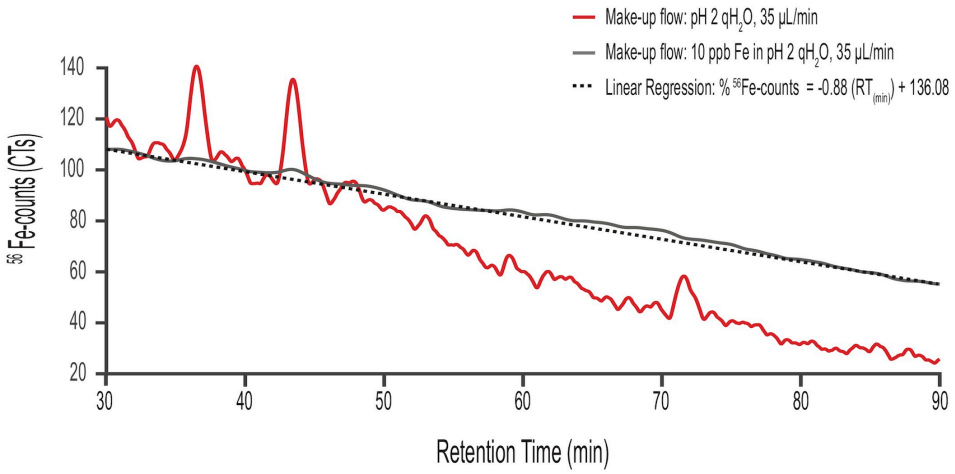

Figure 2.4. LC-ICPMS ^{56}Fe-chromatogram of ferrichrome and ferrioxamine E (200 fmol each), with a make-up flow of 35 µl/min pH 2 qH_2O (red trace). To measure the effect of solvent B on the detection of iron, we performed an identical analysis, but added 10 ppb ^{56}Fe to the make-up flow (grey trace). Iron delivered to the ICPMS in this analysis was dominated by the 10 ppb infusion and was effectively constant over time, making the ^{56}Fe counts a good proxy of Fe sensitivity by ICPMS. A linear regression of ^{56}Fe-counts and time (black solid dashed line) gives a good fit to the data with %Fe = -0.88(retention time (min)) + 136.08% with r^2 = 0.99. For the comparison here, each ^{56}Fe-chromatogram, was normalized to the ^{56}Fe counts at 40 min, the average retention time of the two standards.

The results are shown in Figure 2.4. Even with constant delivery of ^{56}Fe to the ICPMS, the normalized baseline counts (%) for ^{56}Fe drop from 100% to 55% between 40-80 min. We attribute all of this decrease (45%) to the impact of solvent composition (%water to %methanol) on the ICPMS sensitivity for ^{56}Fe. In comparison, when the ferrichrome and ferrioxamine mixture was analyzed without iron added to the make-up flow, the baseline between 40-80 min drops from 100% to 25%. Of the 75% drop in signal, most of the decrease in signal (45%) was attributed to the direct solvent effect, while a lesser amount (30%) was attributed to changes in ^{56}Fe contamination delivered to the ICPMS from the LC hardware and solvents. When 10 ppb Fe is delivered by the make-up flow, a linear regression of ICPMS counts with retention time yields a good fit for the 20-100 min time window (Fig. 2.4), allowing accurate correction for direct solvent

effects on the ICPMS for most every peak in a typical sample chromatogram. Likewise, we can correct for solvent and LC hardware contamination by baseline subtraction of a sample blank. We note that ^{56}Fe contamination by solvents and LC hardware will change with analytical conditions; using solvents direct from the supplier (without distillation in a PTFE still as was used here) may increase contamination while using PEEK lined LC column jackets may decrease it. Finally, we noted that sample matrix effects, the effects of co-eluting organic compounds in the sample, often affect the ionization efficiency of iron (and presumably other elements). These effects are not corrected by baseline subtraction or adjusting the ICPMS response factor for solvent B content. To correct for matrix and solvent effects, we added ^{115}Indium to the make-up flow with the intention of using this rare isotope as an internal calibrant for changes in ICPMS sensitivity in each sample. While the approach offered a good approximation of solvent and effects, we found small differences in the response of ICPMS sensitivity for ^{56}Fe that did not match those measured by ^{115}In, and we set aside any further investigation of this approach. Incorporation of a ^{57}Fe in place of ^{115}In could be used to correct the ICPMS response to iron, but internal calibration standards may have to be element specific.

2.3.2 Mass search algorithm I: Compound Mass Assignment-Time (CMA-T)

Iron-ligand complexes detected by LC-ICPMS are identified or characterized by analyzing the sample a second time with ESIMS detection. To assign masses to Fe ligand complexes, Boiteau and colleagues (Boiteau et al 2016; 2019) applied a mass search algorithm that queries the ESIMS dataset for co-eluting isotopologues for iron, copper and nickel. For iron, the algorithm searched for ^{56}Fe- and ^{54}Fe-containing ion pairs with a mass difference of 1.995 ± 0.002 D and abundance ratio of 15.7 ± 4.7. The approach implicitly assumed that the iron isotopic composition is crustal (15.7). This was a good assumption for some laboratory cultures of siderophore producing microbes (Boiteau and Repeta 2016) and for seawater (Boiteau et al 2016, Bundy et al 2018). However, for some cultures of marine cyanobacteria and for some environmental samples we found a substantial deviation in R from the crustal ^{56}Fe:^{54}Fe ratio, possibly

due to isotopic fractionation during complexation or uptake. In these cases, the algorithm returns false negative results and fails to find masses for Fe-Ls from ESIMS data that are clearly visible in the ICPMS data. Of greater importance, many nutrient metabolites of interest incorporate elements such as cobalt, manganese, iodine, or phosphorus that do not have abundant stable isotope pairs and therefore are not amenable to discovery through our original algorithm.

To address this, we developed two new simple algorithms for feature detection. A feature is a two-dimensional signal (intensity vs. retention time) of a specific m/z that includes one or multiple peaks. Features can be caused by either organic compounds or instrument noise. These two algorithms are collectively named compound mass assignment (CMA) based on time (CMA-T) or carbon (CMA-C) and can be used singularly or in combination.

Annotated code for CMAs (written in Matlab) are available through github (https://github.com/JingxuanJayLi/RepetaLab). To demonstrate the CMA-T algorithm, we used it to assign peaks in the ICPMS Fe-chromatogram of siderophores extracted from spent media from a laboratory culture of *V. cyclitrophicus* strain 1F-53. We selected the starred peak in the LC-ICPMS chromatogram shown in Figure 2.5 as our "unknown" target. We then defined a time window (T_w) centered at the peak's retention time (T_R; here 5063 sec) as $T_w = [(T_R - NT_{PWHH}), (T_R + NT_{PWHH},)]$, where T_{PWHH} represents the peak width in time at half height (code line 62-64). Both T_R and T_{PWHH} were determined from the LC-ICPMS chromatogram. The positive integer N specifies the overall size of the time window used, and is set by the analyst. The value of T_w is adjustable with peak width (T_{PWHH}), which may change with retention time, and with N, which is set depending on the complexity of the chromatogram. Here T_{PWHH} = 30 sec, and we set N = 3, generating a T_w of 180 sec [4973 sec, 5153 sec]. In practice we found that with the gradient used for our siderophore analyses, setting T_{PWHH} = 15-30 sec, N = 3-6 and therefore T_w = 90-360 sec as constants works for most searches.

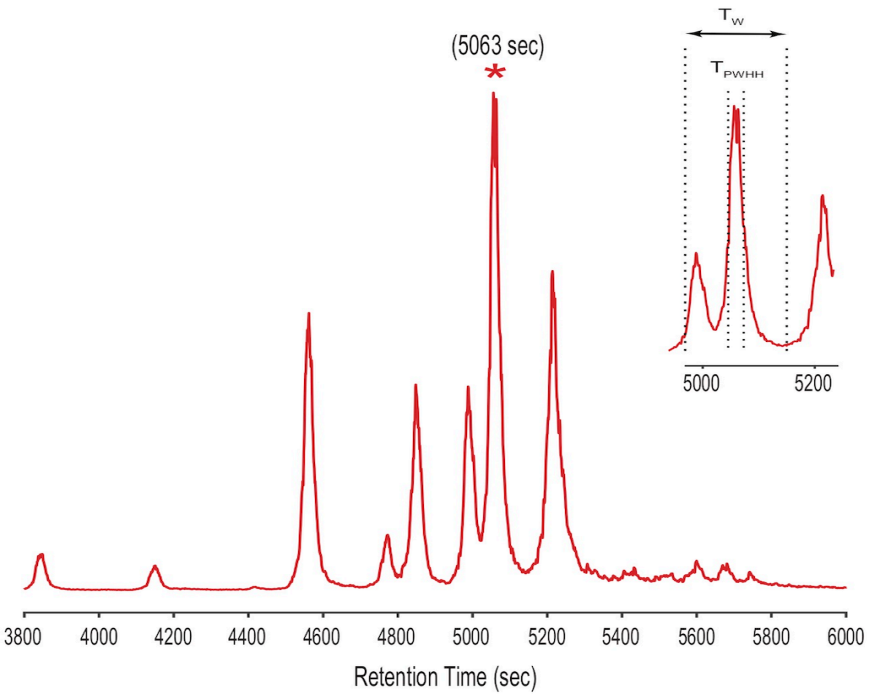

Figure 2.5. LC-ICPMS Fe-chromatogram of the SPE organic extract of *V. cyclitrophicus* strain 1F-53 culture media after addition of iron. The starred peak was selected as our unknown target metabolite to illustrate the application of CMAs. The insert shows the definition of the time window (T_w) in the CMAs, as determined by the retention time (T_R = 5063s) and the peak width at half height (T_{PWHH}).

The sample is analyzed again on LC-ESIMS, the dataset is aligned using the retention time of an internal standard (here Ga-desferrioxamine E, which can be obtained by monitoring m/z of 667.26 on ESIMS and ^{69}Ga on ICPMS, code line 31). Next, the LC-ESIMS mass intensities between 500-1000 D within this T_w were binned by 0.01 D increments, which is well below the mass resolution of the spectrometer (m/Δm = 450,000 at 200 m/z) for this mass range (code line 72). This mass range encompasses most known siderophores, but can be customized to search for any mass window. It is noteworthy that finer binning size could be used, which would provide greater mass accuracy, but also an increase in processing time.

Binning generated thousands of extracted ion chromatograms (EIC). Each EIC was assigned as either a target ion or as noise (code line 72-117). To distinguish the two we define a function as the square of the intensity (I^2) for each ion in the ESIMS data, and integrate the function over time. For compounds that elute from the LC column as Gaussian-shaped peaks, the integral of I^2 over time increases rapidly, ascending from 5% to 95% of its integral total in < $0.2T_w$. In contrast, for ions that appear as noise, the integral of I^2 has as a slow and stepwise increase, rising from 5% to 95% in >> $0.2T_w$. Therefore, we can use $0.2T_w$ as the threshold to distinguish EICs of target ions from noise (Fig. 2.6)

$$Target\ Ion: \quad T95 - T5 \leq 0.2\,Tw;$$

$$Noise: \quad T95 - T5 > 0.2\,Tw;$$

$$where \int_{T0}^{T5} I^2 dt = 0.05 \int_{T0}^{Tf} I^2 dt\,; \int_{T0}^{T95} I^2 dt = 0.95 \int_{T0}^{Tf} I^2 dt\,;$$

$$T0 = 4973\ sec,; Tf = 5153\ sec;\ Tw = Tf - T0 = 180\ sec$$

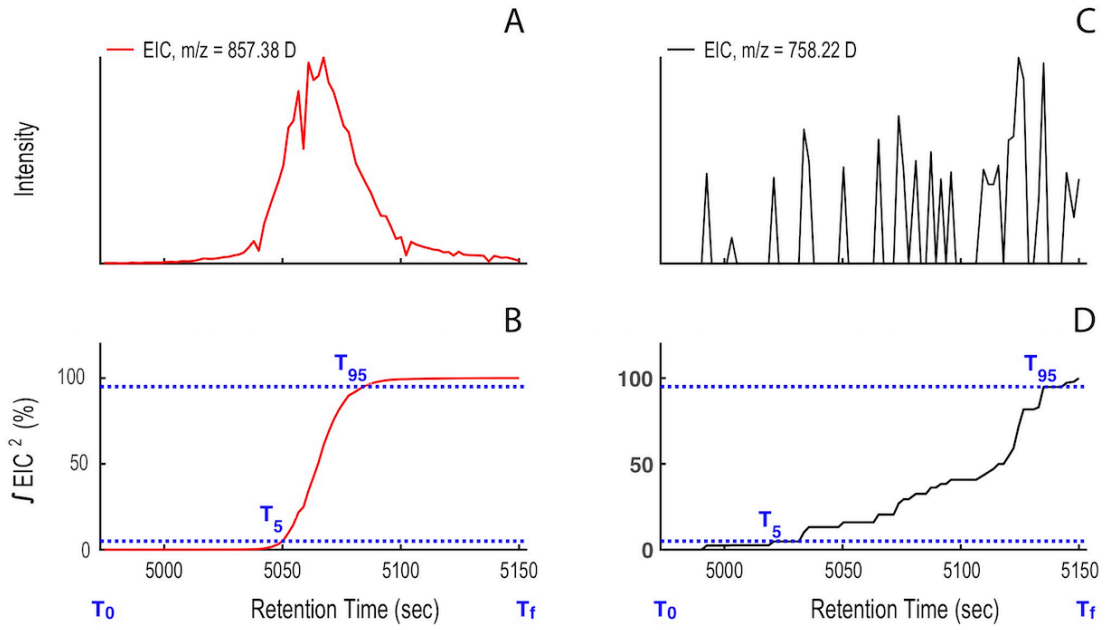

Figure 2.6. Illustration of the compound mass assignment-time (CMA-T) algorithm. A) The ion at 857.38 D targeted by CMA-T has the rise and fall in intensity with time expected for a well-shaped peak eluting from the LC. B) The integral of the square of the 857.38 D ion intensity (I^2) over time ΔT (T_{95}-T_5) rises from 0.05% (T_5) to 0.95% (T_{95}) of its total value in $\Delta T \leqslant 0.2T_w$. C) Ions that arise from noise show a more gradual rise and fall in intensity over time, and D) for the same ΔT, the integral of I^2 between T_5 to $T_{95} \geqslant 0.2\ T_w$. The comparison between ΔT (T_{95}-T_5) and 20% T_w is used as a filter to differentiate target ions from noise.

After applying CMA-T, two additional filters are applied as a quality control step to remove false positive peaks. First, for each ion, if 50% or more of the ESIMS scans within T_w show zero counts, it is removed from the target list (code line 88-109). This eliminates any well-shaped peaks that are poorly of partially captured by the defined time window (Fig. 2.5). In this example, we collected 80 scans across T_w, so a target ion must include at least 40 non-zero data points. Second, if the peak center (maximum in intensity) of its EIC is > T_{PWHH} from T_R, it is removed from the target list (code line 104-106). This eliminates peaks that are significantly shifted in retention time between LC-ICPMS and LC-ESIMS analysis, which is not expected after spectra alignment. When we applied CMA-T with T_R = 5063 sec, T_{PWHM} = 30 sec, T_w = 180 sec and a threshold

value of ≥ 40 data points to the ESIMS data from the *Vibrio* culture media extract, the algorithm identified 12 EICs as target ions that elute within this time window (Fig. 2.7).

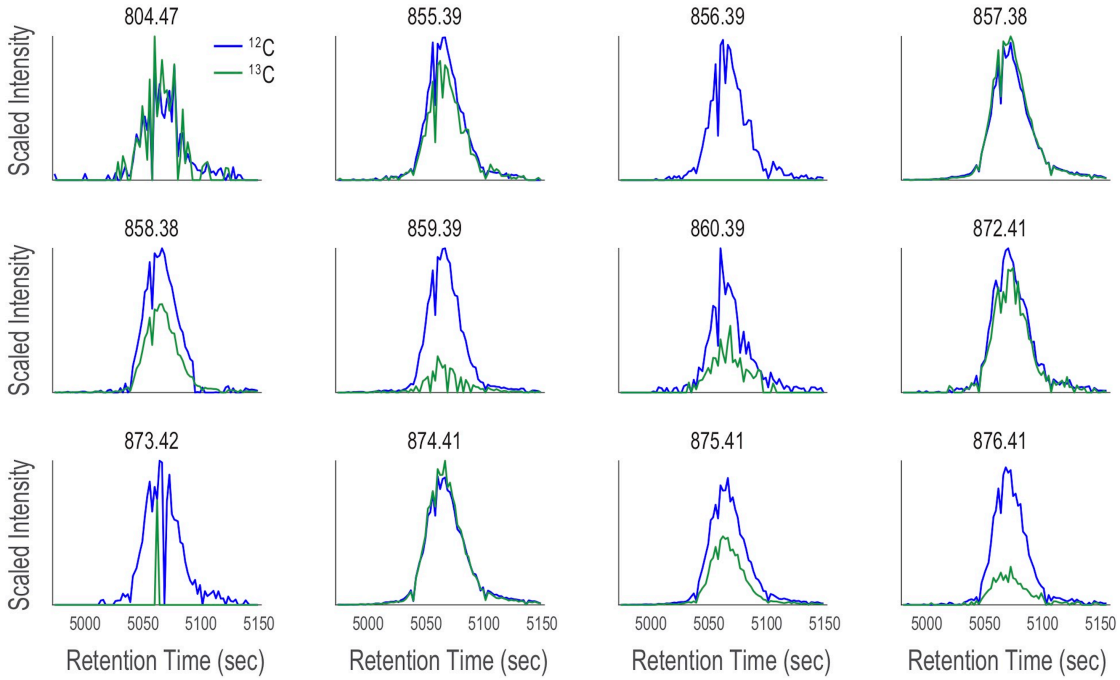

Figure 2.7. Twelve target ions discovered by CMA-T that elute within T_w = 4973-5153 sec in the SPE organic extract of *V. cyclitrophicus* strain 1F-53 culture media after addition of iron. The EIC of each target ion (M; blue traces) is overlaid with the EIC of (M+1.003; green traces), after scaling the latter by the relative abundance of ^{13}C calculated according to Fig. 2.8, under the assumption of a singly charged ion and 50% carbon content.

2.3.3 Mass search algorithm II: Compound Mass Assignment-Carbon (CMA-C)

Spurious noise or co-eluting peaks can yield false positive target ions after the CMA-T algorithm filter. These can be removed by processing the ESIMS data with CMA-C. Originally, CMA-C was designed to find all the organic compounds with a defined fraction of carbon within any given time window, by searching for pairs of isotopologues containing exclusively ^{12}C (M peak) and one ^{13}C (M+1 peak) atoms. This approach is similar to our original mass search algorithm that searches for ^{56}Fe-^{54}Fe isotopologues (Fig. 2.1). In that algorithm, a pair of EICs are attributed to an Fe-containing compound

if their m/z differ by 1.995 D, and their intensities differ by 15.7. In CMA-C, a pair of EICs is attributed to a C-containing compound if their m/z differ by 1.003 D, and their intensities differ by a ratio R. The ratio R in CMA-C is a dynamic parameter, determined by the number of carbon atoms in the compound, which can be estimated by the m/z of the EIC, and the fractional weight of carbon in the compound (code line 43-65). The fractional weight of C in siderophores extracted from a database of 366 known siderophores (Baars et al 2014), is 48% ± 5%, so that for a siderophore of mass m, R = [(0.5)(0.011)(m/z)/(12)], where 0.5, m/z, 0.011 and 12 represent the average carbon content of known siderophores, mass to charge ratio for the target ion, relative abundance of ^{13}C (slope in Fig. 2.8), and atomic mass of ^{12}C respectively.

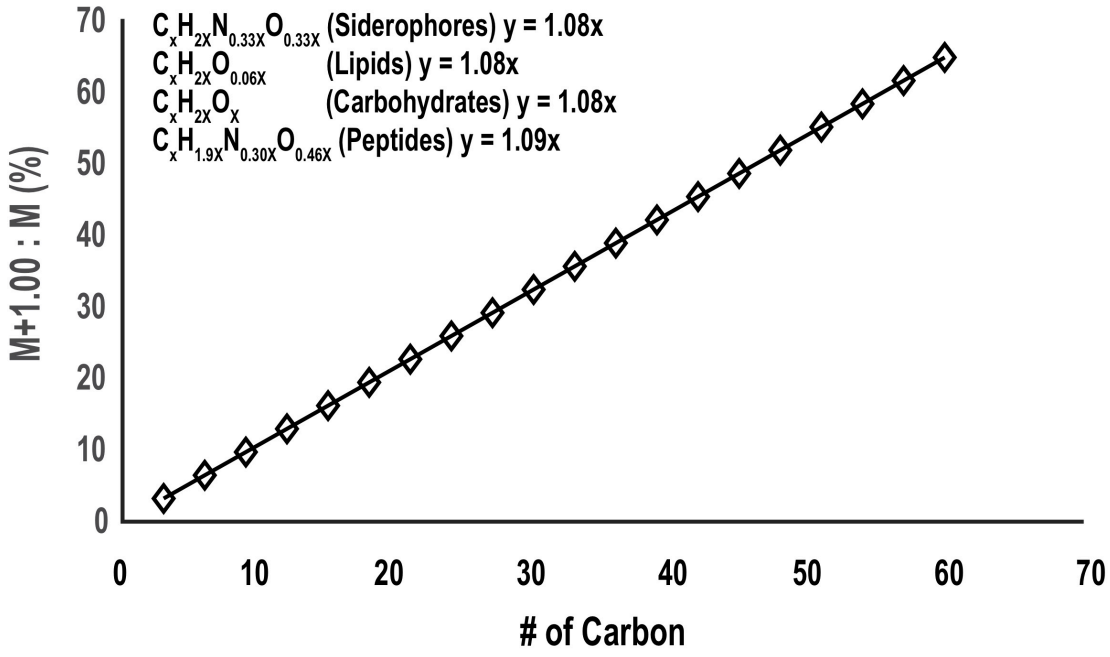

Figure 2.8. The relative abundance of the ^{13}C:^{12}C isotopologue molecular ions (M+1.00/M) as a function of carbon number for siderophores, lipids, carbohydrates, and proteins. Although these classes of metabolites are different in the ratio of H, N, and O they incorporate relative to C, the change in carbon isotopic ratio with carbon number between them is very small and for the mass search algorithms can be approximated by the slope of the plot (1.08).

Although CMA-C can be used independently to generate a list of targeted ions, we here use this algorithm to query the targeted ions by CMA-T. For example, the ^{13}C isotopologue for the target ion 857.38 D will have a mass of 858.38 D and an intensity of 39% of the target ion (857.38 D). We overlaid each of the 12 EICs with the plot of EIC+1.003, (the difference in mass between ^{12}C and ^{13}C) and scaled the plot by the relative abundance of ^{13}C calculated as described above. If the target ion is from a singly charged organic compound, the two EIC should overlay each other closely. Here we assume the ion of interest is singly charged, however other charge states can be assumed as described in Section 2.3.5 for cobalt-containing metabolites. If the target ion has a carbon content significantly different from 50%, is multiply charged, or if the target ion itself is the ^{13}C isotopologue of a peak captured by CMA-T, the two plots will track each other in time, but will be offset in scaled intensity. Finally, if the two plots do not track each other in time or scaled intensity, the target ion is regarded as a false positive.

We used the CMA-C algorithm to query the 12 target ions assigned by CMA-T to the Fe-chromatogram peak at 5063 sec. Five of the 12 target ions passed the CMA-C filter: 804.47 D, 855.39 D, 857.38 D, 872.41 D, and 874.41 D. From the differences in mass between pairs of ions, we can easily assign four of these target ions as the ^{54}Fe:^{56}Fe isotopologue pairs of the ion with m/z = 855.39 and 857.38 D (^{54}Fe m/z_{obs} = 855.386, m/z_{thero} = 855.388, ^{56}Fe m/z_{obs} = 857.382, m/z_{thero} = 857.383) and its ammonium adduct at m/z = 872.41 and 874.41 D (^{54}Fe m/z_{obs} = 872.412, m/z_{thero} = 872.415, ^{56}Fe m/z_{obs} = 874.408, m/z_{thero} = 874.410). A search of our database of known siderophores identified the compound as Amphibactin-T. The ion at 804.47 D has a Δm = 52.912 D less than the Amphibactin-T ion m/z_{obs} = 804.470, m/z_{thero} = 804.472; and arises from nonmetallated (apo-; -Fe+2H) form of the siderophore.

For the seven ions that are rejected by CMA-C, four (856.39 D, 858.38 D, 873. 42 D and 875.41 D) represent the ^{13}C isotopologue of Amphibactin-T and its ammonium adduct. Similarly, the target ions 859.39 D and 876.41 D may contain either additional ^{13}C atoms, or an ^{18}O atom on top of 857. 38 D and 874.41 D. Furthermore, 860.39 D

may contain both a ^{13}C atom and an ^{18}O atom on top of 857. 38 D. These isotopically rare compounds are low in relative abundance, but could be detected when the overall concentration is high, as demonstrated in this example. In summary, the CMA-C returns only the major isotopologue (^{12}C-^{1}H-^{16}O-^{14}N-, etc.) of a compound. The combination of CMA-T and CMA-C was able to correctly identify the molecular ions of Amphibactin-T from the ICPMS and ESIMS data without using isotopes of iron in the search algorithms.

2.3.4 Application I: Targeting monoisotopic-element metabolites in environmental samples

In the sections above, we treated Fe as a 'monoisotopic' nutrient, and successfully assigned masses to siderophores in laboratory culture samples. Here, we use the algorithms to assign the mass of a siderophore complexed to aluminum in an environmental sample. Aluminum is monoisotopic, and in the +3 oxidation state aluminum forms stable complexes with some siderophores. Although siderophore-Al complexes have lower binding constants than siderophores complexed to iron, Al is ~10x more abundant than iron in surface seawater, therefore, many environmental samples that contain siderophores also contain siderophores complexed to aluminum. For example, the ^{27}Al-chromatogram for the North Pacific seawater sample shown in Figure 2.1 looks similar to that of ^{56}Fe. Specifically, it displays four major peaks eluting between 70-82 minutes. We targeted the ^{27}Al peak at 80.6 min (4837 s) for mass assignment.

When we applied CMA-T to the ESIMS data from the North Pacific Seawater extract with following parameterization: T_R = 4837 sec, T_{PWHM} = 30 sec, N=5, T_w = 300 sec, mass window = 500-1100 D, data points in the peak ≥ 20, and T_{95}-T_5 ≤ 0.1 T_w, the algorithm identified 18 EICs as target ions that elute within this time window. We then used the CMA-C algorithm to query these target ions, assuming a carbon fractional weight of 30-70%, which was selected based on the carbon content of siderophores (48% ± 5%).

Two of the 18 EICs identified by CMA-T passed the CMA-C filter: 984.482 D and 1013.434 D. From the differences in their mass (28.952 D), and the presence of a co-eluting peak in the ^{27}Al and ^{56}Fe-chromatograms, we can easily assign the two ions as an ^{27}Al-siderophore and an ^{56}Fe-siderophore. A search of our database of known siderophores identified the two compounds as Al-marinobactin-C (m/z_{thero} = 984.483 D), and Fe-marinobactin-C (m/z_{thero} = 1013.437 D).

2.3.5 Application II: Targeting monoisotopic-element nutrient metabolites using multi-dimensional chromatography with mass search algorithms

For nutrient metabolites that have monoisotopic elements (with respect to stable isotopes), the application of CMA-T and CMA-C filters alone may be insufficient to identify the molecular ion of a compound targeted by ICPMS. This would happen when multiple ions, which could not be easily related to each other, or to a known metabolite, are returned by CMAs. To make these assignments we took advantage of changes in compound selectivity under different chromatographic conditions. Changes in either the mobile (solvent) or stationary (column packing material) phases will move compounds into or out of a particular time (T_w) searched by the algorithms. We expect that compounds co-eluting with a compound targeted by LC-ICPMS, and therefore the suite of ions targeted by CMA-T and CMA-C, will change with chromatographic conditions. To demonstrate this approach, we created a "*Prochlorococcus* sample" by adding cobalamin (vitamin B_{12}) to the SPE extract of spent media from a laboratory culture of the marine cyanobacterium *Prochlorococcus* MIT9215. We note that the media used for this culture was prepared by amending natural seawater with nutrients, so that the "*Prochlorococcus* sample" contains the natural suite of organic matter typically extracted from Sargasso seawater along with organic matter produced by *Prochlorococcus* during growth. Our goal was to determine if the intersection of target ions generated by CMA-T applied to a sample separated using two different chromatographic conditions would identify the correct molecular ion (here 1356.58 D) for a metabolite incorporating cobalt, a monoisotopic element.

The *Prochlorococcus* sample was first analyzed by LC-ICPMS and LC-ESIMS fitted with a C18 column (see Methods). The LC-ICPMS trace shows a cobalt-containing compound at 1832 sec (Fig. 2.9A). ESIMS data were collected between 300-1800 D and binned in 0.01 D increments. CMA-T was applied to the ESIMS data with T_R = 1832 sec, T_{PWHH} = 15 sec and N = 3, identifying 10 target masses (Fig. 2.10; Table 2.1) as potential molecular ions for cobalamin. We then repeated the analyses but replaced the C18 columns with an amide column, which we expected to have a different selectivity of compounds eluting within T_w. The LC-ICPMS Co-chromatogram again shows a single peak for Co, but at a retention time of 1461 sec (Fig. 2.9B). After generating the complement LC-ESIMS data with the amide column, we applied CMA-T with T_R = 1461 sec and T_{PWHH} = 15 sec and N = 3, and found 19 target ions that elute within T_w (Table 2.1).

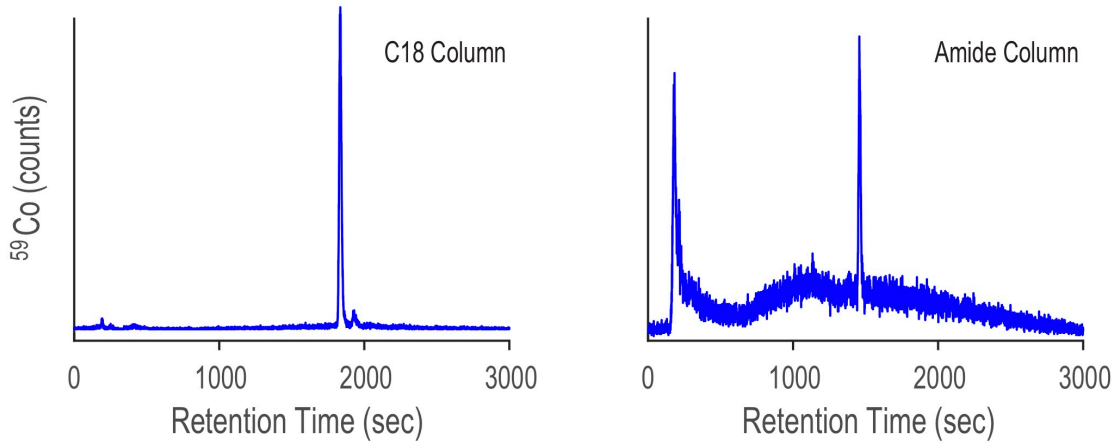

Figure 2.9. LC-ICPMS Co-chromatograms of the SPE organic extract of *Prochlorococcus* MIT9215 culture media, separated with a C18 column (left) and an amide column (right). The large peak in both chromatograms is due to the elution of the cobalamin spike. The difference in cobalamin retention time between the two separations is due to the change in selectivity of each column.

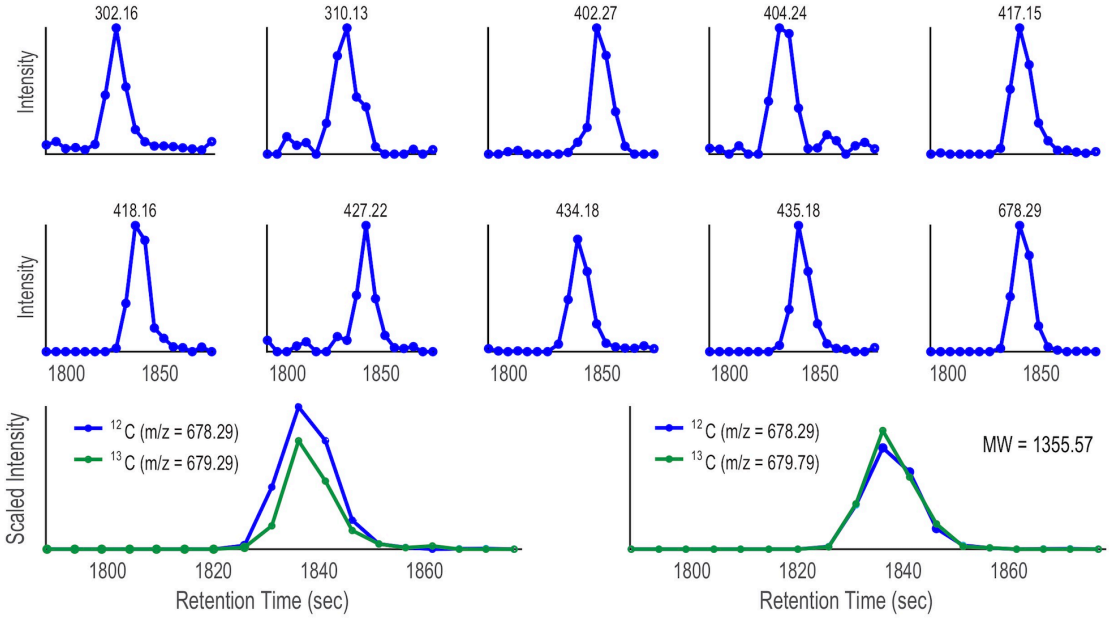

Figure 2.10. Plots of mass vs retention time for ten target ions discovered by CMA-T that elute within T_w = 3357-3537 sec in the SPE organic extract of *Prochlorococcus* MIT9215 culture media. When the target ion 678.29 D is assumed to be singly charged, CMA-C scales the ion at 679.29 D (green trace; 678.29 D+1.003 D, assumed ^{13}C isotopologue) in each scan by a factor of 3.2 which is overlaid with the EIC of 678.29 D (^{12}C isotopologue, blue trace) in the lower left of the Figure. When the ion 678.29 D is assumed to be doubly charged, CMA-C scales the ion at 679.79 D (green trace, 678.29 D + (1.003 D)/2 = 678.79 D) in each scan by a factor of 1.6, and overlays the result with the EIC of 678.29 D (lower right). The better fit of 679.79 plot suggests the ion is doubly charged and that the molecular weight of the ^{12}C isotopologue is 1354.57 D.

Table 2.1. Targeted ions (D) found by CMA-T from LC-ESIMS dataset with C18 column and Amide column, with overlapping ion bold in font.

C18	302.16	310.13	402.27	404.24	417.15	418.16	427.22
	434.18	435.18	**678.29***				
Amide	312.19	358.24	371.23	386.24	415.25	416.26	432.18
	432.19	432.20	432.21	432.28	433.28	434.28	440.31
	442.22	475.29	605.30	622.36	**678.29***		

For C18, (m/z_{obs} = 678.292, m/z_{theor} = 678.292);

For Amide, (m/z_{obs} = 678.292, m/z_{theor} = 678.292);

Comparing the CMA-T outputs from the two separations, we found only one common target ion at 678.29 D. We tentatively assigned this mass to the Co-containing compound. Next, we used CMA-C to determine the charge state of the ion. As shown in Fig. 2.10 when the ion 678.29 D is plotted using CMA-C we found the expected carbon isotopic pattern only under the assumption of a +2 charge. Therefore, we conclude that the Co-compound has a molecular weight of 1354.57, which is the mass of the ^{12}C isotopologue of cobalamin. CMA-T and CMA-C did not find the singly charged molecular ion for cobalamin because it was not detected by ESIMS; the compound was only ionized as the doubly charged species. In summary, CMA-T and CMA-C, when combined with multi-dimensional chromatography was able to assign the correct molecular ion to a compound (in this case cobalamin) incorporating a monoisotopic element even in a complex mixture of organic matter.

2.3.6 Application III: of Characterization of iodine metabolites from *Prochlorococcus* MIT 9215

Marine phytoplankton reduce iodate, the most stable species of iodine in seawater, to iodide (Wong et al 2002). They also produce a broad suite of organic iodine metabolites, for processes including thyroid signaling (Javier et al 2018), that can be detected by LC-ICPMS. Like cobalt, iodine is monoisotopic with respect to stable

isotopes, making organic iodine metabolites particularly challenging to isolate and characterize.

The spent media we used to assign the mass of cobalamin in the previous discussion from cultured *Prochlorococcus* strain MIT 9215 also had a complex suite of iodine metabolites detected as well resolved peaks by LC-ICPMS. We are unable to conclude the axenicity of the culture, or attribute the source of the ligands to *Prochlorococcus*. However, we would use the data for the demonstration of the algorithms.

The complexity and distribution of iodine metabolites illustrated by the ^{127}I chromatogram shown in Figure 2.11 are characteristic of virtually all seawater and culture media samples we have analyzed to date. Organic iodine metabolites are abundant, diverse, and common in marine samples. The C18- and amide- columns used for our cobalamin analyses show different selectivity for iodine metabolites, as illustrated by the change in iodine distribution across each chromatogram. To investigate iodine metabolites further, we assumed the largest peak in each ICPMS chromatogram was the same metabolite, and targeted this compound for characterization by CMA-T and CMA-C. For the C18 separation, we targeted the ^{127}I peak with a retention time of 3447 sec, collected ESIMS data between 200-1800 D and binned this data in 0.01 D increments. CMA-T was applied to the ESIMS data with T_{PWHH} = 15 sec and N = 6, identifying 29 target masses as potential molecular ions for the iodine metabolite. For the amide column separation, we collected ESIMS data in the same manner, targeted the ^{127}I peak at 3630 sec and applied CMA-T with T_{PWHH} = 15 sec and N = 6, to find 16 target ions that elute within T_w. Comparing the CMA-T outputs from the two separations, we found only two common target ions at 205.09 D and 279.16 D. These ions were queried by CMA-C and the target ion at 205.09 D was rejected as having insufficient data points in the EIC+1.003 output, leaving the target ion at 279.16 D as the most likely candidate for this metabolite (Fig. 2.11). CMA-C also confirmed this ion was singly charged.

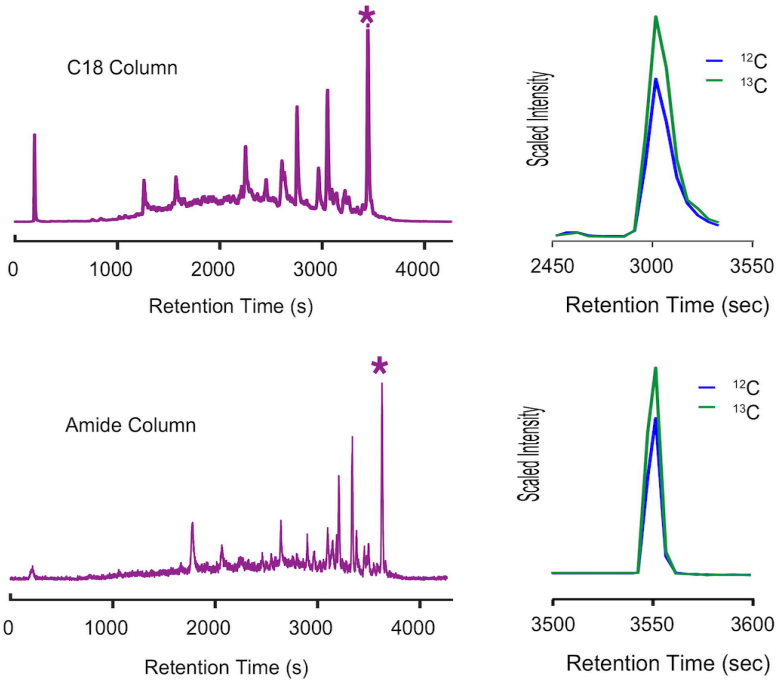

Figure 2.11. LC-ICPMS ^{127}I-chromatogram of organic iodine metabolites in spent media from a culture of *Prochlorococcus* MIT9215 separated on a C18 column (top, let) and an amide column (bottom, left). The complex mixture of organic iodine metabolites shown in the chromatograms is typical of culture media and seawater samples. When the ESIMS data from each analysis are processed with CMA-T and CMA-C we only find one target ion at 279.16 D (top and bottom, right) that is common to both datasets.

2.4 Conclusion

The low abundance of metabolites, and the presence of a complex organic matrix in environmental samples, make the identification and quantitative analyses of metabolites challenging. The element-targeted approach described here offers advantages for characterizing metabolites that incorporate elements other than C, N, H and O. LC-ICPMS allows the analyst to quickly find and quantify these metabolites, while LC-ESIMS allows for their identification or characterization. The approach also assists in defining the elemental composition of a metabolite, which is helpful in applying high resolution mass spectral data to determine elemental formulas. This is particularly useful in targeting metabolites that are involved in biogeochemical cycles of elements

such as metals, halogens, and nutrients that have not been previously described due to their low abundance within complex organic samples. In seawater we have detected metabolites that incorporate manganese, copper, nickel, zinc, iodine, and many other elements that, to the best of our knowledge, have not been previously described. Sensitivity is important for enabling the detection of these trace species, and the approach presented here provides a five-fold increase compared to our previous method.

For metabolites that incorporate trace metals, mass search algorithms utilize the mass difference and relative abundance ratio of isotopologues to assign molecular ions (Baars et al 2014; Boiteau et al 2015). The CMA-T and CMA-C algorithms described here approach the assignment of molecular ions to ICPMS data somewhat differently. CMA-T only requires that the retention time and peak width of a targeted metabolite are known, and that the peaks are well-shaped. However, metabolites with isomers that have similar retention times might show double peaks on the EIC, which could be classified as noise by CMA-T, resulting in false negatives. CMA-C requires an estimate of the fractional mass of carbon in the class of metabolites of interest, and the algorithm works best for metabolites with > C_{10}, below which the detection of the ^{13}C-isotopologue may be compromised, and the carbon content is less predictable. Both CMAs do not require the presence of isotopes (other than for carbon) and can be used with ICPMS, or optical (absorption, fluorescence) detection. For elements with stable isotopes, the combination of an isotope-based mass search algorithm with CMA-T and CMA-C is usually successful in assigning molecular ions to ICPMS data. However, in some cases, particularly for metabolites incorporating monoisotopic elements, the combination of CMA-T and CMA-C alone were often insufficient to assign unique molecular ions. In these instances, we found the most convenient way to make assignments from the suite of target ions identified by the algorithms was to change the separation conditions that determine the masses of co-eluting compounds within T_w until a unique solution is obtained.

Acknowledgements

The authors would like to thank the Captain, crew, and scientific party on the *RV Roger Revelle* cruise 1814 GEOTRACES GP-15 for sample collection, and Mr. Luis Valentin-Alvarado for providing us with the *Prochlorococcus* culture. This work was generously supported by the National Science Foundation grant OCE-1829761 to RMB and OCE-1356747 and -1736280 to DJR. DJR also received generous support from the Simons Foundation Life Sciences Project Award 49476. This paper is a contribution from the Simons Collaboration on Ocean Processes and Ecology (SCOPE).

2.5 References

Petras, D., Koester, I., Da Silva, R., Stephens, B. M., Haas, A. F., Nelson, C. E., ... & Dorrestein, P. C. (2017). High-resolution liquid chromatography tandem mass spectrometry enables large scale molecular characterization of dissolved organic matter. Frontiers in Marine Science, 4, 405.

Patriarca, C., Bergquist, J., Sjöberg, P. J., Tranvik, L., & Hawkes, J. A. (2018). Online HPLC-ESI-HRMS method for the analysis and comparison of different dissolved organic matter samples. Environmental science & technology, 52(4), 2091-2099.

Soule, M. C. K., Longnecker, K., Johnson, W. M., & Kujawinski, E. B. (2015). Environmental metabolomics: Analytical strategies. Marine Chemistry, 177, 374-387.

Cajka, T., & Fiehn, O. (2016). Toward merging untargeted and targeted methods in mass spectrometry-based metabolomics and lipidomics. *Analytical chemistry*, *88*(1), 524-545.

Boiteau, R. M., & Repeta, D. J. (2015). An extended siderophore suite from Synechococcus sp. PCC 7002 revealed by LC-ICPMS-ESIMS. *Metallomics*, *7*(5), 877-884.

Boiteau, R. M., Mende, D. R., Hawco, N. J., McIlvin, M. R., Fitzsimmons, J. N., Saito, M. A., ... & Repeta, D. J. (2016). Siderophore-based microbial adaptations to iron scarcity across the eastern Pacific Ocean. *Proceedings of the National Academy of Sciences*, *113*(50), 14237-14242.

Bundy, R. M., Boiteau, R. M., McLean, C., Turk-Kubo, K. A., McIlvin, M. R., Saito, M. A., ... & Repeta, D. J. (2018). Distinct siderophores contribute to iron cycling in the mesopelagic at station ALOHA. *Frontiers in Marine Science*, *5*, 61.

Boiteau, R. M., Till, C. P., Coale, T. H., Fitzsimmons, J. N., Bruland, K. W., & Repeta, D. J. (2019). Patterns of iron and siderophore distributions across the California current system. *Limnology and Oceanography*, *64*(1), 376-389.

Gledhill, M., & Buck, K. N. (2012). The organic complexation of iron in the marine environment: a review. *Frontiers in microbiology*, *3*, 69.

Buckley, P. J., & van den Berg, C. M. (1986). Copper complexation profiles in the Atlantic Ocean: A comparative study using electrochemical and ion exchange techniques. *Marine Chemistry*, *19*(3), 281-296.

Coale, K. H., & Bruland, K. W. (1988). Copper complexation in the Northeast Pacific. *Limnology and Oceanography*, *33*(5), 1084-1101.

Coale, K. H., & Bruland, K. W. (1990). Spatial and temporal variability in copper complexation in the North Pacific. *Deep Sea Research Part A. Oceanographic Research Papers*, *37*(2), 317-336.

Bruland, K. W. (1989). Complexation of zinc by natural organic ligands in the central North Pacific. *Limnology and Oceanography*, *34*(2), 269-285.

Saito, M. A., & Moffett, J. W. (2001). Complexation of cobalt by natural organic ligands in the Sargasso Sea as determined by a new high-sensitivity electrochemical cobalt speciation method suitable for open ocean work. *Marine chemistry*, *75*(1-2), 49-68.

Achterberg, E. P., & Van Den Berg, C. M. (1997). Chemical speciation of chromium and nickel in the western Mediterranean. *Deep Sea Research Part II: Topical Studies in Oceanography*, *44*(3-4), 693-720.

Kuma, K., Katsumoto, A., Kawakami, H., Takatori, F., & Matsunaga, K. (1998). Spatial variability of Fe (III) hydroxide solubility in the water column of the northern North Pacific Ocean. *Deep Sea Research Part I: Oceanographic Research Papers*, *45*(1), 91-113.

Millero, F. J. (1998). Solubility of Fe (III) in seawater. *Earth and Planetary Science Letters*, *154*(1-4), 323-329.

Hutchins, D. A., Witter, A. E., Butler, A., & Luther, G. W. (1999). Competition among marine phytoplankton for different chelated iron species. *Nature*, *400*(6747), 858-861.

Wells, M. L., & Trick, C. G. (2004). Controlling iron availability to phytoplankton in iron-replete coastal waters. *Marine chemistry*, *86*(1-2), 1-13.

Hassler, C. S., Schoemann, V., Nichols, C. M., Butler, E. C., & Boyd, P. W. (2011). Saccharides enhance iron bioavailability to Southern Ocean phytoplankton. *Proceedings of the National Academy of Sciences*, *108*(3), 1076-1081.

Aristilde, L., Xu, Y., & Morel, F. M. (2012). Weak organic ligands enhance zinc uptake in marine phytoplankton. *Environmental science & technology*, *46*(10), 5438-5445.

Lis, H., Shaked, Y., Kranzler, C., Keren, N., & Morel, F. M. (2015). Iron bioavailability to phytoplankton: an empirical approach. *The ISME journal*, *9*(4), 1003-1013.

Boyd, P. W., Jickells, T., Law, C. S., Blain, S., Boyle, E. A., Buesseler, K. O., ... & Harvey, M. (2007). Mesoscale iron enrichment experiments 1993-2005: synthesis and future directions. *science*, *315*(5812), 612-617.

Moore, C. M., Mills, M. M., Arrigo, K. R., Berman-Frank, I., Bopp, L., Boyd, P. W., ... & Jickells, T. D. (2013). Processes and patterns of oceanic nutrient limitation. *Nature geoscience*, *6*(9), 701-710.

Reid, R. T., Livet, D. H., Faulkner, D. J., & Butler, A. (1993). A siderophore from a marine bacterium with an exceptional ferric ion affinity constant. *Nature*, *366*(6454), 455-458.

Martinez, J. S., Zhang, G. P., Holt, P. D., Jung, H. T., Carrano, C. J., Haygood, M. G., & Butler, A. (2000). Self-assembling amphiphilic siderophores from marine bacteria. *Science*, *287*(5456), 1245-1247.

Martinez, J. S., Haygood, M. G., & Butler, A. (2001). Identification of a natural desferrioxamine siderophore produced by a marine bacterium. *Limnology and Oceanography*, *46*(2), 420-424.

Hopkinson, B. M., & Barbeau, K. A. (2012). Iron transporters in marine prokaryotic genomes and metagenomes. *Environmental microbiology*, *14*(1), 114-128.

Tang, K., Jiao, N., Liu, K., Zhang, Y., & Li, S. (2012). Distribution and functions of TonB-dependent transporters in marine bacteria and environments: implications for dissolved organic matter utilization. *PLoS One*, *7*(7), e41204.

Hider, R. C., & Kong, X. (2010). Chemistry and biology of siderophores. *Natural product reports*, *27*(5), 637-657.

Baars, O., Morel, F. M., & Perlman, D. H. (2014). ChelomEx: Isotope-assisted discovery of metal chelates in complex media using high-resolution LC-MS. *Analytical chemistry*, *86*(22), 11298-11305.

Boiteau, R. M., Fitzsimmons, J. N., Repeta, D. J., & Boyle, E. A. (2013). Detection of iron ligands in seawater and marine cyanobacteria cultures by high-performance liquid chromatography–inductively coupled plasma-mass spectrometry. *Analytical chemistry*, *85*(9), 4357-4362.

Hu, Z., Hu, S., Gao, S., Liu, Y., & Lin, S. (2004). Volatile organic solvent-induced signal enhancements in inductively coupled plasma-mass spectrometry: a case study of methanol and acetone. *Spectrochimica Acta Part B: Atomic Spectroscopy*, *59*(9), 1463-1470.

Wong, G. T., Piumsomboon, A. U., & Dunstan, W. M. (2002). The transformation of iodate to iodide in marine phytoplankton cultures. *Marine Ecology Progress Series*, *237*, 27-39.

Javier, L. H., Benzekri, H., Gut, M., Claros, M. G., Van Bergeijk, S., Canavate, J. P., & Manchado, M. (2018). Characterization of iodine-related molecular processes in the marine microalga Tisochrysis lutea (Haptophyta). Frontiers in Marine Science.

Chapter 3 Siderophore distribution in the Pacific Ocean along the US GEOTRACES GP15 transect

3.1 Introduction

Across large regions of the surface ocean, the essential micronutrient iron (Fe) limits the growth of microbes, including phytoplankton (Martin and Fitzwater, 1988; de Baar et al 1990; Price et al 1994; Boyd et al 2007) and heterotrophic bacteria (Pakulski et al 1996; Kirchman et al 2000; Cochlan 2001; Oliver et al 2004). This is due to the high cellular Fe quota of phytoplankton (60 μmol/mol-C in Fe sufficient medium, Ho et al 2003; 2.5 μmol/mol-C in Fe deficient medium, Sunda and Huntsman 1995) and heterotrophic bacteria (44 μmol/mol-C in Fe sufficient medium, 7.5 μmol/mol-C in Fe deficient medium, Tortell et al 1996), as well as the low dissolved Fe (dFe) concentration in surface seawater (generally < 0.2 nM, Boyd and Ellwood, 2010).

In order to adapt to chronic low Fe conditions, microbes inhabiting Fe limited regions could decrease cellular demand or increase Fe uptake. One example for the latter strategy is the production of siderophores by heterotrophic bacteria and cyanobacteria. Siderophores are small (< 1000 Da) organic ligands that exhibit an extraordinarily high stability constant for Fe(III) (For the thermodynamic equilibrium constant K = [Fe(III)S]/[Fe(III)] [S]. where S is a siderophore, K = 10^{29} for ferrichrome, K = 10^{31} for ferrioxamine B, and K = 10^{52} for enterobactin, Schwarzenbach and Schwarzenbach 1963; Harris et al 1979). After binding to Fe, the Fe-siderophore complex is transported across the cell membrane by TonB dependent transporters (Moeck and Coulton 1998), which show high affinity and high specificity to siderophores. In eukaryotic phytoplankton, siderophore synthesis has not been demonstrated. However, eukaryotic phytoplankton are able to take up Fe bound to exogenous siderophores by cell surface Fe reduction of Fe(III) to Fe(II) (Shaked et al 2005), endocytosis (Kazamia et al 2018), or combination of the two mechanisms (Coale et al 2019).

Mass spectrometry based techniques allow for the characterization and quantification of siderophores in seawater (Mawji et al 2008; Boiteau et al 2013). To date, siderophore samples for LC-MS measurement have only been collected from a few depth profiles and surface transects, generating a dataset of less than 100 samples. According to these data, two major classes of siderophores have been found in seawater, including the polar ferrioxamines, which have a peptidic Fe binding group, and the non polar amphibactins, marinobactins and synechobactins, which have a peptidic Fe binding group linked to a fatty acid chain (Mawij et al 2008; Boiteau et al 2016; Bundy et al 2018; Boiteau et al 2019; Gledhill et al 2022; Park et al 2022). Ferrioxamines seem to be prevalent in surface (0-20 m) waters (Mawij et al 2008; Boiteau et al 2016; Bundy et al 2018). Amphibactins are found in both surface and upper mesopelagic (300-400 m) waters. (Boiteau et al 2016; Bundy et al 2018). Marinobactins and synechobactins have been found in coastal regions, but not in the open ocean (Boiteau et al 2019; Gledhill et al 2022). Because many samples collected in prior studies do not have a paired sample for dFe, the relationship between siderophore and dFe concentrations remains unclear.

No studies have analyzed siderophores in suspended particulate matter. Due to the high polarity of ferrioxamines, these siderophores are expected to be released into the environment after production. The presence of ferrioxamines in seawater samples support this expectation (Mawij et al 2008; Boiteau et al 2016; Bundy et al 2018). In contrast, amphibactins and marinobactins are non-polar metabolites due to the incorporation of a fatty acid chain into their structure. Therefore, these siderophores are expected to be associated with cells (Martinez et al 2000; Martinez et al 2003). Since all measurements made to date are of dissolved siderophores, we might have missed most of the siderophores in seawater, and the contribution of particles to the distribution of siderophores remains unknown.

To determine how nutrient conditions and microbial cycling impact siderophore production, and to assess the likely role of siderophores in Fe acquisition, we participated in the US GEOTRACES Pacific Meridional Transect (PMT) GP15 and collected samples for molecular speciation measurements of Fe (Figure 3.1). The PMT

is a section that extends from 56 °N to 20 °S along 152 °W longitude, which crosses several biogeochemical provinces, including coastal waters along the South Alaskan Shelf, two high nutrient low chlorophyll (HNLC, North Pacific Subarctic Gyre and East Pacific Equatorial upwelling) regions, and two oligotrophic subtropical (North and South Pacific) gyres. Overall, this transect offered an opportunity to directly compare siderophore concentration, production and consumption at sample sites with different nutrient conditions, thereby providing a window into microbial responses to nutrient stress. We expect to find higher concentration of siderophores in the HNLC regions than in the gyres, and higher concentrations at surface than at depth, because these regions are more likely to be Fe limited.

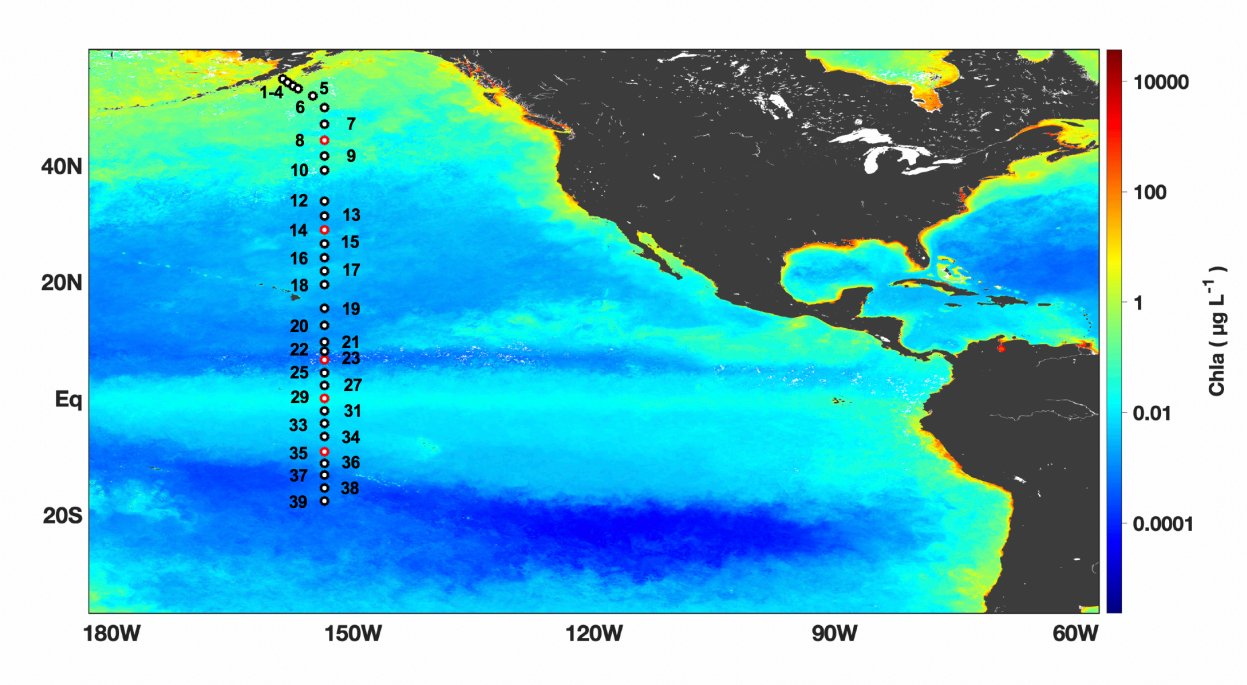

Figure 3.1: US GEOTRACES PMT GP15 cruise track map with Aqua-MODIS-derived average sea surface chlorophyll (October-December 2018) during the time of the cruise. A subset of stations was sampled from 0 to 1000 m, and other stations are sampled from the surface to the sea floor. Siderophore data are reported only for samples from 0-1000 m.

3.2 Methods

3.2.1 Sample collection and processing for dissolved siderophores

Seawater samples were collected on the US GEOTRACES cruise GP15, Pacific Meridional Transect (R/V Revelle, RR1814 and RR1815) using GEOTRACES sampling protocols. Each sample was filtered directly from the trace metal clean GTC rosette/Go-Flo bottle through a 0.2 µm Pall Acropak-200 Supor cartridge into a trace metal grade acid-cleaned 4 L polycarbonate bottle. Samples were pumped at 20 mL/min through Bond-Elut ENV solid phase extraction (SPE) columns (1 g, 6 mL, P/N 12255012, Agilent Technologies, Figure 3.2) that had been previously activated by passing 6 mL each of distilled methanol (MeOH, Optima LCMS grade, Fisher Scientific) and ultrapure water (qH_2O, 18.2 MΩ) through the column.

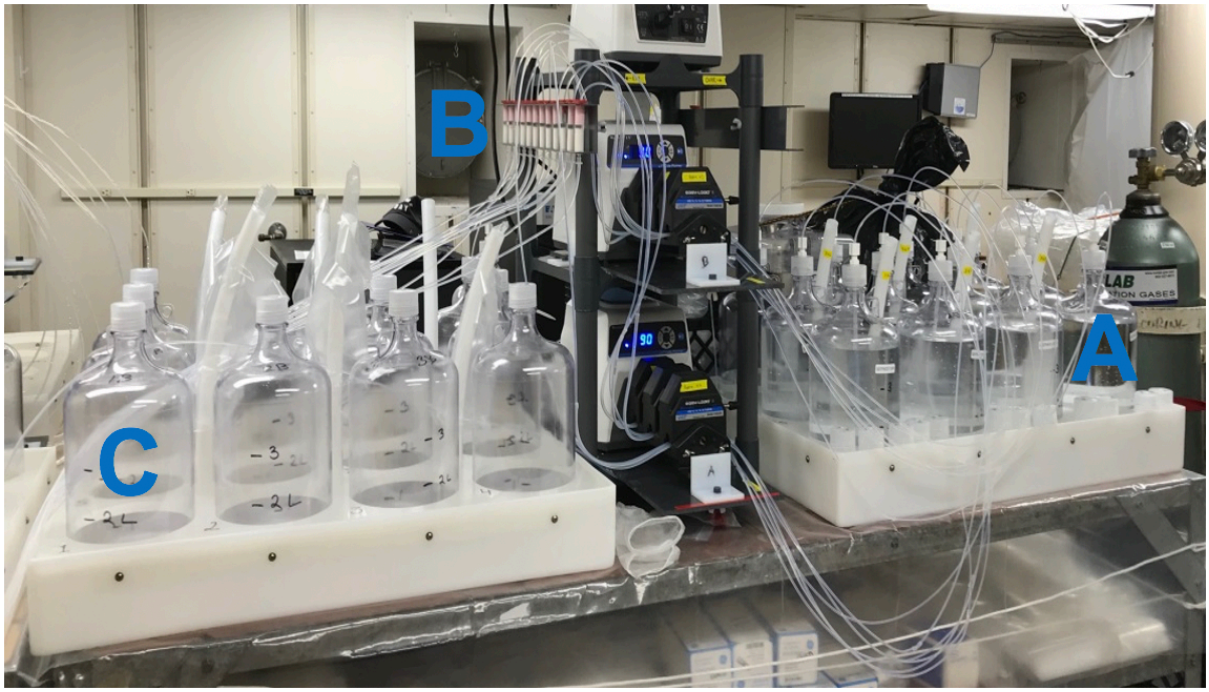

Figure 3.2: Apparatus for shipboard siderophore sample processing. Twelve dissolved seawater samples of 4 L each (**A**) were pumped through Bond-Elut ENV SPE column (**B**). For select samples, the ENV extracted seawater (**C**) was acidified with HCl (1 mL/L) and pumped back through SPE-CHAR columns, to expand the window of ligand extraction and detection.

SPE columns were frozen (-20 °C) immediately after sample collection and returned to the laboratory for processing. Columns were thawed and washed with 6 mL qH_2O (to reduce salts) and the qH_2O wash was discarded. Ligands were then eluted with 6 mL distilled MeOH into acid-cleaned 10 mL polypropylene tubes. Process blanks were prepared in parallel by eluting activated ENV columns with 6 mL qH_2O followed by 6 mL MeOH. The methanol fraction was collected as the process blank. A 10 µL stock solution of 2.2 µM Ga-Desferrioxamine-E (Ga-DFOE) was added to each sample as an internal standard. The sample was concentrated to about 500 µL by vacuum centrifugation (SpeedVac, Thermo Scientific; 35 °C, 5 hrs). A 100 µL aliquot of the sample was taken, mixed with 100 µL of qH_2O, and immediately analyzed by LC-MS.

To prepare the Ga-DOFE internal standard, 0.5 mg desferrioxamine-E (DFOE; Biophore Research) was dissolved with sonication in 1 mL distilled MeOH. Then, 10 µL of 200 mM gallium nitrate in qH_2O adjusted to pH 1 with nitric acid (Optima grade, Fisher Scientific) was added to complex DFOE. The solution was diluted by adding 4 mL qH_2O to make 5 mL of standard. To remove excess Ga, 500 µL of the solution was applied to a C18 SPE column (100 mg, 1 mL, Agilent Technologies), which had been previously activated with 2 mL each of distilled MeOH and qH_2O. The cartridge was washed with 2 mL qH_2O to remove excess Ga, and the Ga-DFOE eluted with 2 mL MeOH. The MeOH eluant was collected and then diluted with qH_2O to a final volume of 20 mL.

3.2.2 Sample collection and processing for siderophores in suspended POM

Suspended particulate organic matter (POM) samples were collected by McLane pumps according to GEOTRACES sampling protocols (Lam et al 2018). Seawater was pumped through a 51 µm polyester prefilter and a Whatman QMA quartz filter (Cytiva). The particles collected on the QMA filter represents 1-51 µm size fraction of suspended POM. Up to 1500 L of seawater is pumped through each pair of filters, and we received a subsample equivalent to 1/16 of each QMA filter, representing 50-100 L of seawater. Filters were frozen (-20 °C) immediately after sample collection and returned to the laboratory for processing.

Filters are first extracted with 10 mL MQ under ultrasonication at 35% power for 5 min (Branson Ultrasonics, model 102C). The MQ extract was collected and the filter was extracted again with 10 mL distilled MeOH under ultrasonication at 35% power for 10 min. Then, the MQ extract and MeOH extract were combined, and diluted with 200 mL MQ. The sample was pumped through a 0.2 µm PES filter capsule (P/N SLGPM33RS, MilliporeSigma) and a Bond-Elut ENV SPE cartridge (1 g, 6 mL, P/N 12255012, Agilent Technologies) activated as described earlier. The SPE column was washed with 6 mL qH_2O water, the sample recovered by extracting with 6 mL MeOH, 10 µL of Ga-DFOE standard were added, and the sample analyzed for siderophores as described below.

3.2.3 High pressure liquid chromatography-Inductively coupled plasma mass spectrometry

Chromatographic analyses were performed on a bioinert Dionex Ultimate 3000 LC system fitted with a loading pump, a nano pump, and a 10-port switching valve (Li et al 2021). During the loading phase, 200 µL of sample were withdrawn into the sample loop, then applied to a C18 trap column (3.5 µm, 0.5 mm x 35 mm, P/N 5064-8260, Agilent Technologies) by the loading pump at 25 µL/min for 10 min. The loading solvent is a mixture of 95% solvent A (5 mM aqueous ammonium formate, Optima, Fisher Scientific) and 5% solvent B (5 mM methanolic ammonium formate). During the elution phase, the solvent was delivered by a nano pump at 10 µL/min, and the trap column outflow directed onto two C18 columns (3.5 µm, 0.5 mm x 150 mm, P/N 5064-8262, Agilent Technologies) connected in series. Samples were separated with an 80 min linear gradient from 95% solvent A and 5% solvent B to 95% solvent B, followed by isocratic elution at 95% solvent B for 10 minutes. Meanwhile, the loading pump solvent was switched to 100% qH_2O, increased to 35 µL/min and directed as a post column make-up flow, which was infused with the column eluant into the ICPMS (Li et al 2021). The high aqueous content of the combined flow serves to minimize the effect of changes in solvent composition (in this case increasing methanol content during the analysis) on the detector response to Fe, Ga, and Al (Boiteau et al 2013). For Station 39, the HPLC eluant at 10 µL/min was directed into the ICPMS without post column infusion of qH_2O.

The combined flow from the LC (45 µL/min) was analyzed using a Thermo Scientific iCAP Q quadrupole mass spectrometer fitted with a perfluoroalkoxy micronebulizer (PFA-ST, Elemental Scientific), and a cyclonic spray chamber cooled to 4 °C (Boiteau and Repta, 2015). Measurements were made in kinetic energy discrimination (KED) mode, with a helium collision gas flow of 4-4.5 mL/min to minimize isobaric $^{40}Ar^{16}O^{+}$ interferences on ^{56}Fe. Oxygen was introduced into the sample carrier gas at 25 mL/min to prevent the formation of reduced organic deposits onto the ICPMS skimmer and sampling cones. Isotopes monitored were ^{56}Fe (integration time 0.05 s), ^{54}Fe (0.02 s), ^{57}Fe (0.02 s), ^{69}Ga (0.05 s), ^{71}Ga (0.02 s) and ^{27}Al (0.02 s).

3.2.4 External and Internal Standards

The Fe detector response was calibrated using the siderophore ferrichrome which elutes at ~40 min in our chromatographic analysis. Stock solutions of 250 µM ferrichrome were diluted to prepare standards with 2 nM, 5 nM, 10 nM, 20 nM, and 40 nM of the siderophore. Then, 5 µL of 2.2 µM Ga-DFOE was added to 995 µL of each standard. Next, a 100 µL aliquot was taken, mixed with 100 µL of qH_2O, and analyzed by LC-ICPMS. A plot of the ratio of ^{56}Fe(ferrichrome):^{69}Ga (Ga-DFOE) peak areas against ferrichrome/Ga-DFOE concentration yields a linear relationship (r^2 ~0.999) for the response of the ICPMS detector to Fe between 0.2-4 pmoles of ferrichrome. Calibrations and process blanks were made for every 10-20 samples analyzed, with only small changes (RSD ~30%) were observed in the slope of the calibration relationship over the course of the two years of sample analysis. Concentrations of Fe ligands in each sample were measured by plotting the FeL/Ga-DFOE peak area on the most appropriate calibration curve.

Al-siderophores are quantified by converting peak area of Al-siderophores on ICPMS to peak area of Fe-siderophores. Before each standard curve, a metal stock solution containing 10 ppb Fe and 10 ppb Al in 5% Optima HNO_3 (Fisher Scientific) was introduced into the ICPMS, and the counts of ^{56}Fe and ^{27}Al were collected for 5 min.

Then, the sensitivity ratio of Fe:Al is averaged, and used in the normalization of Al-siderophore peak area to Fe-siderophore peak area, which is then quantified using the standard curve.

3.2.5 High pressure liquid chromatography-Electrospray ionization mass spectrometry (LC-ESIMS)

To verify the assignment of Fe-Ls to known siderophores, select samples were analyzed by LC-ESIMS. The eluant from the LC, without qH_2O infusion, was coupled to a Thermo Scientific Orbitrap Fusion mass spectrometer equipped with a heated electrospray ionization source. ESI source parameters were set to a capillary voltage of 3500 V, sheath, auxiliary and sweep gas flow rates of 5, 2, and 0 (arbitrary units), and ion transfer tube and vaporizer temperatures of 275 °C and 20 °C. MS^1 scans for a m/z range of 150-1900 were collected in high resolution (450K) positive ion mode.

The LC-ESIMS data was converted from raw file format to mzXML (MSconvert, Chambers et al 2012). The mzXML was imported to Matlab, and aligned with ICPMS data using the retention time of Ga-DFOE, which was obtained by monitoring m/z of 667.26 by ESIMS and ^{69}Ga by ICPMS. Then, the m/z and intensity from each scan were extracted and ordered by scan number into a scan number/mass (m/z)/intensity matrix, which is then interrogated by mass search algorithms (Boiteau and Repeta, 2015, Li et al 2021). The algorithms find pairs of co-eluting peaks with a mass difference of 1.995 D (ΔD = ^{56}Fe - ^{54}Fe) and a ratio of 15.7 in intensity, which represents the crustal abundance ratio of ^{56}Fe and ^{54}Fe.

3.3 Results and discussion

3.3.1 The section features discrete siderophore "hotspots"

All the samples show a broad "hump" in intensity of the ^{56}Fe-ICPMS chromatogram between 20-100 min (Figure 3.3). This hump in intensity is greater than the baseline signal between 20-100 min that appears in the process blank, which represents Fe from

the SPE cartridge, HPLC instrument, solvents and columns. The elevated hump in the samples relative to the baseline in the process blank represents organically bound Fe extracted from seawater, which includes a complex mixture of compounds of low individual concentration.

Some samples show well defined peaks on top of the hump, and the GP15 section is dominated by three classes of peaks (Figure 3.3). In coastal region, particularly Station 01 and Station 02, we find sharp polar peaks with retention times of 30-40 min, similar to the retention time of ferrichrome and ferrioxamine standards. The open ocean portion of the transect between Station 03 and Station 39 is dominated by a suite of non-polar peaks with retention time of 60-90 min (Figure 3.3), similar to the retention time of amphibactins. These non-polar peaks are found at most stations, and they are the most prevalent peaks in the transect. South of Station 23 at 7.7 °N, we found broad peaks with retention time of 50-60 min, which is the first time these peaks are found in seawater (Figure 3.3).

The SPE extractable dFe could be calculated by subtracting the total area of the appropriate process blank from the area of the total chromatogram. The fraction of Fe complexed to siderophores was then calculated as the summed area of discrete peaks relative to total area. In the samples shown in Figure 3.3, siderophores account for 5%, 25% and 12% of the SPE extractable dFe in the sample at 40 m of Station 01, 400 m at Station 16, and 400 m at Station 39.

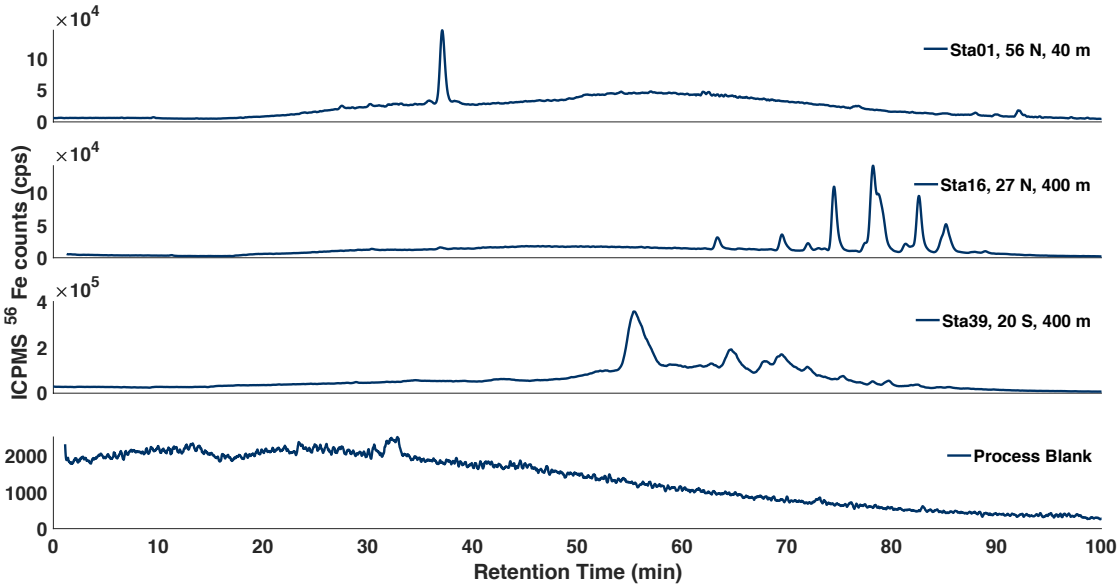

Figure 3.3: Representative LC-ICPMS chromatograms of samples with polar siderophores, non-polar siderophores, intermediate polarity broad peaks and a process blank. Note the change in Fe counts scales between the different chromatograms.

We quantified all the Fe siderophore peaks in each sample to generate the section plot in Figure 3.4. Siderophore concentration ranges from 0-70 pM, with the highest concentration found at 400 m of Station 25. The concentrations of siderophores we found in the GP15 transect are similar to the concentrations of 0-95 pM in a transect of the North Pacific (Park et al 2022). In the Atlantic Ocean, siderophore concentration in surface waters is 3-20 pM (Mawji et al 2008). In the eastern tropical Pacific Ocean, siderophores in surface water are 1-9 pM (Boiteau et al 2016). At Station ALOHA, siderophores are present at multiple depths at 0.1-11 pM (Bundy et al 2018). In the California Coastal upwelling system, siderophores are found at 1-18 pM in the water column (Boiteau et al 2019).

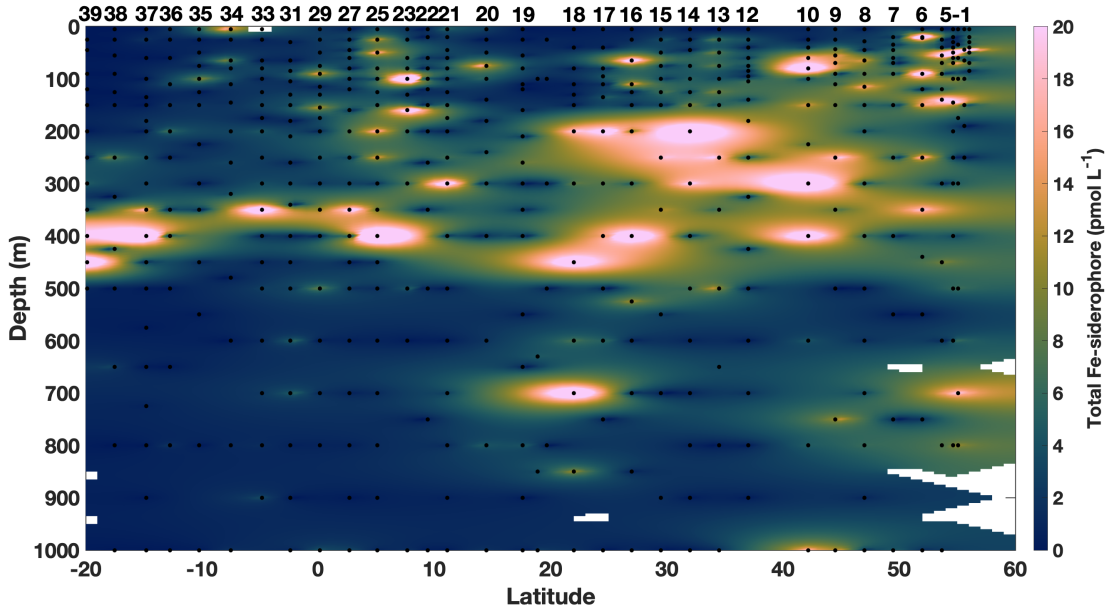

Figure 3.4: The distribution of total Fe-siderophores in the upper 1000 m of US GEOTRACES GP15. The total concentration of Fe-siderophores in each sample is calculated by combining all Fe peaks on the LC-ICPMS chromatogram that have a concentration higher than 0.5 pM. The concentration does not include non-metallated "apo" siderophores or Al-siderophores.

At Station ALOHA, the concentration of soluble Fe (< 20 nm) is 350 pM at 400 m (Fitzsimmons et al 2015). Due to the low molecular weight (< 1000 D) and small size (1 nm), Fe-siderophores are expected in the soluble Fe fraction. Assuming the distribution of soluble Fe is the same at Station ALOHA (Fitzsimmons et al 2015) and Station 25 in GP15, Fe-siderophore concentration of 70 pM and soluble Fe concentration of 350 pM at 400 m would result in a contribution of 20% by Fe-siderophore to soluble Fe.

Siderophores are widely distributed across the entire section, suggesting that siderophore mediated Fe transport is common in the Pacific Ocean. We define a "hotspot" as any sample with a total concentration of Fe-siderophore that is above 20 pM. This threshold is higher than values (0.1-20 pM) typical of seawater reported in other studies (Mawji et al 2008; Boiteau et al 2016; Bundy et al 2018). In GP15, hotspots occur as discrete features, suggesting that the siderophores are produced and consumed locally and that lateral transport of siderophores is likely limited in distance.

3.3.2 Most hotspots are found in nitracline

There are 33 hotspots across the entire transect, with 29 hotspots found in the nitracline (Figure 3.5). In the NPSG and SPSG, the hotspots are found at mesopelagic depths between 200-400 m. At Station ALOHA in the NPSG, a maximum in siderophore concentration in the water column was also found at 300 m (Bundy et al 2018), supporting our results here. In the upwelling regions of around 50° N and 10° N where nitracline is lifted to shallower depths, the hotspots are also lifted (Figure 3.5).

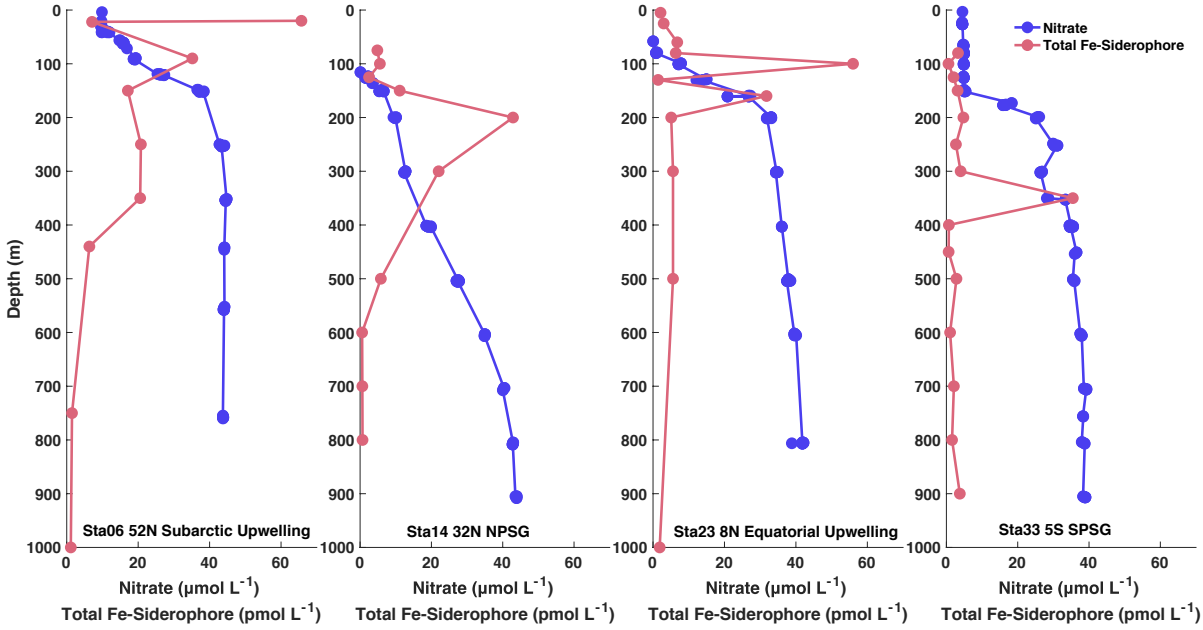

Figure 3.5: The distribution of nitrate and total Fe-siderophores at representative stations in different biogeochemical regions, including Subarctic Upwelling (50-56 °N), NPSG (15-50 °N), Equatorial Upwelling (5 °S-15 °N) and SPSG (20-5 °S).

For example, at Station 05 located at 54 °N, the hotspots are found at 55 and 140 m, where nitrate concentration is 15 and 41 μM. At Station 06 at 52 °N, the total concentration of siderophores is 66 pM at 20 m, where nitrate concentration is 10 μM. At Station 23 at 8 °N, the total concentration of siderophores is 56 pM at 100 m, where

nitrate concentration is 7 μM. These hotspots suggest a shallower depth for Fe limitation in the upwelling region than in the gyres.

3.3.3 Low dFe:NO_3^- ratio seems to be a necessary condition for siderophore hotspots

Our expectation was that as dFe concentrations decrease, production and therefore concentrations of siderophores would increase. However, we found no correlation between dFe and siderophore concentrations (Figure 3.6; dFe data from Sieber and Conway, personal communication). The locations of siderophore hotspots led us to suspect that high concentration of nitrate is another necessary condition for siderophore production, because most of the siderophores found in the ocean are N rich compounds. Therefore, we expected to find siderophores in samples with low dFe and high nitrate, and low dFe:NO_3^- ratio. Indeed, when siderophore concentration is plotted against dFe:NO_3^- ratio, most hotspots are associated with a ratio lower than 50 μmol/mol, and only one hotspot is associated with a ratio higher than 50 μmol/mol (Figure 3.6). In addition, the average concentration of dFe for the hotspots is 0.35 nM, suggesting that low dFe is a necessary condition, but not sufficient condition for high concentration of siderophores.

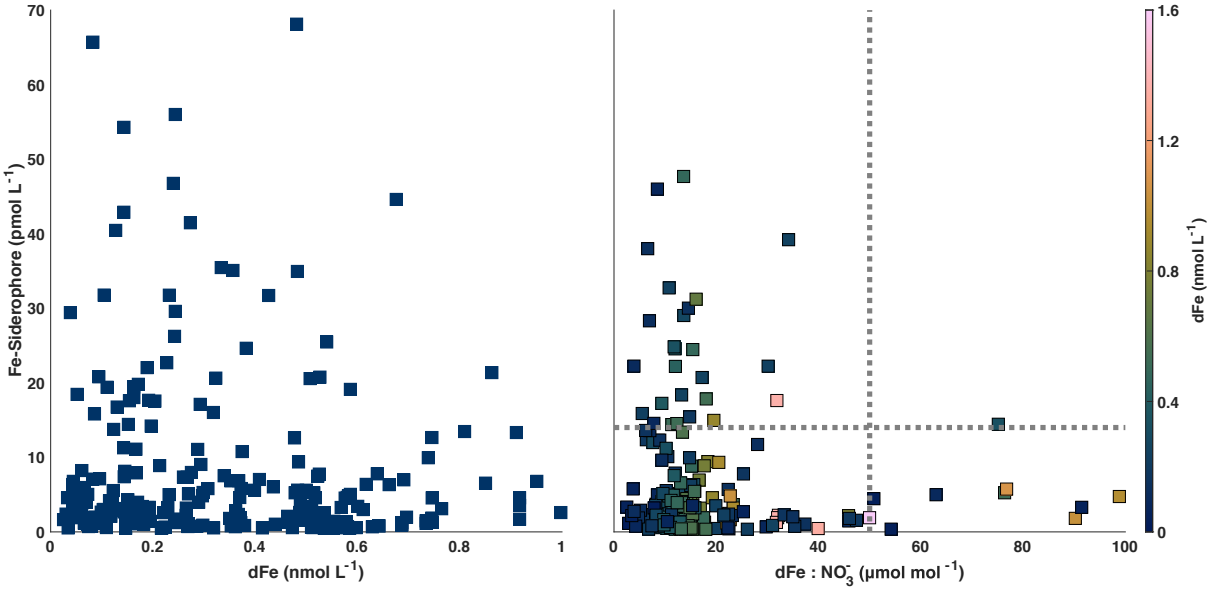

Figure 3.6: The relationship between the concentration of Fe-siderophores and dFe, (left panel) and siderophore concentration and dFe:NO_3^- ratio (right panel). The color of the symbol in the right panel represents concentration of dFe associated with each sample. No strong relationship between dFe concentration and siderophore concentration was found in our data, but most hotspots of siderophore concentration (> 20 pM, horizontal dotted line in the right panel) were characterized by a Fe:NO_3^- ratio of < 50 µmol/mol (vertical dotted line in the right panel). The dFe data is from Sieber and Conway, personal communication. When the samples for siderophores and dFe or nitrate are not collected from the same depth, the dFe and nitrate data from the closest depth of the same station are used to pair the siderophore data.

Heterotrophic bacteria including *Pseudomonas* spp. grown under low Fe concentrations have a cellular Fe:C ratio of 8 µmol/mol (Tortell et al 1996), or an dFe:NO_3^- ratio of 50 µmol/mol assuming Redfield stoichiometry. At 200-400 m of the NPSG, dFe:NO_3^- ratio in seawater is 10-80 µmol/mol (Figure 3.7), much lower than the dFe:NO_3^- ratio of 80-80000 µmol/mol characteristic of seawater at 0-200 m. At 200-400 m of the NPSG, the dFe:NO_3^- ratio in seawater, which represents the supply of Fe relative to NO_3^-, is similar to the cellular Fe:N ratio for Fe limited heterotrophic bacteria, which represents the minimum demand of Fe relative to N. Therefore, heterotrophic bacteria are likely to be

Fe limited between 200 and 400 m of the NPSG (Moore et al 2013), and a subset of heterotrophic bacteria would produce siderophores as a response.

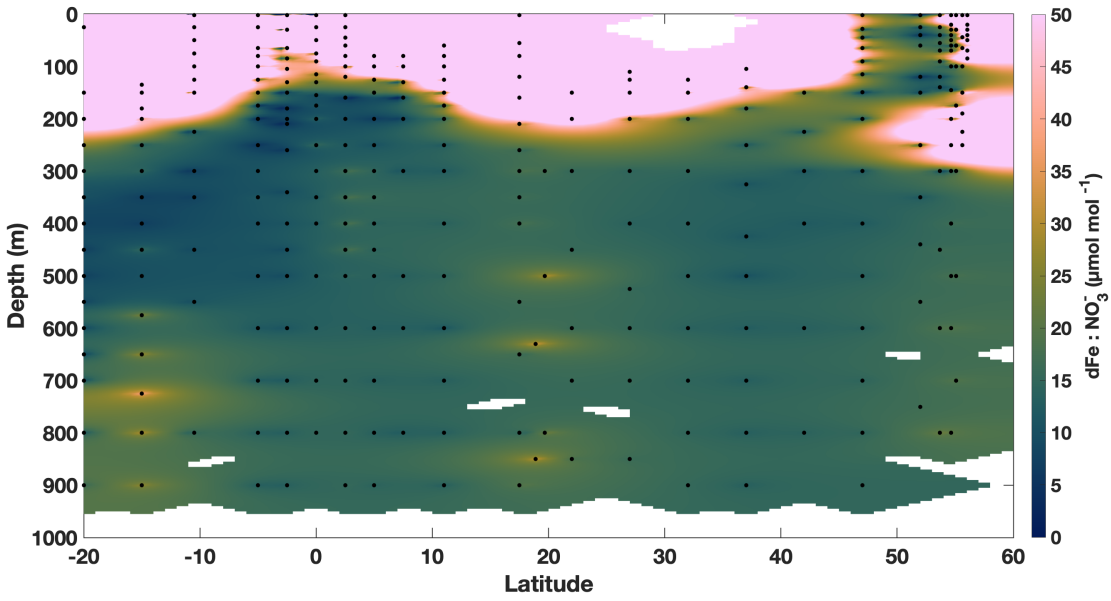

Figure 3.7: The distribution of Fe:NO_3^- in the upper 1000 m of US GEOTRACES GP15. The dFe data is from Sieber and Conway, personal communication. When the samples for dFe and nitrate are not collected from the same depth, the nitrate data from the closest depth of the same station were used to calculate the dFe:NO_3^- ratio.

At 0-200 m of the NPSG, the concentration of dFe is lower than 200-400 m (Fitzsimmons et al 2015). Therefore, we expected more extensive Fe limitation of heterotrophic bacteria, and higher concentration of siderophores in surface waters than between 200-400 m. However, siderophore concentration is lower at 0-200 m than 200-400 m in the NPSG. This likely could not be explained by C limitation on siderophore production, because the production of both POM and labile C substrate were higher at 0-200 m than at 200-400 m. However, surface waters are characterized by a dFe:NO_3^- ratio of 80-80000 µmol/mol (Figure 3.7), which is higher than this ratio between 200-400 m (due to lower nitrate concentrations in surface waters). Therefore, siderophore production by heterotrophic bacteria between 0-200 m in the NPSG seems to be limited by N.

The control of dFe:NO_3^- ratio on siderophore concentration would also explain the shallower hotspots in the upwelling regions. For example, at around 50 °N, deep water associated with a low dFe:NO_3^- ratio is upwelled to around 50 m (Figure 3.7), and the entire water column features a dFe:NO_3^- ratio that is lower than 50 μmol/mol, which is similar to the minimum Fe demand for Fe limited heterotrophic bacteria (Tortell et al 1996). In this HNLC region, there is consistent Fe deficiency in the entire water column. Furthermore, the shallow hotspots at 55 and 140 m of Station 05, 20 m at Station 06, and 100 m at Station 23 all have high concentration of NO_3^- which could be used for siderophore production. Therefore, the hotspots of siderophores are found at surface of the HNLC regions.

The importance of N in siderophore production has been shown for freshwater cyanobacteria *Anabaena* 7120, which is known to produce N rich hydroxamate siderophores (Hutchins et al 1991). Cultures were grown with and without 300 μM NO_3^- and 1 μM Fe in all four possible combinations. Siderophores were produced only by cultures with added NO_3^- and no added Fe. In the treatment of no NO_3^- and no Fe addition, the cyanobacteria is expected to be Fe limited, and the absence of siderophore production suggest the importance of N in siderophore production, at least for hydroxamate siderophores, which includes most of the siderophores found in seawater.

The concentration of siderophores below 400 m is low or non-detectable. Water below 400 m features a dFe:NO_3^- ratio that is < 50 μmol/mol (Figure 3.7), the Fe limitation threshold for heterotrophic bacteria. Therefore, based on dFe:NO_3^- ratio alone we expected to see siderophores below 400 m. The absence of siderophores in GP15 samples below this depth suggests that other nutrients limit siderophore production, most likely labile organic carbon. Because the nitrate concentration generally increases with depth, but POC flux decreases with depth, bacterial production in the deep ocean are probably limited by the supply of labile carbon. Therefore, although siderophore production on the cellular level might be favored, siderophore concentration would scale down with bacterial production.

At Station 16, we measured the siderophores in samples below 1000 m, and found siderophores at 4000 m (Figure 3.8). The presence of siderophores is not continuous in the water column. In this example the suite of siderophores at 4000 m was the same as the siderophores at 25 m, but the concentration of the siderophores is below 1 pM at 4000 m.

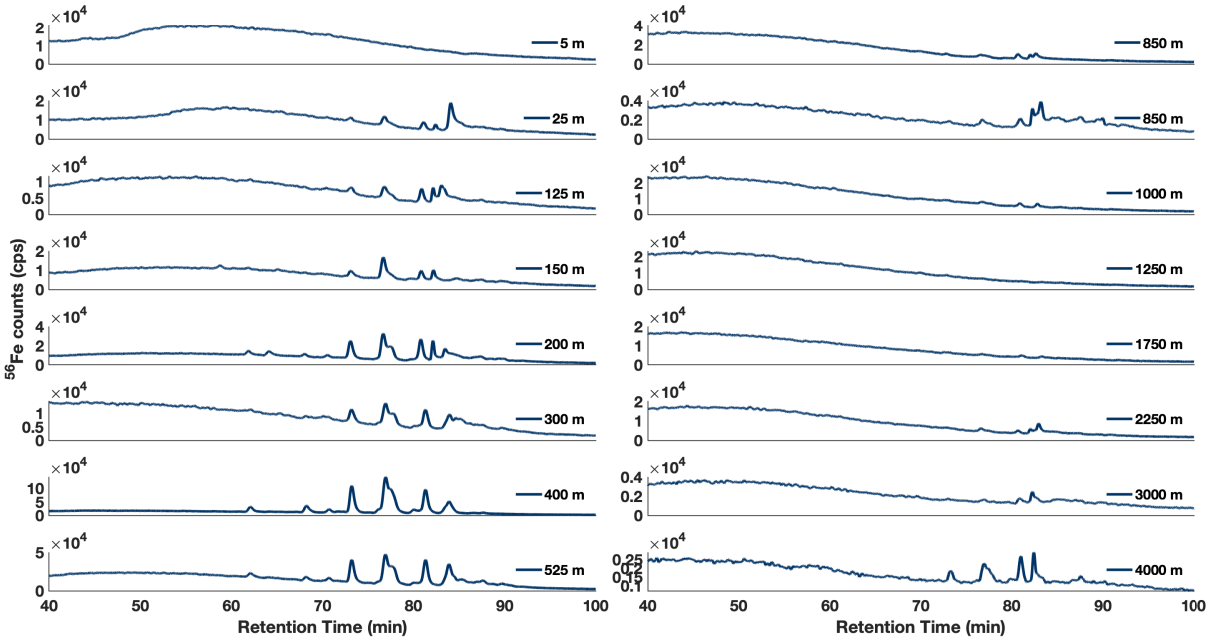

Figure 3.8: LC-ICPMS ^{56}Fe chromatogram of samples for the entire water column at Station 16.

3.3.4 GP15 transect is dominated by Marinobactins

A chromatogram for a sample at 400 m of Station 16, representative of most GP15 samples, shows that the section was dominated by a suite of non-polar peaks (Figure 3.9). The molecular weights of these Fe-siderophores were found by searching for ion pairs in the LC-ESIMS data with the same mass difference and relative abundance as isotopologues of ^{56}FeL and ^{54}FeL. Then, the molecular weights of the putative ^{56}Fe-complex were compared to a library of 366 known siderophores (Hider and Kong 2010). From this the major siderophores in the samples were putatively identified as a suite of marinobactins, including Marinobactin A-E as well as novel marinobactins that have not

been described in the literature (Table 3.1). To confirm the identification of some marinobactins, the retention time of each peak was normalized to Ga-DFOE (internal standard, RT ~2700 s), and compared to the relative retention time of Marinobactins A-E isolated from a *Alteromonas* spp. culture (Boiteau 2016). Finally, the retention times of the marinobactins in the culture sample was compared to the ^{56}Fe chromatogram of the GP15 samples (Figure 3.9). Marinobactins have been previously found in European Shelf seawater (Gledhill et al 2022), and our results show the prevalence of marinobactins in the open ocean.

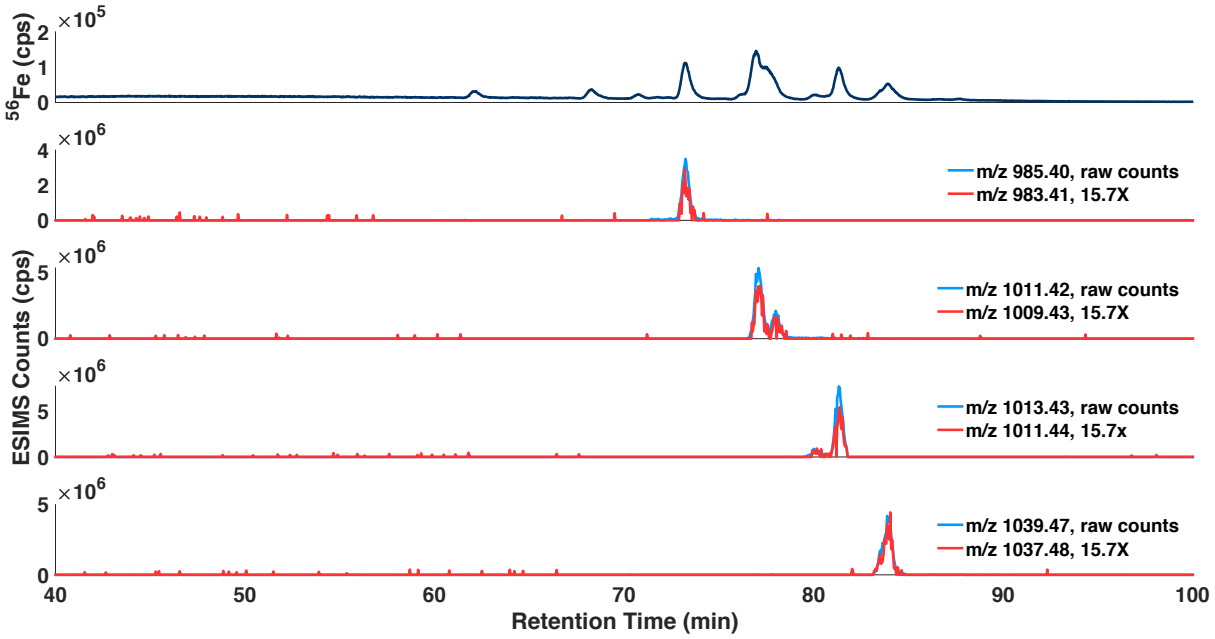

Figure 3.9: Marinobactin A-D characterization. The top panel is the ^{56}Fe LC-ICPMS chromatogram from the sample at 400 m of Station 16 (27 °N). The lower panels are the extracted ion chromatograms (EIC) from positive mode LC-ESIMS of the same sample. Blue lines correspond to the ^{56}Fe-siderophore $[M+H]^+$ isotopologue and red lines correspond to the ^{54}Fe-siderophore $[M+H]^+$ isotopologue. The intensity of the ^{54}Fe- isotopologue has been scaled by the natural (crustal) abundance ratio of ^{56}Fe/^{54}Fe (15.7) so that the isotopologues overlap.

Table 3.1: Marinobactins detected by LC-ICPMS and LC-ESIMS from a representative sample at 400 m of Station 27. The relative retention time was calculated by normalizing the retention time of siderophore to the retention time of the internal standard Ga-DFOE, which elutes at ~2700 s. The relative retention time of standards were determined for marinobactins produced by *Alteromonas* spp. (Boiteau 2016). The authenticity of the standards is confirmed in Chapter 4.

Siderophore	$[M+H]^+$ Observed	$[M+H]^+$ Calculated	Molecular Formula	Relative Retention Time	Relative Retention Time of Standard
Marinobactin A $C_{12:0}$	985.4005	985.4055	$C_{40}H_{66}N_9O_{16}Fe$	1.68	1.66
Marinobactin B $C_{14:1}$	1011.4163	1011.4212	$C_{42}H_{68}N_9O_{16}Fe$	1.76	1.75
Marinobactin C $C_{14:0}$	1013.4321	1013.4368	$C_{42}H_{70}N_9O_{16}Fe$	1.86	1.85
Marinobactin D $C_{16:1}$	1039.4518	1039.4525	$C_{44}H_{72}N_9O_{16}Fe$	1.91	1.92
Marinobactin E $C_{16:0}$	1041.4658	1041.4681	$C_{44}H_{74}N_9O_{16}Fe$	1.99	2.00
Marinobactin $C_{13:0}$	999.4155	999.4212	$C_{41}H_{68}N_9O_{16}Fe$	1.78	
Marinobactin $C_{13:0}$ + O	1015.4107	1015.4161	$C_{41}H_{68}N_9O_{17}Fe$	1.76	
Marinobactin $C_{15:1}$	1025.4321	1025.4369	$C_{43}H_{70}N_9O_{16}Fe$	1.85	
Marinobactin $C_{15:0}$	1027.4519	1027.4525	$C_{43}H_{72}N_9O_{16}Fe$	1.92	

The putative Marinobactins A-E in GP15 samples show nearly identical retention times to authentic standards of Marinobactin A-E, confirming their identity (Table 3.1). In addition to the known marinobactins, we also found a suite of novel marinobactins in GP15 samples. For example, one siderophore is putatively identified as Marinobactin $C_{13:0}$, which has one more -CH_2- group on the fatty acid chain relative to Marinobactin A ($C_{12:0}$), and one less -CH_2- group than Marinobactin C ($C_{14:0}$). The relative retention time of marinobactin $C_{13:0}$ is 1.78, which is between Marinobactin A (1.68) and Marinobactin C (1.86, Table 3.1). Similarly, the relative retention time of novel Marinobactin $C_{15:1}$ (1.85) is between the relative retention time of Marinobactin B ($C_{14:1}$, 1.76) and Marinobactin D ($C_{16:1}$, 1.91), and the relative retention time of novel Marinobactin $C_{15:0}$ (1.92) is between the relative retention time of Marinobactin C ($C_{14:0}$, 1.86) and Marinobactin E ($C_{16:0}$, 1.99).

We measured 13 samples associated with high concentration of siderophores, from different station and depths. According to the LC-ICPMS data, the retention time for the suite of non-polar siderophores seems consistent among samples. Therefore, we used this subset of samples to represent the suit of non-polar siderophores in the entire GP15 transect. We found amphibactins in 2 out of the 13 samples, and marinobactins in 11 out of the 13 samples, suggesting that marinobactins occur much more frequently in samples than amphibactins.

Table 3.2: The GP15 samples analyzed by LC-ESIMS, the concentration of dissolved siderophore in the sample, and the identity of the siderophores in the sample.

Sample	Station	Depth (m)	Dissolved [Fe-siderophore] (pM)	Siderophore found by ICPMS	Siderophore identified by ESIMS
GT12434	1	70	8.2	Non-polar	Marinobactins
GT12438	1	40	6.8	Polar	
GT12470	2	44	31.8	Polar and non-polar	Marinobactins
GT12499	3	500	13.5	Polar and non-polar	Marinobactins
GT13049	9	1000	14.3	Non-polar	Marinobactins
GT13057	9	250	20.2	Non-polar	Marinobactins
GT13361	13	250	20.8	Non-polar	Marinobactins
GT13369	13	75	8.1	Non-polar	Marinobactins
GT13596	15	250	18.9	Non-polar	Marinobactins
GT13645	16	400	41.5	Non-polar	Marinobactins
GT13736	17	200	27.5	Non-polar	Marinobactins and Amphibactins
GT15502	36	200	7.4	Non-polar	Marinobactins
GT15684	38	250	9.5	Non-polar	Amphibactins

The head group of amphibactins includes three molecules of N^5-acyl N^5-hydroxy ornithine, and each of them has a hydroxamate group that binds Fe. Two N^5-acyl N^5-hydroxy ornithine are connected by a serine, and the third N^5-acyl N^5-hydroxy ornithine is connected directly by a peptic bond (Figure 3.10). The head group of marinobactins includes two molecules of N^5-acyl N^5-hydroxy ornithine, and a third dipeptide of aspartic acid and diaminobutryic acid. The three subunits are connected by two molecules of serine (Figure 3.10).

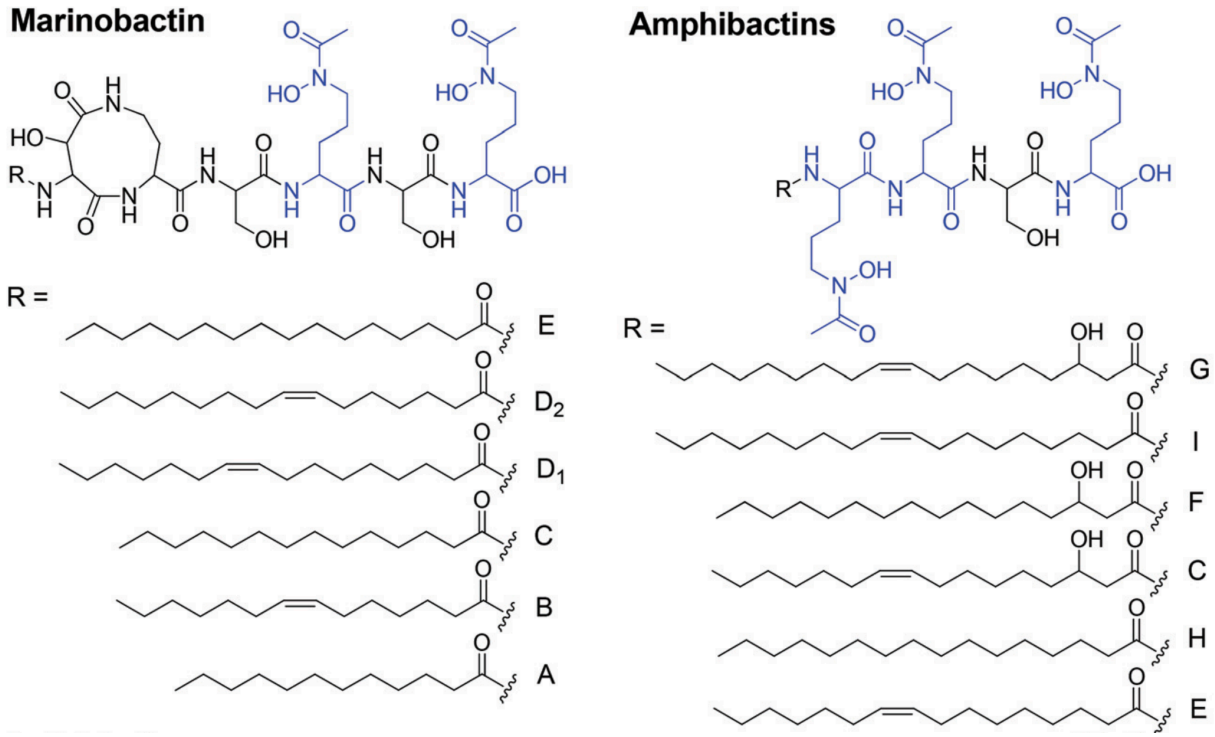

Figure 3.10: Structures of representative marinobactins and amphibactins (Cherkupally et al 2015).

Because the amino acids used in the assembly of amphibactins are a subset of those used in the synthesis of marinobactins, there is no reason *a priori* to expect that marinobactins should have been more prevalent than amphibactins in the GP15 samples. Although conditional stability constants for amphibactins have been reported (Bundy et al 2018), conditional stability constants for marinobactins have not been measured, because they have been found in seawater only recently. Therefore, the

benefit of marinobactins over amphibactins remains unknown. At this stage, we are unable to explain the dominance of marinobactins over amphibactins in the GP15 samples.

In addition to marinobactins and amphibactins, we found polar Fe binding ligands with similar retention time to ferrichromes and ferrioxamines exclusively in 10 samples at Station 01-03 near the Alaskan coast. These polar siderophores were absent in all samples collected from Station 04 to Station 39. For the polar peak in the sample at 44 m of Station 02 (Figure 3.11), we found an ion in the LC-ESIMS data, with a m/z of 771.25 Da corresponding to ferricrocin, a type of ferrichrome. The intensity of the 771.25 Da ion was too low to retrieve the ^{54}Fe isotopologue or the ^{27}Al-pseudoisotopologue. However, the authentic standard of ferricrocin showed the same retention time as the polar peak. In addition, the MS^2 of the 771.25 Da ion show major fragments of m/z 455, 542, 599 and 753 Da (Figure 3.11), which are characteristic for ferricrocin (Mawji et al 2008). The fragments at m/z 455, 542 and 599 represent the cleavage of different peptidic bonds (Mawji et al 2008), and the fragment at m/z 753 Da represents the loss of water.

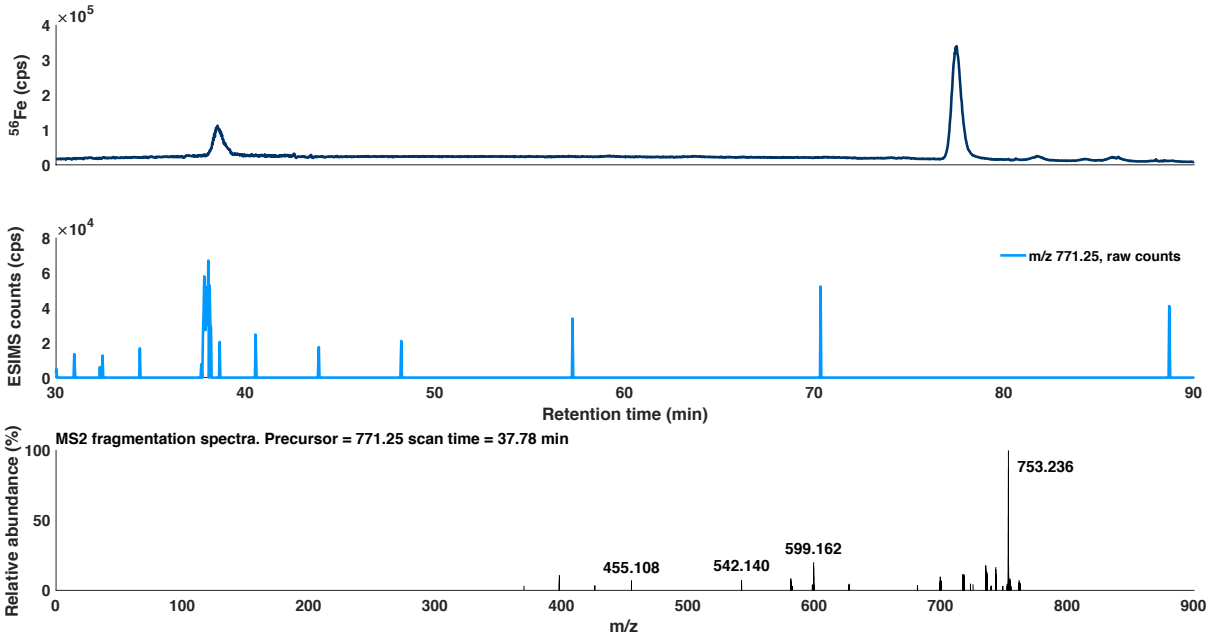

Figure 3.11: Ferricrocin characterization from the sample at 44 m of Station 02 (6 °N). The top panel is ^{56}Fe LC-ICPMS chromatogram. The mid panel is extracted ion chromatograms (EIC) from positive mode LC-ESIMS chromatograms. The blue line corresponds to the ^{56}Fe-siderophore $[M+H]^+$ isotopologue. The ^{54}Fe-siderophore $[M+H]^+$ isotopologue is not found. The bottom panel is the MS^2 fragmentation spectra of the ^{56}Fe-Ferricrocin.

The dFe:NO_3^- ratio in seawater appears to affect both the concentration and the type of siderophores in our GP15 samples. For example, waters characterized by a dFe:NO_3^- ratio higher than 50 µmol/mol, which are associated with euphotic zone of oligotrophic gyre and coastal waters, feature the prevalence of ferricrocin, whereas waters characterized by low dFe:NO_3^- ratios, which are associated with upper mesopelagic waters of the oligotrophic gyre and upwelling regions, feature the dominance of amphibactins and marinobactins.

These patterns agree with other studies. In the Altantic Ocean, ferrioxamines are widely distributed in surface waters (Mawji et al 2008) which is associated with a dFe:NO_3^- ratio > 50 µmol/mol (GEOTRACES IDP2021), whereas amphibactins are not found. In a surface transect of the eastern tropical Pacific Ocean, ferrioxamines are found in coastal and oligotrophic waters, and amphibactins are found exclusively in a narrow

region of upwelling (Boiteau et al 2016), which is associated with a dFe:NO_3^- ratio that is < 50 μmol/mol (GEOTRACES IDP2021). At Station ALOHA, ferrioxamines are found at 15 m and 125 m, where the dFe:NO_3^- ratio is 700-800 μmol/mol, whereas amphibactins are found at 300 m and 400 m, where the dFe:NO_3^- ratio is 100-200 μmol/mol (Bundy et al 2018). In California Current System, amphibactins are found in surface samples in the upwelling region (Boiteau et al 2019).

3.3.5 Marinobactins bind not only Fe, but also Al

In addition to their high affinity for Fe, some siderophores are known to bind Al (Hu and Boyer 1996; Martell and Smith 2004). For most Fe-Marinobactins in our GP15 samples, we find a co-eluting Al-Marinobactin (Figure 3.12). Al siderophore complexes have not been previously found in environmental samples. Our high sensitivity method (Li et al 2021) allows us to detect Al siderophore complexes on LC-ICPMS for the first time. For example, at 400 m of Station 16, we found both Fe-siderophores and Al-siderophores. According to ICPMS, the concentration of Al-siderophore is 10-20% of the concentration of Fe-siderophore for the three major peaks, which represents Marinobactin A-C.

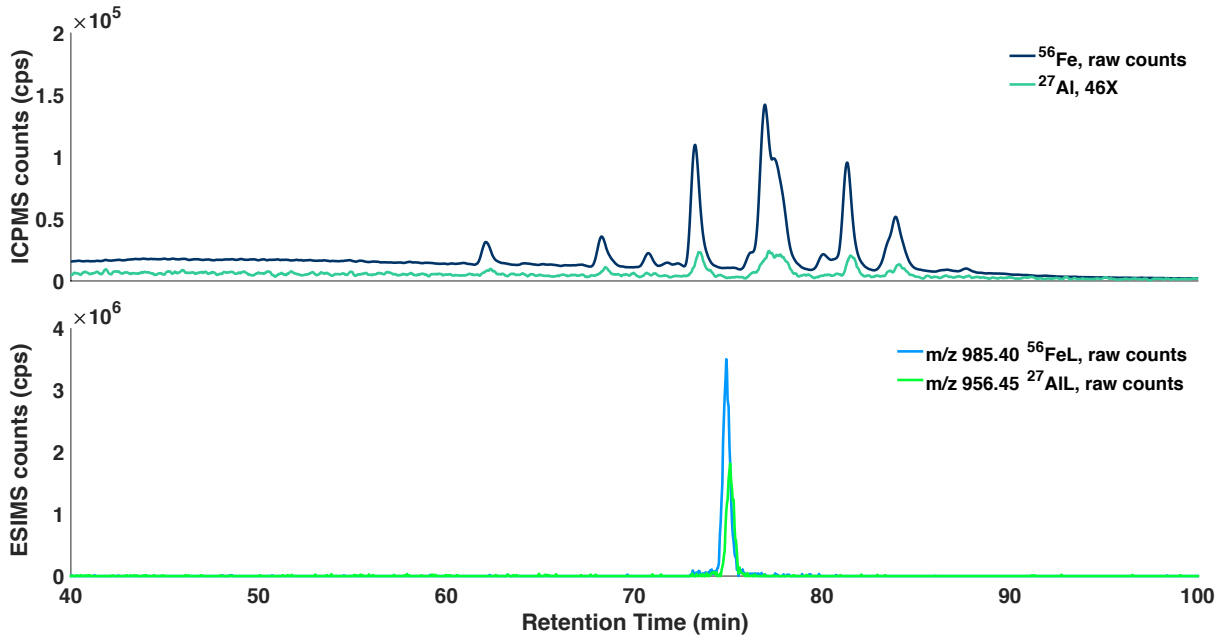

Figure 3.12: Al-Marinobactins in the sample at 400 m of Station 16. The dark blue trace in the top panel is the ^{56}Fe LC-ICPMS chromatogram, and the green trace is the ^{27}Al chromatogram, which has been scaled up by 46, to correct for the difference in detector response for Al and Fe. The blue line in the lower panel corresponds to the ^{56}Fe-siderophore $[M+H]^+$ isotopologue of Marinobactin A and the green line corresponds to the ^{27}Al-siderophore $[M+H]^+$ isotopologue. The counts for ^{27}Al-siderophore have not been scaled in LC-ESIMS data.

Although Al siderophore complexes have not been reported in environmental samples, they have been found in nutrient amended seawater, where high concentration of ferrioxamines and amphibactins are produced by microbial community after a few days of incubation (Gledhill et al 2004). Because the stability constant of Fe-Ferriomixane B is six orders of magnitude stronger than Al-Ferrioxamine B (Martell and Smith 2004), Gledhill and colleagues concluded that Al siderophore complexes would only be found when siderophores are in excess to Fe. However, in our samples concentrations of total siderophores were well below the concentration of dFe and soluble Fe, assuming a dFe to soluble iron ratio of 2 (Fitzsimmons et al 2015).

The coexistence of pM Al-siderophore and nM dFe in seawater is not expected. The persistence of Al-siderophore could not be explained by slow dissociation of Al-

siderophores. The dissociation constant of Al-DFB is 9.6×10^{-4} s^{-1} (Garrison and Crumbliss 1987). Therefore, in the absence of the formation of Al-DFB, the half life of Al-DFB would be 722s. Al-Marinobactin is expected to be weaker than Al-DFB, which would result in a faster dissociation and shorter half life, precluding Al-Marinobactin from accumulation in seawater. The persistence of Al-Marinobactin suggests a high formation rate of Al-Marinobactin, which is not expected in the presence of nM dFe that competes for siderophores. From an equilibrium perspective, similar concentration of Al-Marinobactin and Fe-Marinobactin and a six order of magnitude higher stability constant for Fe than Al would reflect a six order of magnitude lower concentration for Fe^{3+} than Al^{3+}.

In seawater, the majority of dFe is bound to organic ligands (Fe-Ls), and some of these Fe-Ls are solid phase extractable, which contribute to the hump on the chromatogram of LC-ICPMS (Figure 3.3). In contrast, we have not found a hump for Al in any of the samples, although some studies suggest the presence of organic ligands for Al (van den Berg et al 1994). Therefore, it is possible that inorganic Al and Al^{3+} account for a higher portion of dAl, which is also on the order of nM in seawater, than the portion of inorganic Fe and Fe^{3+}, and a higher concentration of Al^{3+} than Fe^{3+} allow Al to compete against Fe for siderophores.

The similar concentration of Al-Marinobactin and Fe-Marinobactin could also be partly due to the low bioavailability of Al siderophores. In heterotrophic bacteria, iron siderophores are transported across the outer membrane by TonB-Dependent Transporters, and then transported across the inner membrane by a periplasmic binding protein and an ABC transporter. In the cytoplasm, iron in the siderophore is reduced from Fe(III) to Fe(II), resulting in a decrease in the stability constant and release of Fe from the siderophore. The Fe can then be stored or incorporated into enzymes (Noinaj et al 2010). In contrast to Fe, Al does not have an oxidation state of +2. Therefore, it is likely that Al could not be reduced or used in the cytoplasm, so that Al siderophore complexes may be released back into seawater. If the equilibrium concentration is

higher for Fe-siderophore than Al-siderophore, fast uptake of Fe-siderophore and accumulation of Al-siderophore would buffer the difference in concentration.

In some samples, with low concentrations of ^{56}Fe-siderophore, the concentration of ^{54}Fe-siderophore drops below the detection limit on LC-ESIMS, thereby complicating mass search algorithms that rely on the detection of both Fe isotopologues. The high concentration of Al-siderophores allows us to use ^{27}Al as a pseudoisotope of Fe in the mass search algorithms, which is beneficial for samples with low siderophore concentrations. For example, at 200 m of Station 14 (24.5 °N, 152 °W), there is a peak at 88 min on the chromatogram of ^{56}Fe by LC-ICPMS (Figure 3.13), suggesting the presence of an Fe siderophore complex. In addition, this siderophore also binds Al according to LC-ICPMS (Figure 3.13). However, the mass search algorithm that relies on the detection of both ^{56}FeL and ^{54}FeL by LC-ESIMS did not find the mass for the Fe-siderophore complex. Using the new algorithm described in Chapter 2, we were able to find the mass for each organic compound that elutes within this time window, and find the pair of isotopologue for ^{56}FeL and ^{27}AlL, and identified the siderophore as Marinobactin E (Figure 3.13).

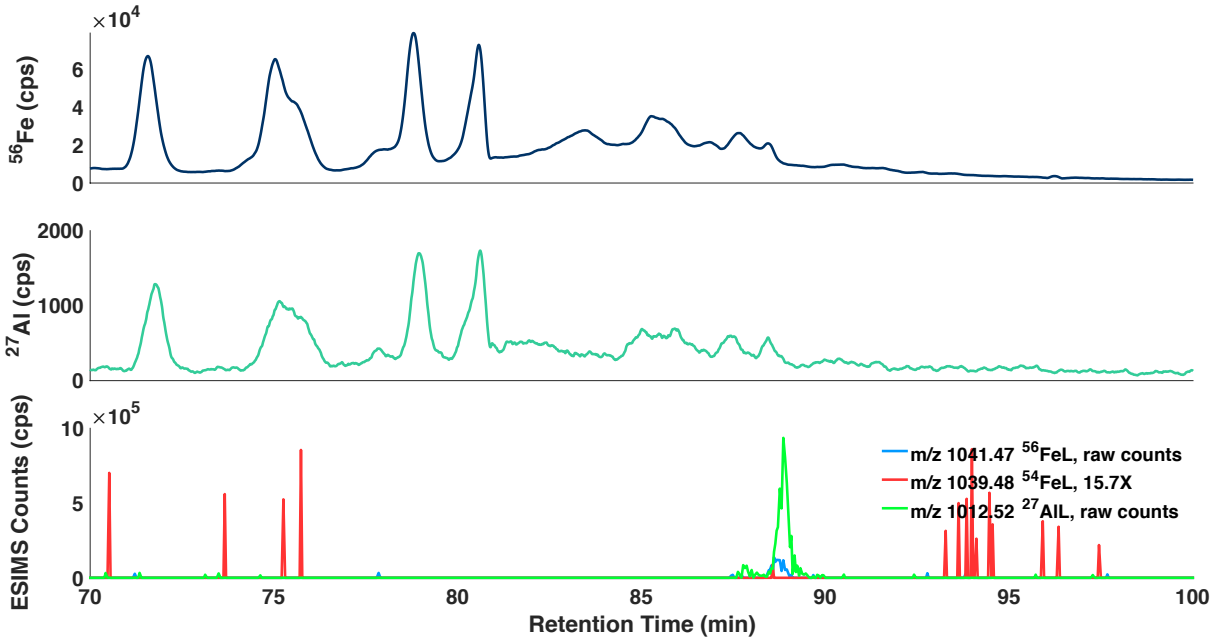

Figure 3.13: Characterization of Marinobactin E using ^{27}Al as a pseudoisotope for ^{56}Fe. The top panel is the ^{56}Fe LC-ICPMS chromatogram from the sample at 200 m of Station 17 (25 °N). The mid panel is the ^{27}Al LC-ICPMS chromatogram of the same sample. The lower panel is the extracted ion chromatograms (EIC) from positive mode LC-ESIMS of the same sample. The blue line corresponds to the ^{56}Fe-siderophore $[M+H]^+$ isotopologue, the red line corresponds to the ^{54}Fe-siderophore $[M+H]^+$ isotopologue, and the green line corresponds to the ^{27}Al-siderophore $[M+H]^+$ pseudoisotopologue.

In the surface waters of the Southeast Pacific (GEOTRACES GP16) Boiteau et al (2016) found that addition of Fe increased Fe-siderophore concentrations by 40–65%, and concluded that a large fraction of siderophores in their samples were originally metal free (apo). However, the discovery of Al-siderophore in GP15 samples led us to suspect that there might also be Al-siderophore in GP16 samples, which was converted to Fe-siderophore after Fe addition, and resulted in the increase of Fe-siderophore concentration observed by Boiteau and colleagues. In GP16 samples, Boiteau et al (2016) found Fe-siderophores (Figure 3.14), but did not report Al-siderophores, probably due to the low sensitivity of Al on ICPMS. However, upon examining the ESIMS data in Boiteau et al (2016), we found Al-siderophores in the sample before Fe addition, including Al-Amphibactin D and Al-Siderophore 959 (Figure 3.14). Therefore,

Al-siderophores were prevalent in the GP16 samples, and the conversion from Al-siderophore to Fe-siderophore might have contributed to the increase of siderophore concentration under Fe addition (Boiteau et al 2016).

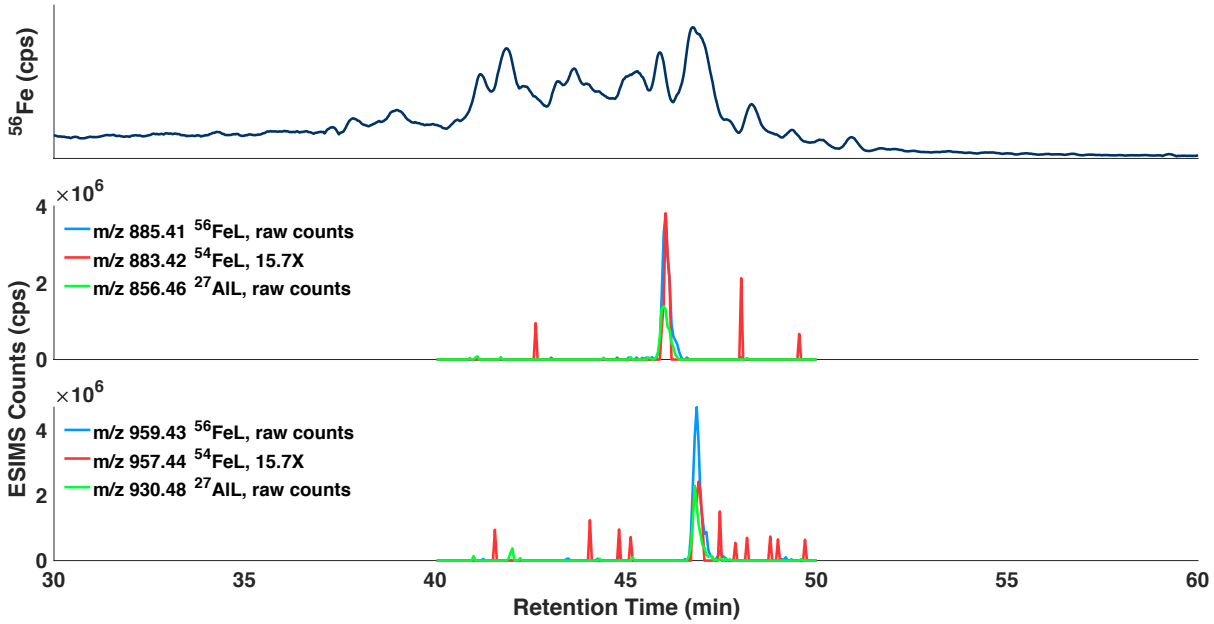

Figure 3.14: Al-Siderophores in the Sample 2 at the surface of the GP16 East Pacific Zonal Transect (Boiteau et al 2016). The blue trace in the top panel is the ^{56}Fe LC-ICPMS chromatogram. Blue lines in the lower panels correspond to the ^{56}Fe-siderophore $[M+H]^+$ isotopologue of Amphibactin D and an unknown siderophore that has a m/z of 959 for ^{56}FeL. Red lines correspond to the ^{54}Fe-siderophore $[M+H]^+$ isotopologue. Green lines correspond to the ^{27}Al-siderophore $[M+H]^+$ pseudoisotopologue. The counts for ^{27}Al-siderophore have not been scaled in LC-ESIMS data.

The discovery of Al-siderophore raises an issue on the presence of apo siderophores in the ocean. We did not find apo siderophores in LC-ESIMS data of GP15 samples. However, in incubation samples with high concentration of both Fe-siderophore and apo siderophores (measured by the addition of ^{57}Fe to the sample), we are able to detect the Fe-siderophore, and unable to detect the apo siderophores on LC-ESIMS (Chapter 4), which suggests that the sensitivity of apo siderophore is at least 20 times lower than the sensitivity of Fe-siderophores. Therefore, we cannot rule out the existence of apo

siderophores in GP15 samples and it is possible that a portion of siderophores in the North Pacific is also metal-free, which would result in even higher concentration of total siderophores.

3.3.6 Particulate organic matter contains only ferrioxamine, not amphibactins or marinobactins

In addition to low dFe:NO_3^- ratio, another explanation for the high concentrations of siderophores between 200-400 m is that siderophores are introduced by the dissolution of sinking particles sourced from the euphotic zone. In some studies, siderophore production and release to seawater was postulated to be an ineffective strategy for Fe uptake (Hutchins et al 1991; Volker and Wolf-Gladrow 1999), because a cell might not recapture the siderophores it produced, due to diffusive loss of the siderophore (Leventhal et al 2018). Therefore, Hopkinson and Morel (2009) suggests that heterotrophic bacteria produce siderophores primarily when attached to particles where losses by diffusion could be reduced.

Indeed, marinobactins are expected to be associated with POM, due to their fatty acid chain and presumed membrane affinity (Martinez et al 2000). To investigate the partitioning of siderophores between POM associated and dissolved siderophores, we measured siderophores in fourteen suspended POM samples that were located near hotspots of dissolved siderophores (Table 3.3). The 14 samples are selected from 3 stations, including Station 06 in the upwelling region, Station 08 in the transition zone between the subarctic and subtropical gyres, and Station 14 in the NPSG. Each POM sample was associated with a dissolved sample that displayed high concentrations of marinobactins or amphibactins. Therefore, these 14 POM samples are more likely to contain marinobactins or amphibactins than other POM samples.

Table 3.3: The locations where POM sample was measured for siderophores, the concentration of dissolved siderophore in the sample of closest depth, and the concentration of Ferrioxamine G in the POM samples.

Sample	Station	Depth (m)	Dissolved [Fe-siderophore]	[Ferrioxamine G] in POM
GT12706	6	38	66 pM at 20 m	7.8 pM
GT12707	6	58	35 pM at 90 m	2.8 pM
GT12709	6	248	21 pM at 250 m	0.04 pM
GT12710	6	348	21 pM at 350 m	0.02 pM
GT12875	8	61	14 pM at 65 m	0.26 pM
GT12876	8	86	8 pM at 90 m	0.04 pM
GT12877	8	145	4 pM at 150 m	
GT12878	8	195	3 pM at 200 m	
GT13395	14	71	5 pM at 75 m	0.33 pM
GT13396	14	96	6 pM at 100 m	0.32 pM
GT13397	14	121	3 pM at 125 m	0.16 pM
GT13398	14	145	11 pM at 150 m	0.05 pM
GT13399	14	296	22 pM at 300 m	
GT13400	14	499	6 pM at 500 m	

We found no marinobactins or amphibactins in any of the 14 samples of suspended POM. Therefore, our data show that amphiphilic siderophores occur primarily in the dissolved phase.

However, a polar siderophore was detected in 12 out of the 14 POM samples, and we were able to identify that siderophore as Ferrioxamine G (Figure 3.15). The MS^2 of the compound show major fragments of m/z 472, 554 and 572, which are also found in the authentic standard of Ferrioxamine G (Mawji et al 2008). The fragments at m/z 472 represents the cleavage of a peptidic bond (Mawji et al 2008). The fragments at m/z 572

represents the cleavage of a C-N bond in the hydroxamate group. The fragments at m/z 554 represents the loss of a H_2O from the fragment of 572.

Ferrioxamine G is most likely located intracellularly, and is released during our extraction process. However, the paired dissolved samples were dominated by marinobactins and amphibactins, and ferrioxamines were entirely absent in the dissolved samples from the open ocean. At this stage, we are unable to explain the presence of ferrioxamines in the POM, and their absence in seawater, which is different from the expected partitioning according to their molecular structure.

This is the first study to investigate siderophores in suspended particulate matter. However, the connection between marine particles and ferrioxamines is found to be prevalent. For example, in the presence of dust, epibionts associated with *Trichodesmium* produce ferrioxamines to promote dust dissolution and Fe uptake of *Trichodesmium* (Basu et al 2019), suggesting that ferrioxamine production might be a response to transient Fe input. This would explain not only the exclusive presence of ferrioxamines in seawater with high dFe or Fe input from dust, including coastal region (Boiteau et al 2016) and the Atlantic Ocean (Mawji et al 2008), but also the presence of ferrioxamines in the surface of the NPSG (Bundy et al 2018) and SPSG (Boiteau et al 2016), where nitrogen concentration is low and siderophore production is not expected. In contrast, amphibactins and marinobactins are found exclusively in seawater with a low Fe:NO_3^- ratio, suggesting that the production of these siderophores is a response to Fe limitation by heterotrophic bacteria.

Indeed, fast production of Ferrioxamine E by particle-associated bacteria has been reported during incubation of freshly collected sinking organic matter at 150 m of Station ALOHA (Bundy et al 2018). Similarly, production of Ferrioxamine B and Ferrioxamine G by particle-associated bacteria has been reported during incubation of suspended and slow sinking particles (> 5 μm) at 30 m of a station in the subtropical waters east of New Zealand (Velasquez et al 2016). These authors concluded that ferrioxamines were produced to acquire Fe during particle remineralization, and the presence of

ferrioxamines in suspended particles from GP15 seems to be in accordance with this conclusion.

We have no samples for siderophores in the sinking particles (e.g. > 51 μm), and we cannot rule out the production of marinobactins occurred after suspended particles aggregate into sinking particles. Metabolite composition of sinking particles could differ from surface suspended particles from which they are likely derived, suggesting that some metabolite could be produced during degradation of sinking particles (Johnson et al 2020), which could include marinobactins. At this stage, there is no evidence suggesting the existence of marinobactins in sinking particles, and it seems unlikely that the hotspots in GP15, which are dominated by marinobactins, are due to the release of siderophores from sinking POM.

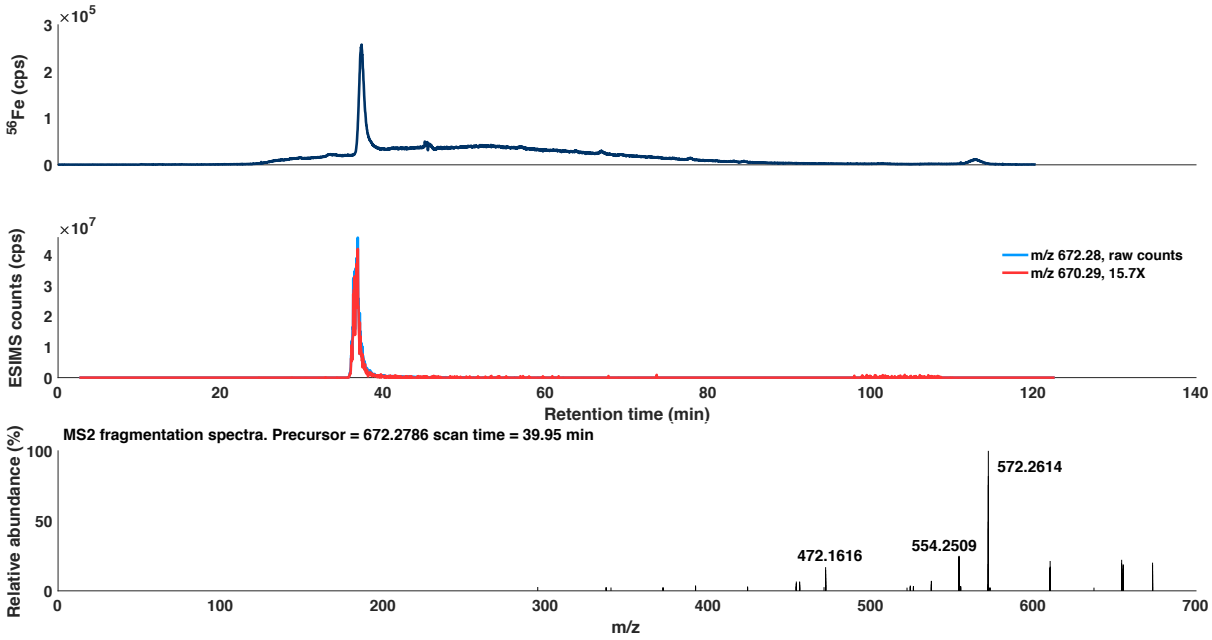

Figure 3.15: Ferrioxamine G characterization from POM samples. The top panel is ^{56}Fe LC-ICPMS chromatogram. The mid panel is extracted ion chromatograms (EIC) from positive mode LC-ESIMS chromatograms. The blue line corresponds to the ^{56}Fe-siderophore $[M+H]^+$ isotopologue and the red line corresponds to the ^{54}Fe-siderophore $[M+H]^+$ isotopologue. The intensity of the ^{54}Fe isotopologue has been scaled by 15.7, so that the isotopologues overlap. The bottom panel is the MS^2 fragmentation spectra of the ^{56}Fe-Ferrioxamine G.

3.4 Conclusion

We report the distribution of siderophores in the upper 1000 m of the US GEOTRACES GP15 Pacific Meridional Transect, from 56 °N to 20 °S along 152 °W longitude. The concentration of dissolved siderophores ranges from 0-70 pM. The distribution of siderophores features prevalent hotspots across the entire transect, suggesting that the siderophore mediated Fe transport is common in the Pacific Ocean. Most hotspots are found in the nitracline. In the NPSG and SPSG, the hotspots are found at mesopelagic depths between 200-400 m. In the upwelling regions of around 50 °N and 10 °N where nitracline is lifted to shallower depths, the hotspots are also lifted, to up to 20 m. Most hotspots are associated with a dFe:NO_3^- ratio lower than 50 µmol/mol, suggesting that low dFe and high nitrate concentration are both necessary for siderophore production. The transect is dominated by marinobactins and amphibactins. In addition to Fe-siderophores, we also find Al-siderophores, which is the first time they are reported in seawater samples.

In addition to siderophores in dissolved samples, we also measured siderophores in 14 suspended POM samples, which is the first time siderophores are measured in POM. These samples are selected at hotspots for dissolved siderophores, and are more likely to contain marinobactins or amphibactins than other POM samples. We found no marinobactins in any of the 14 samples of suspended POM, suggesting that the marinobactins and amphibactins in dissolved samples are not due to contribution of siderophores in POM. However, we found a polar siderophores in 12 out of the 14 POM samples, and we were able to identify the peak as Ferrioxamine G.

3.5 References

Martin, J. H., & Fitzwater, S. E. (1988). Iron deficiency limits phytoplankton growth in the north-east Pacific subarctic. *Nature*, *331*, 341-343.

de Baar, H. J., Buma, A. G., Nolting, R. F., Cadée, G. C., Jacques, G., & Tréguer, P. J. (1990). On iron limitation of the Southern Ocean: experimental observations in the Weddell and Scotia Seas. *Marine ecology progress series*, 105-122.

Price, N. M., Ahner, B. A., & Morel, F. M. (1994). The equatorial Pacific Ocean: Grazer-controlled phytoplankton populations in an iron-limited ecosystem 1. *Limnology and Oceanography*, *39*(3), 520-534.

Boyd, P. W., Jickells, T., Law, C. S., Blain, S., Boyle, E. A., Buesseler, K. O., ... & Watson, A. J. (2007). Mesoscale iron enrichment experiments 1993-2005: synthesis and future directions. *science*, *315*(5812), 612-617.

Pakulski, J. D., Coffin, R. B., Kelley, C. A., Holder, S. L., Downer, R., Aas, P., ... & Jeffrey, W. H. (1996). Iron stimulation of Antarctic bacteria. *Nature*, *383*, 133-134.

Kirchman, D. L., Meon, B., Cottrell, M. T., Hutchins, D. A., Weeks, D., & Bruland, K. W. (2000). Carbon versus iron limitatio

Cochlan, W. P. (2001). The heterotrophic bacterial response during a mesoscale iron enrichment experiment (IronEx II) in the eastern equatorial Pacific Ocean. *Limnology and Oceanography*, *46*(2), 428-435.

Oliver, J. L., Barber, R. T., Smith Jr, W. O., & Ducklow, H. W. (2004). The heterotrophic bacterial response during the Southern Ocean iron experiment (SOFeX). *Limnology and oceanography*, *49*(6), 2129-2140.

Ho, T. Y., Quigg, A., Finkel, Z. V., Milligan, A. J., Wyman, K., Falkowski, P. G., & Morel, F. M. (2003). The elemental composition of some marine phytoplankton 1. *Journal of phycology*, *39*(6), 1145-1159.

Sunda, W. G., & Huntsman, S. A. (1995). Iron uptake and growth limitation in oceanic and coastal phytoplankton. *Marine chemistry*, *50*(1-4), 189-206.

Tortell, P. D., Maldonado, M. T., & Price, N. M. (1996). The role of heterotrophic bacteria in iron-limited ocean ecosystems. *Nature*, *383*(6598), 330-332.

Boyd, P. W., & Ellwood, M. J. (2010). The biogeochemical cycle of iron in the ocean. Nature Geoscience, 3(10), 675-682.

Schwarzenbach, G., & Schwarzenbach, K. (1963). Hydroxamatkomplexe I. Die Stabilität der Eisen (III)-Komplexe einfacher Hydroxamsäuren und des Ferrioxamins B. *Helvetica Chimica Acta*, *46*(4), 1390-1400.

Harris, W. R., Carrano, C. J., Cooper, S. R., Sofen, S. R., Avdeef, A. E., McArdle, J. V., & Raymond, K. N. (1979). Coordination chemistry of microbial iron transport compounds. 19. Stability constants and electrochemical behavior of ferric enterobactin and model complexes. *Journal of the American Chemical Society*, *101*(20), 6097-6104.

Moeck, G. S., & Coulton, J. W. (1998). TonB-dependent iron acquisition: mechanisms of siderophore-mediated active transport. *Molecular microbiology*, *28*(4), 675-681.

Shaked, Y., Kustka, A. B., & Morel, F. M. (2005). A general kinetic model for iron acquisition by eukaryotic phytoplankton. *Limnology and Oceanography*, *50*(3), 872-882.

Kazamia, E., Sutak, R., Paz-Yepes, J., Dorrell, R. G., Vieira, F. R. J., Mach, J., ... & Lesuisse, E. (2018). Endocytosis-mediated siderophore uptake as a strategy for Fe acquisition in diatoms. *Science Advances*, *4*(5), eaar4536.

Coale, T. H., Moosburner, M., Horák, A., Oborník, M., Barbeau, K. A., & Allen, A. E. (2019). Reduction-dependent siderophore assimilation in a model pennate diatom. *Proceedings of the National Academy of Sciences*, *116*(47), 23609-23617.

Mawji, E., Gledhill, M., Milton, J. A., Tarran, G. A., Ussher, S., Thompson, A., ... & Achterberg, E. P. (2008). Hydroxamate siderophores: occurrence and importance in the Atlantic Ocean. *Environmental science & technology*, *42*(23), 8675-8680.

Boiteau, R. M., Fitzsimmons, J. N., Repeta, D. J., & Boyle, E. A. (2013). Detection of iron ligands in seawater and marine cyanobacteria cultures by high-performance liquid chromatography–inductively coupled plasma-mass spectrometry. *Analytical chemistry*, *85*(9), 4357-4362.

Boiteau, R. M., Mende, D. R., Hawco, N. J., McIlvin, M. R., Fitzsimmons, J. N., Saito, M. A., ... & Repeta, D. J. (2016). Siderophore-based microbial adaptations to iron scarcity across the eastern Pacific Ocean. *Proceedings of the National Academy of Sciences*, *113*(50), 14237-14242.

Bundy, R. M., Boiteau, R. M., McLean, C., Turk-Kubo, K. A., McIlvin, M. R., Saito, M. A., ... & Repeta, D. J. (2018). Distinct siderophores contribute to iron cycling in the mesopelagic at station ALOHA. *Frontiers in Marine Science*, *5*, 61.

Boiteau, R. M., Till, C. P., Coale, T. H., Fitzsimmons, J. N., Bruland, K. W., & Repeta, D. J. (2019). Patterns of iron and siderophore distributions across the California Current System. *Limnology and Oceanography*, *64*(1), 376-389.

Gledhill, M., Zhu, K., Rusiecka, D., & Achterberg, E. P. (2022). Competitive interactions between microbial siderophores and humic-like binding sites in european shelf sea waters. *Frontiers in Marine Science*, *9*, Art-Nr.

Park, J., Durham, B. P., Key, R. S., Groussman, R. D., Pinedo-Gonzalez, P., Hawco, N. J., ... & Bundy, R. M. (2022). Siderophore production and utilization by microbes in the North Pacific Ocean. *bioRxiv*, 2022-02.

Martinez, J. S., Zhang, G. P., Holt, P. D., Jung, H. T., Carrano, C. J., Haygood, M. G., & Butler, A. (2000). Self-assembling amphiphilic siderophores from marine bacteria. *Science*, *287*(5456), 1245-1247.

Martinez, J. S., Carter-Franklin, J. N., Mann, E. L., Martin, J. D., Haygood, M. G., & Butler, A. (2003). Structure and membrane affinity of a suite of amphiphilic siderophores produced by a marine bacterium. *Proceedings of the National Academy of Sciences*, *100*(7), 3754-3759.

Lam, P. J., Lee, J. M., Heller, M. I., Mehic, S., Xiang, Y., & Bates, N. R. (2018). Size-fractionated distributions of suspended particle concentration and major phase composition from the US GEOTRACES Eastern Pacific Zonal Transect (GP16). Marine Chemistry, 201, 90-107.

Li, J., Boiteau, R. M., Babcock-Adams, L., Acker, M., Song, Z., McIlvin, M. R., & Repeta, D. J. (2021). Element-Selective Targeting of Nutrient Metabolites in Environmental Samples by Inductively Coupled Plasma Mass Spectrometry and Electrospray Ionization Mass Spectrometry. *Frontiers in Marine Science*, *8*, 630494.

Boiteau, R. M., & Repeta, D. J. (2015). An extended siderophore suite from Synechococcus sp. PCC 7002 revealed by LC-ICPMS-ESIMS. *Metallomics*, *7*(5), 877-884.

Chambers, M. C., Maclean, B., Burke, R., Amodei, D., Ruderman, D. L., Neumann, S., ... & Mallick, P. (2012). A cross-platform toolkit for mass spectrometry and proteomics. Nature biotechnology, 30(10), 918-920.

Fitzsimmons, J. N., Hayes, C. T., Al-Subiai, S. N., Zhang, R., Morton, P. L., Weisend, R. E., ... & Boyle, E. A. (2015). Daily to decadal variability of size-fractionated iron and iron-binding ligands at the Hawaii Ocean Time-series Station ALOHA. *Geochimica et Cosmochimica Acta*, *171*, 303-324.

Moore, C. M., Mills, M. M., Arrigo, K. R., Berman-Frank, I., Bopp, L., Boyd, P. W., ... & Ulloa, O. (2013). Processes and patterns of oceanic nutrient limitation. *Nature geoscience*, *6*(9), 701-710.

Hutchins, D. A., Rueter, J. G., & Fish, W. (1991). Siderophore production and nitrogenfixation are mutually exclusive strategies in Anabaena 712. *Limnology and oceanography*, *36*(1), 1-12.

Hider, R. C., & Kong, X. (2010). Chemistry and biology of siderophores. Natural product reports, 27(5), 637-657.

Boiteau, R. M. (2016). Molecular determination of marine iron ligands by mass spectrometry (Doctoral dissertation, Massachusetts Institute of Technology).

Cherkupally, P., Ramesh, S., Govender, T., Kruger, H. G., Beatriz, G., & Albericio, F. (2015). An efficient solid-phase strategy for total synthesis of naturally occurring amphiphilic marine siderophores: amphibactin-T and moanachelin ala-B. *Organic & Biomolecular Chemistry*, *13*(16), 4760-4768.

Hu, X., & Boyer, G. L. (1996). Siderophore-mediated aluminum uptake by Bacillus megaterium ATCC 19213. *Applied and Environmental Microbiology*, *62*(11), 4044-4048.

Martell, A. E., Smith, R. M., & Motekaitis, R. J. (2004). Critically Selected Stability Constants of Metal Complexes: Version 8.0. *National Insitutue of Standards and Technology, Gainesburg*.

Gledhill, M., McCormack, P., Ussher, S., Achterberg, E. P., Mantoura, R. F. C., & Worsfold, P. J. (2004). Production of siderophore type chelates by mixed bacterioplankton populations in nutrient enriched seawater incubations. *Marine Chemistry*, *88*(1-2), 75-83.

Garrison, J. M., & Crumbliss, A. L. (1987). Hydroxamic acid ligand-exchange kinetics at hexaaquoaluminum ion. Inorganic Chemistry, 26(22), 3660-3664.

van den Berg, C. M., Boussemart, M., Yokoi, K., Prartono, T., & Campos, M. L. A. (1994). Speciation of aluminium, chromium and titanium in the NW Mediterranean. Marine Chemistry, 45(4), 267-282.

Noinaj, N., Guillier, M., Barnard, T. J., & Buchanan, S. K. (2010). TonB-dependent transporters: regulation, structure, and function. *Annual review of microbiology*, *64*, 43-60.

Völker, C., & Wolf-Gladrow, D. A. (1999). Physical limits on iron uptake mediated by siderophores or surface reductases. Marine Chemistry, 65(3-4), 227-244.

Leventhal, G. E., Ackermann, M., & Schiessl, K. T. (2019). Why microbes secrete molecules to modify their environment: the case of iron-chelating siderophores. *Journal of the Royal Society Interface*, *16*(150), 20180674.

Hopkinson, B. M., & Morel, F. M. (2009). The role of siderophores in iron acquisition by photosynthetic marine microorganisms. *Biometals*, *22*, 659-669.

Basu, S., Gledhill, M., de Beer, D., Prabhu Matondkar, S. G., & Shaked, Y. (2019). Colonies of marine cyanobacteria Trichodesmium interact with associated bacteria to acquire iron from dust. Communications biology, 2(1), 284.

Velasquez, I. B., Ibisanmi, E., Maas, E. W., Boyd, P. W., Nodder, S., & Sander, S. G. (2016). Ferrioxamine siderophores detected amongst iron binding ligands produced during the remineralization of marine particles. *Frontiers in Marine Science*, *3*, 172.

Johnson, W. M., Longnecker, K., Kido Soule, M. C., Arnold, W. A., Bhatia, M. P., Hallam, S. J., ... & Kujawinski, E. B. (2020). Metabolite composition of sinking particles differs from surface suspended particles across a latitudinal transect in the South Atlantic. *Limnology and Oceanography*, *65*(1), 111-127.

Chapter 4 Fast Fe uptake from siderophores at 200-400 m in the North Pacific Subtropical Gyre

4.1 Introduction

It has been well established that Fe limits phytoplankton growth in ~30% of the surface ocean (Boyd et al 2007). In these regions, deep water with an dFe:NO_3^- ratio of 20 μmol/mol (dFe ~0.8 nM, NO_3^- ~40 μM, Schlitzer et al 2018) upwells to the surface, where phytoplankton take up the two nutrients in a ratio of 500 μmol/mol in Fe sufficient cultures (Ho et al 2003). Therefore, in the absence of external Fe input, iron is depleted before nitrate and thereby becomes the principal nutrient that limits phytoplankton growth. This concept has been confirmed by mesoscale Fe fertilization experiments where addition of exogenous Fe leads to an increase in chlorophyll and a drawdown of nitrate in virtually all experiments (de Baar et al 2005).

Iron limitation of heterotrophic bacteria is less well understood. In the surface waters with low concentrations of dFe (< 0.2 nM, Boyd and Ellwood, 2010), the growth of heterotrophic bacteria is constrained primarily by labile organic carbon, instead of dFe (Church et al 2000; Kirchman et al 2000; Fourques et al 2020). Below the euphotic zone, dissolved iron concentrations rise, and the supply of labile carbon falls. Iron limitation of heterotrophic bacteria seems less likely in the mesopelagic.

However, our analyses of water column profiles from the GEOTRACES GP15 Pacific Meridional Transect showed elevated concentrations of siderophores at mesopelagic depths of 200-400 m in the North and South Pacific Subtropical Gyres (NPSG and SPSG, Chapter 3, Figure 3.4). The distribution of siderophores in the mesopelagic was dominated by marinobactins and less frequently by amphibactins, which are produced by heterotrophic bacteria grown in low Fe media to facilitate Fe uptake. Therefore, one explanation for the high concentrations of marinobactins in the mesopelagic is that siderophores are being produced by heterotrophic bacteria in response to the unexpected Fe limitation.

Bacterial production in the mesopelagic is limited by the supply of labile organic carbon substrates. Marinobactins and amphibactins are low molecular weight peptide and lipid hybrid compounds, that are easily taken up and metabolized by bacteria. For example, when seawater from 25-100 m of Station ALOHA was incubated with 20 nM leucine, the leucine uptake rate in the dark was 14-34 pM/h (Church et al 2004), and the turnover time was 59-143 h. We expect marinobactins and amphibactins to be bioavailable as labile carbon substrate, although the turnover might be slower than leucine. If these siderophores are being used in the mesopelagic to facilitate Fe uptake, then uptake must be fast enough to effectively compete with loss to metabolism as labile carbon. This line of reasoning suggests that siderophores cycling in the mesopelagic must be dynamic.

In contrast, high concentrations of siderophores in the mesopelagic could also be attributed to slow uptake of siderophores that were introduced by lateral transport or locally from rapidly sinking particles. In this scenario both consumption and production are slow, which suggests that siderophores are not a dynamic Fe pool, and heterotrophic bacteria are not Fe limited. Because our GP15 data represents only a snapshot of siderophore concentrations at the time of sampling, they do not allow us to distinguish these two possibilities. To evaluate potential Fe limitation of heterotrophic bacteria in the mesopelagic, and the processes that lead to elevated siderophore concentrations in this region, we need to make rate measurements of Fe uptake from siderophores.

The Fe uptake rate from siderophores could be measured by radio- or stable isotope tracers. In radiotracer uptake experiments, ^{55}Fe or ^{59}Fe is bound to siderophores, and the complexes are incubated with natural populations of microbes in seawater for a few hours. After incubation, the sample is filtered, and the intracellular ^{55}Fe or ^{59}Fe activity is measured to determine the Fe uptake rate. Indeed, this has been the only approach that has been used to measure Fe uptake rates in seawater, and it has largely promoted our understanding on the bioavailability of Fe in multiple siderophores to different

phytoplankton and bacteria (Hutchins et al 1999, Maldonado et al 1999, Lis et al 2015). However, due to the low specific activity of the radiotracers, uptake measurements often involve addition of nM amendments of Fe-siderophores. Therefore, the Fe speciation in the experiment does not represent natural, unperturbed conditions, as in situ siderophore concentrations are typically on the order of pM. In addition, while these experiments measure the uptake of Fe, iron uptake in these experiments account for only a small portion of the Fe addition, and the turnover of siderophore after Fe uptake is not reported, because siderophores were not directly measured. Furthermore, iron uptake rate data are rare, due to the constraints of using radiotracers and the intensive onboard sample processing required for these experiments.

In this chapter, I introduce an Fe uptake measurement based on LC-ICPMS, using ^{57}Fe as a stable isotope tracer. This method does not involve radiotracer, which makes it more logistically applicable. The limit of detection for Fe-siderophore complexes by LC-ICPMS is 30-250 femtomoles (Boiteau et al 2013), and the limit of quantification is 100-800 femtomoles. Therefore, the incubation could be performed with pM additions of ^{57}Fe-siderophores in 2 L seawater, which allows for a more realistic Fe speciation in the experiment. Siderophore concentration, including ^{57}Fe-siderophore, ^{56}Fe-siderophore, ^{27}Al-siderophore and non-metallated (apo) siderophores in the media are quantified before and after the incubation, which allows Fe uptake and siderophores to be tracked independently.

To investigate the turnover of siderophores in the upper water column around Station ALOHA, we labeled suites of amphibactin and marinobactin siderophores with ^{57}Fe. Amphibactins and Marinobactins were the two most prevalent classes of siderophores found between 200-500 m in the NPSG sampled by GEOTRACES GP15, and at Station ALOHA (Bundy et al 2018). We performed Fe uptake experiments by amending unfiltered seawater collected between 75-500 m for five days and measuring the loss of ^{57}Fe siderophores over time.

4.2 Methods

4.2.1 Culturing for the production of amphibactins and marinobactins

Amphibactins were produced by *Vibrio* 1F53 culture under Fe limitation induced by the addition of desferrioxamine B (Li et al., 2021). One liter of culture was pumped at 20 mL/min through a 0.2 μm PES capsule filter (Millipore), and Bond-Elut ENV solid phase extraction (SPE) column (1 g, 6 mL, Agilent Technologies) that had been previously activated by passing 6 mL each of distilled methanol (MeOH, Optima LCMS grade, Fisher Scientific) and ultrapure water (qH_2O, 18.2 MΩ) through the column. After extraction, the column was washed with 6 mL qH_2O (to reduce salts) and the qH_2O wash was discarded. Amphibactins were then eluted with 6 mL distilled MeOH into acid-cleaned 10 mL polypropylene tubes.

Marinobactins were produced by *Alteromonas* 2E5 and *Pseudoalteromonas* 2E11 culture (Boiteau 2016). For each culture, 25 mL of media was pumped through 0.2 μm PES Sterivex (MilliporeSigma), and C18 SPE columns (0.5 g, Biotage). The column was rinsed with qH_2O and eluted with 5 mL MeOH. The extracts were concentrated to ~300 μL under a stream of nitrogen.

4.2.2 Labeling of amphibactins and marinobactins with ^{57}Fe

The amphibactins produced by *Vibrio* are dominated by non-metallated (apo) siderophores, due to the induction of Fe limitation arising from the presence of 10 nM desferrioxamine B in culture media (Li et al 2021). To prepare isotopically labeled amphibactins, ^{57}Fe oxide (Cambridge Isotope Laboratories) was dissolved in concentrated HCl (Optima, Fisher Scientific) as a stock solution of 33.9 mM ^{57}Fe (180 μL HCl per 1 mg $^{57}Fe_2O_3$). Five microliters (5 μL) of this ^{57}Fe stock solution was added to an aliquot of 500 μL of MeOH extract of SPE column, which contained amphibactins from the *Vibrio* culture. After one hour, the mixture is diluted with 500 mL of qH_2O, which results in a MeOH content of 0.1% for the solution. The solution was extracted by a Bond-Elut ENV cartridge (1 g, 6 mL, Agilent Technologies) at 20 mL/min, to remove excess ^{57}Fe. The SPE columns were then washed with 6 mL of MQ and eluted with 6

mL of MeOH. The MeOH extract was concentrated to approximately 500 µL by vacuum centrifugation (SpeedVac, Thermo Scientific), and used as amphibactin stock solution.

The marinobactins produced by *Alteromonas* and *Pseudoalteromonas* were dominated by ^{56}Fe-siderophores, due to higher concentration of Fe (125 nM), and the absence of desferrioxamine B in the growth media (Boiteau 2016). To label marinobactin with ^{57}Fe, 100 µL of ^{57}Fe stock solution was added to 10 mL of qH_2O, to create an ^{57}Fe stock solution of pH ~1, which facilitates the isotope exchange from ^{56}Fe to ^{57}Fe. Then, 500 µL of MeOH extract of *Alteromonas* and *Pseudoalteromonas* were combined and added to the ^{57}Fe stock solution. After two days, the mixture was diluted with 1000 mL of MQ, neutralized with 10 mL 100 mM $NaHCO_3$, and extracted by a Bond-Elut ENV column, to remove excess ^{56}Fe and ^{57}Fe. Then, the column was washed with qH_2O and eluted with MeOH. The MeOH extract was concentrated to approximately 500 µL by vacuum centrifugation and used as marinobactin stock solution.

4.2.3 Incubation for Fe-siderophore uptake rate measurement

Samples for Fe uptake experiments were collected onboard the *R/V* Kilo Moana at three stations near Station ALOHA (22.45 °N, 158.0 °W) during PARAGON I in August 2021 (PG2021, 21.87 °N, 156.30 °W) and PARAGON II in August 2022 (PG2022, Station 2 at 23.41 °N, 154.63 °W, Station 3 at 23.29 °N, 155.32 °W). For example, seawater for the incubation of PG2022-S3C2 was collected using a 24×12 L Niskin bottle rosette equipped with a conductivity, temperature, depth package (SBE 911Plus; Sea-Bird Scientifc) along with fluorescence, oxygen and transmissometer sensors. Two liters (2 L) of unfiltered seawater was sampled from 10 depths between 75-500 m into acid cleaned 2 L polycarbonate bottles. Additional samples of filtered and unfiltered seawater were taken at 200 m and 400 m for experimental controls and measurements of the initial conditions. For the filtered control, samples were filtered directly from the Niskin bottle through an in-line 0.2 µm Acropak-1500 Supor cartridge (Pall).

For each of the fourteen samples, 20 µL of amphibactin stock solution and 20 µl of marinobactin stock solution were added. Then, the two samples for time zero (T0) measurements were pumped at 10 mL/min through 0.2 µm PES capsule filter (MilliporeSigma), and immediately extracted by Bond-Elut ENV SPE columns. Processing took ~3 hours between introduction of the siderophore amendment and the removal of microbial cells by filtration. The twelve samples for uptake experiments were wrapped in 4 mil black plastic, and placed in a temperature-controlled water bath incubator at 25 °C. After 5 days, the final timepoint samples (Tf) were filtered and extracted using the same procedure as for the T0 samples. SPE columns were frozen (-20 °C) immediately after sample collection and returned to the laboratory for processing.

4.2.4 High pressure liquid chromatography-Inductively coupled plasma mass spectrometry

The LC-ICPMS analyses were described in detail in Chapter 2, except that the post-column addition of 35 µL/min water was not implemented. Therefore, the 10 µL of LC eluant was directly introduced into ICPMS. Isotopes monitored were ^{56}Fe (integration time 0.05 s), ^{54}Fe (0.02 s), ^{57}Fe (0.02 s), ^{69}Ga (0.05 s), ^{71}Ga (0.02 s) and ^{27}Al (0.02 s).

4.3 Results and discussion

4.3.1 ^{57}Fe labeling was successful for both amphibactins and marinobactins

The integrity of the ^{57}Fe-siderophere amendment was established by measuring the chromatographic and isotopic properties of the amphibactin or marinobactin mixture by LC-ICPMS. The results show that the impurity of ^{56}Fe-siderophore accounted for 5-10% of the ^{56}Fe-siderophore concentration (Figure 4.1, Table 4.1). In addition, both siderophore stock solutions show no peak in Fe at the solvent front on LC-ICPMS, suggesting that the stock solution does not contain inorganic ^{57}Fe or ^{56}Fe. The baseline is low for both ^{57}Fe and ^{56}Fe, suggesting that the concentration of other Fe ligand complexes is low in the stock solutions. Therefore, the Fe-siderophore addition to the

incubation would be dominated by ^{57}Fe-siderophore, with little contamination from other Fe ligands, inorganic Fe, or ^{56}Fe-siderophores.

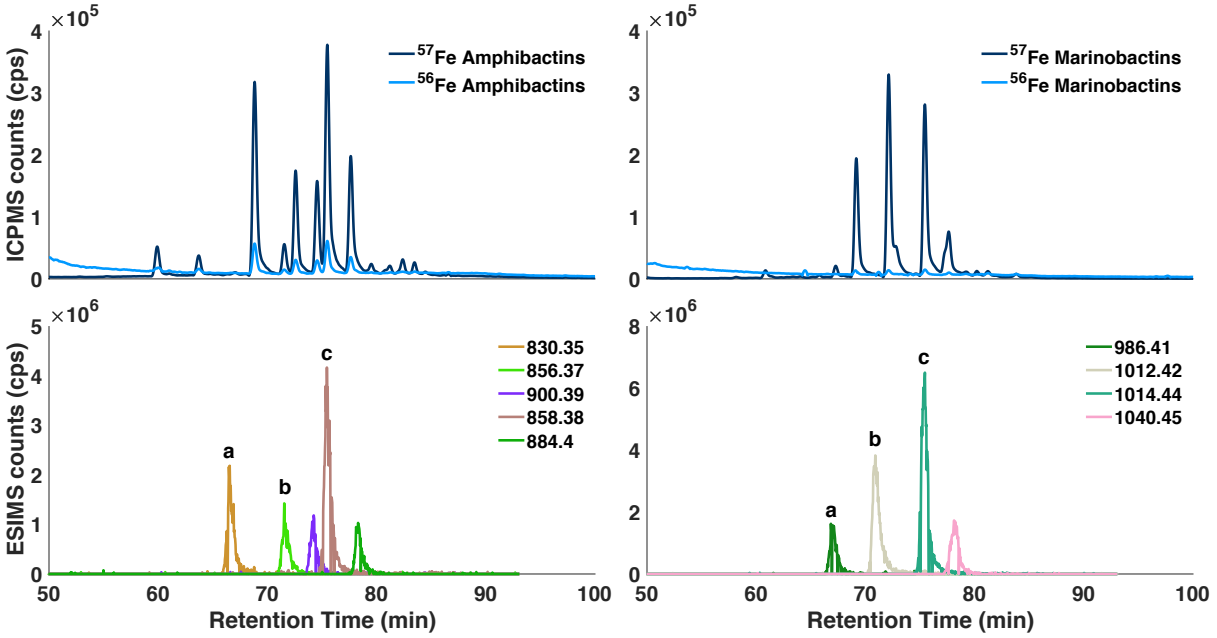

Figure 4.1: Top panels show the LC-ICPMS chromatograms of amphibactin stock solution (left) and marinobactin stock solution (right). The dark blue line indicates the counts for ^{57}Fe and the light blue line indicates the counts for ^{56}Fe. Bottom left panels show the extracted ion chromatograms (EIC) from positive mode LC-ESIMS for ^{57}Fe-amphibactins in the amphibactin stock solution. Peaks **a-c** represent ^{57}Fe-Amphibactin-$C_{10:0}$ (m/z 830.35), ^{57}Fe- Amphibactin-$C_{12:1}$ (m/z 856.37), and ^{57}Fe-Amphibactin-T (m/z 858.38). Bottom right panel show the EIC for ^{57}Fe-marinobactins in the marinobactin stock solution. Peaks **a-c** represent ^{57}Fe-Marinobactin A (m/z 986.41), ^{57}Fe-Marinobactin B (m/z 1012.42), and ^{57}Fe-Marinobactin-C (m/z 1014.44).

When amphibactins and marinobactins were mixed, some siderophores coeluted under the LC conditions used for this study, and in some cases multiple siderophores eluted as a single peak on ICPMS. For example, the peak **a** on the chromatogram of amphibactin stock solution and the peak **a** on the chromatogram of marinobactin stock solution coeluted, due to similar retention time (Figure 4.1).

In the mixture, we found 10 different peaks in the ^{57}Fe-chromatogram representing > 20 different siderophores using our chromatographic conditions. All of the peaks were quantified before and after the incubation, but the following discussion will focus only on the three major peaks as representative of all siderophores in the mixture. The bold letters **a-c** were used to represent the three major peaks on the chromatogram of ICPMS, recognizing that each peak includes an Fe-amphibactin and an Fe-marinobactin. Peak **a** is a combination of ^{57}Fe-Amphibactin-$C_{10:0}$. and ^{57}Fe-Marinobactin A (Figure 4.1). Amphibactin $C_{10:0}$ is a novel amphibactin that has not been previously reported in the literature. Amphibactin $C_{10:0}$ differs from Amphibactin T by -C_2H_4- on the fatty acid chain. Peak **b** is a combination ^{57}Fe-Amphibactin $C_{12:1}$ and ^{57}Fe-Marinobactin B. Amphibactin $C_{12:1}$ is also a novel amphibactin that differs from Amphibactin T by having two fewer hydrogens. Peak **c** is a combination ^{57}Fe-Amphibactin T and ^{57}Fe-Marinobactin C.

These assignments are verified by analysis of the MS^2 spectra. For example, the MS^2 of ^{57}Fe-Amphibactin T (m/z = 858.38) show major fragments of m/z 486.12, 581.26 and 668.29 (Figure 4.2). The fragment at m/z 486 represents the cleavage of a peptidic bond on the head group, and it retains ^{57}Fe according to the fragment mass. The fragments at m/z 581 and 668 represent the cleavage of another two peptidic bonds on the head group and they do not retain ^{57}Fe. These fragmentation patterns are characteristic of amphibactins (Vraspir et al 2011; Boiteau et al 2016).

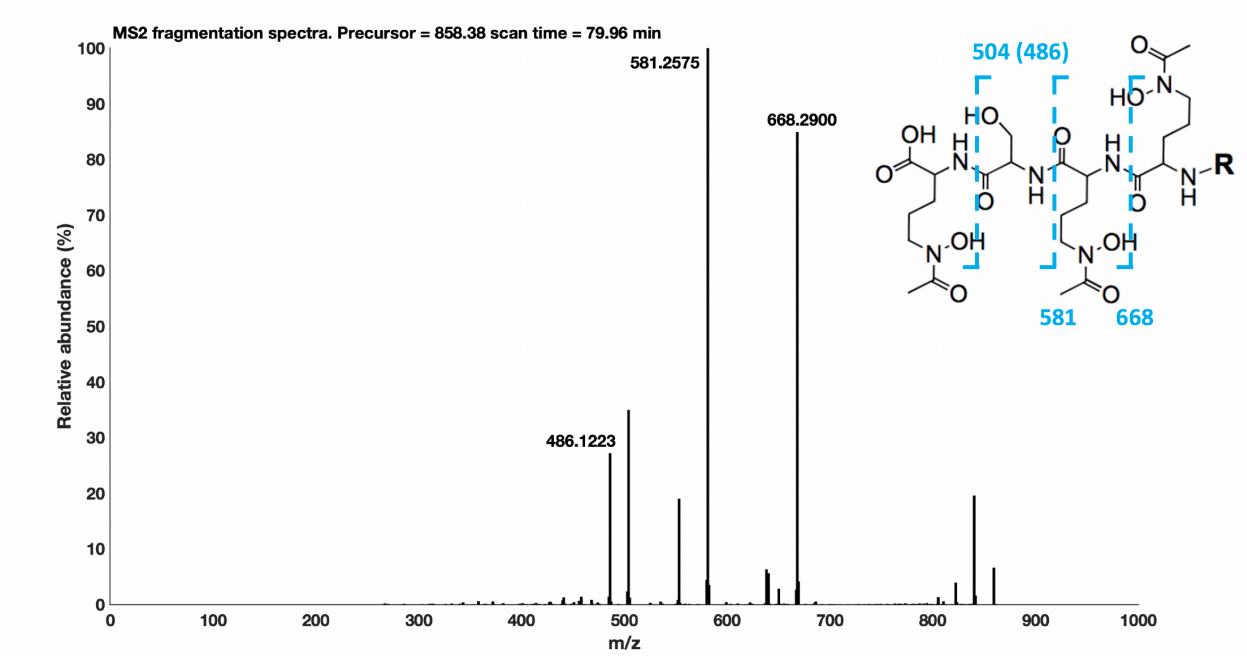

Figure 4.2: MS^2 fragmentation spectra of the ^{57}Fe-Amphibactin T. The blue dashed lines indicate characteristic cleavage of peptidic bonds in amphibactins, which results in fragments as shown in the spectra.

The MS^2 fragmentation spectrum of ^{57}Fe-Marinobactin C (m/z = 1014.44) shows major fragments at m/z 486.12, 573.15 and 743.22 (Figure 4.3). We also grew culture of *Pseudomonas mendocina* (P/N 25411, ATCC) in nutrient broth (P/N 234000, BD) with 10 nM DFB to induce Fe limitation, and found a suite of marinobactins in the spent media. The MS^2 fragmentation spectrum of ^{56}Fe-Marinobactin C isolated from *Pseudomonas mendocina* (m/z = 1013.44) shows major fragments at m/z 485.12, 572.15 and 742.23.

According to the comparison between ^{57}Fe-Marinobactin C and ^{56}Fe-Marinobactin C, all three fragments retain Fe, and the difference of ^{57}Fe and ^{56}Fe results in the difference of 1.0005 amu for these pairs of fragments. For ^{57}Fe-Marinobactin C, the fragment at m/z 486 represents diagnostic cleavage of a peptidic bond (Kem et al 2015), and a further loss of H_2O (m/z 18). The fragment at m/z 486 was also found in the MS^2 of ^{57}Fe-Amphibactin T, due to the same structure of Fe-Marinobactin C and Fe-Amphibactin T

after the neutral loss (the loss of small molecules that are neutral in charge, Figure 4.2 and Figure 4.3). Similarly, the fragment at m/z 573 represents a diagnostic cleavage of another peptidic bond, and a further loss of H_2O.

The fragment at m/z 743 has not been reported for marinobactins, but it was present in all ^{57}Fe-Marinobactins, including Marinobactins A-E, which differ only on the fatty acid chain. Therefore, the common fragment at 743 does not retain the fatty acid chain. For the fragment of 743 in ^{57}Fe-Marinobactin C, the exact mass of the neutral loss is 271.2158, and two molecular formula could be assigned for the neutral loss, within three times of mass deviation (Δ m), including $C_{15}H_{29}NO_3$ and $C_{18}H_{27}N_2$. However, neither of the two formula seem reasonable, and we are not able to explain the fragment of 743 at this stage.

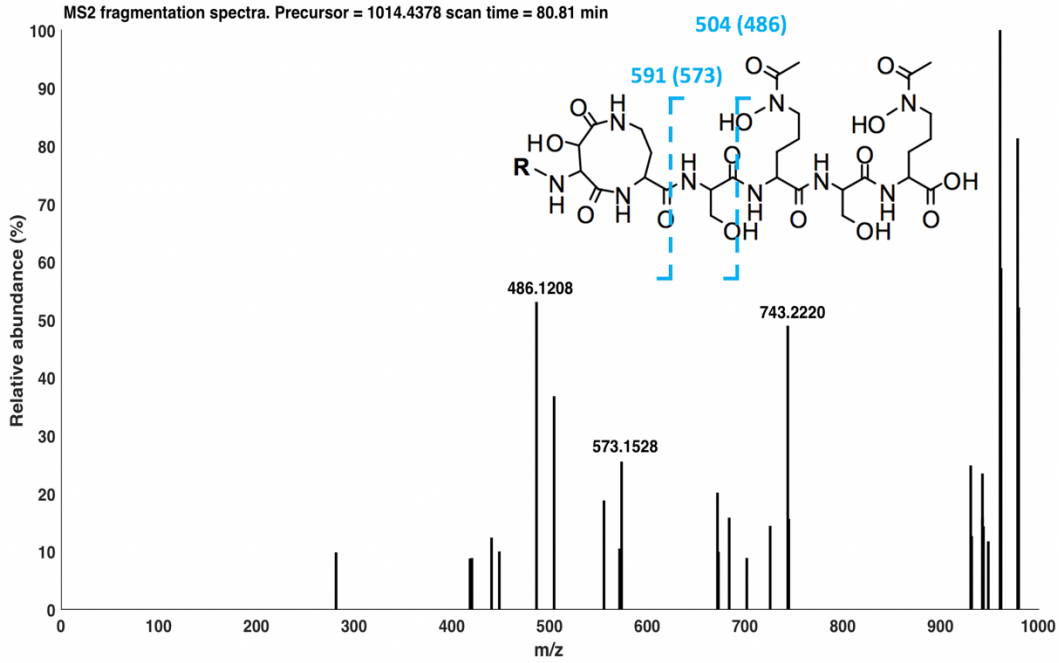

Figure 4.3: MS^2 fragmentation spectra of the ^{57}Fe-Marinobactin C. The blue dashed lines indicate characteristic cleavage of peptidic bonds for marinobactins, which results in fragments as shown in the spectra.

4.3.2 Fast drawdown of ^{57}Fe-siderophore was found in the upper mesopelagic in PG2021

Station ALOHA is a long-term oceanographic study site representative of the ecology and biogeochemistry of the North Pacific Subtropical Gyre (NPSG). At Station ALOHA, high irradiance throughout the year increases the temperature of surface waters and decreases the density of surface waters, which results in a permanent mixed layer of ~60 m. Therefore, there is little seasonal or interannual changes in nutrient distribution, chlorophyll a distribution and euphotic zone integrated primary production (Karl et al 2021).

The permanent stratification results in depletion of nutrients and extreme oligotrophy in the surface mixed layer, represented by low chlorophyll a (< 100 ng/L), low nitrate (< 10 nmol/L, Figure 4.4), and low biomass (< 2 µgC/L Karl and Church 2014). As a result, Station ALOHA features a deep chlorophyll maximum (DCM) at 100-125 m, where phytoplankton community could access both light from above, and inorganic nutrients from below.

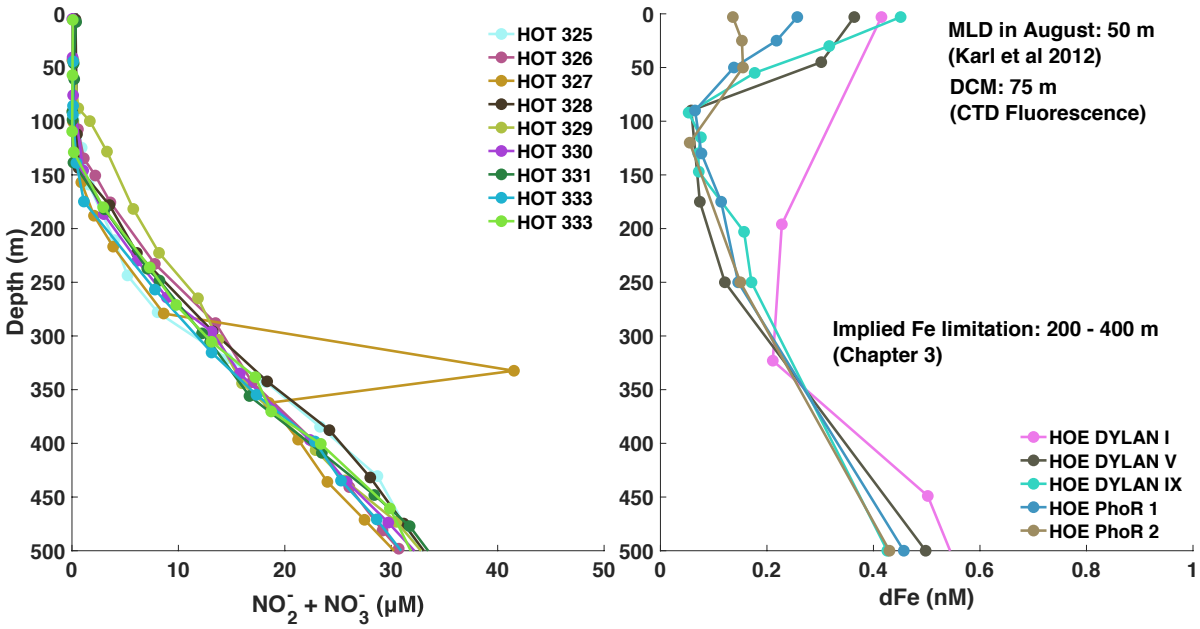

Figure 4.4: Distribution of nitrate and nitrite, and dissolved Fe at Station ALOHA. The N data is retrieved from Hawaii Ocean Time-series program (HOT) for the recent 9 cruises from December 2020 to November 2021. The dFe data is reproduced from Fitzsimmons et al (2015), and the samples were collected between May and September. The mixed layer depth at Station ALOHA in August is 50 m (Karl et al 2012). The DCM at the station for our incubation experiment was 75 m, according to the CTD fluorescence. The depth for implied Fe limitation on heterotrophic bacteria is 200-400 m, according to the siderophore distribution in Chapter 3.

In the euphotic zone of Station ALOHA, *Prochlorococcus* is the numerically dominant phytoplankton, and the highest abundance is found near the DCM (Campell et al 1997). *Synechococcus* is less abundant numerically than *Prochlorococcus* and is generally restricted to the upper 100 m. The eukaryotic algae show similar abundance to *Synechococcus*. The vertical distribution of heterotrophic bacteria abundance is uniform, but typically the maximum abundance is found in the surface mixed layer. Below the euphotic zone, the abundance of prokaryotic decrease exponentially with depth (Martinez-Garcia 2017), following the pattern of POC flux (Karl et al 2022).

At Station ALOHA, the vertical distribution of dFe features a decrease from ~400 pM at the surface to ~50 pM at the DCM (Figure 4.4, Fitzsimmons et al 2015). Then, dissolved

iron concentrations gradually increase with depth to ~600 pM at 750 m. Even though the dFe concentration show some temporal variation between 0-200 m (Fitzsimmons et al 2015) due to sporadic dust input (Boyle et al 2005; Hayes et al 2015) or mesoscale eddies (Hawco et al 2021), the dFe concentration at 200-750 m shows little temporal variation (Fitzsimmons et al 2015). The nitracline is found at the similar depths as the ferricline (Figure 4.4), but the increase in concentration with depth for nitrate is much faster than for Fe, from below detection limit at the DCM, to ~30 μM at 500 m (Figure 4.4).

As a result, the mesopelagic depths of 200-500 m are associated with a dFe:NO_3^- ratio lower than 50 μmol/mol, whereas the surface water is associated with a dFe:NO_3^- ratio higher than 50 μmol/mol. Heterotrophic bacteria including *Pseudomonas* spp. grown under low Fe concentrations have a cellular Fe:C ratio of ~8 μmol/mol (Tortell et al 1996), or an Fe:N ratio of ~50 μmol/mol assuming Redfield stoichiometry. Therefore, between 200 and 500 m, heterotrophic bacteria are likely to be Fe limited with respect to N.

To investigate the possible Fe limitation on heterotrophic bacteria in the upper water column of NPSG, we performed an uptake experiment in 2021 (PG2021) at a station near Station ALOHA. At the station, no siderophores were detected in seawater samples collected at the depths of the uptake experiments.

The mixture of ^{57}Fe-marinobactins and ^{57}Fe-amphibactins shown in Figure 4.1 was added to unfiltered seawater from different depths, and incubated at 50% of surface light for 5 days. In addition to unfiltered samples, we added ^{57}Fe-siderophores to a sample of filtered seawater collected at 75 m, and incubated the filtrate for 5 days as a control.

On Tf, we found almost complete consumption of all of the siderophores between 200 and 350 m (Figure 4.5). In this experiment, we did not have a sample for T0, and we assumed that the concentration of ^{57}Fe-siderophore in the filtered control could

represent the concentration on T0. This assumption will be tested below. During the incubation, there might be siderophore production. However, the ^{57}Fe-siderophore will not measurably form, due to the low natural abundance of ^{57}Fe (2%). Therefore, there is only a sink, but not a source of ^{57}Fe-siderophore, allowing it to be used as a tracer of Fe uptake. The drawdown of ^{57}Fe-siderophore in unfiltered samples from the filtered control, and presumably from samples on T0, represents the uptake of Fe or siderophore by microbes.

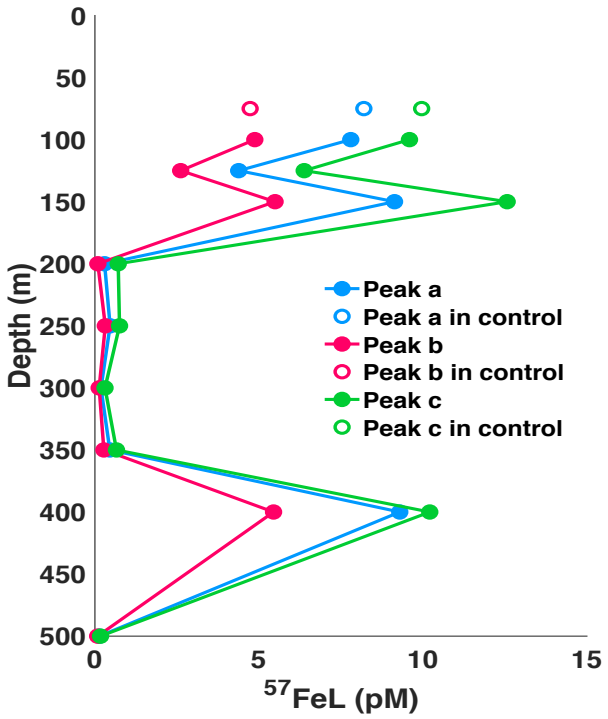

Figure 4.5: The results of incubation in PG2021. The blue line indicates the concentration for peak **a**, the red line indicates the concentration for peak **b**, the green line indicates the concentration for peak **c**. Solid circle indicates the concentration in the unfiltered sample on Tf, and open circle indicates the concentration in the filtered control on Tf, which was only prepared at 75 m.

This depth interval of fast consumption of ^{57}Fe-marinobactins and ^{57}Fe-amphibactins coincides with the depth of siderophore hotspots in NPSG (200-400 m, Chapter 3), which were dominated by marinobactins and amphibactins, and earlier measurements

of water column siderophore distribution by Bundy et al (2018), which showed high concentration of amphibactins at 300 m. Therefore, the depths of 200-400 m feature both a high concentration of Fe-siderophores and a fast turnover of Fe-siderophores.

However, it is not clear whether the drawdown was due to the acquisition of ^{57}Fe, or the metabolism of siderophores as N-rich labile carbon substrates, which could also cause the drawdown of ^{57}Fe-siderophores. Furthermore, it is unknown whether the uptake was dominated by phytoplankton or heterotrophic bacteria, as the incubation was performed under light.

4.3.3 Fast drawdown of ^{57}Fe-siderophore was found again at upper mesopelagic in PG2022.

To address these issues, we performed three additional experiments at two stations near Station ALOHA in 2022, including two experiments at Station 2 (PG2022-S2TM2 and PG2022-S2TM3), and one experiment at Station 3 (PG2022-S3C2). Siderophore concentration in situ were below the detection limit of our analyses at all incubation depths at all stations at the time of our experiment.

All three experiments show similar results, and the discussion will focus on PG2022-S3C2. The other two experiments will be summarized at the end of the discussion. The siderophore mixture was added to unfiltered seawater from 10 depths, and incubated in the dark for 5 days. Similar to PG2021, we collected samples for filtered controls from 200 m and 400 m, which bracketed the depth interval of fast Fe-siderophore uptake in PG2021, and siderophore hotspots in the NPSG (Chapter 3). In addition, we collected two samples from 200 m and 400 m, added ^{57}Fe-siderophores, and immediately filtered and extracted the sample for an initial timepoint (T0).

Table 4.1: The concentration of siderophores for peak **a-c** in the experiment of PG2022-S3C2

	Peak **a** (pM)				Peak **b** (pM)				Peak **c** (pM)			
	^{57}FeL	^{56}FeL	^{27}AlL	Total	^{57}FeL	^{56}FeL	^{27}AlL	Total	^{57}FeL	^{56}FeL	^{27}AlL	Total
75 m	45.4	12.6	0	58.0	41.5	8.6	0	50.1	52.8	12.1	0	64.9
100 m	33.1	16.3	0.3	49.8	27.1	6.7	0.7	34.5	34.8	18.9	0.9	54.6
150 m	38.2	9.0	0	47.1	37.9	6.2	0	44.1	57.6	10.3	0	67.9
200 m	1.9	9.5	0.6	12.0	3.0	6.3	3.8	13.0	0.8	13.3	1.8	15.9
250 m	6.9	4.4	2.0	13.3	6.4	3.5	4.3	14.3	10.6	5.7	3.9	20.2
300 m	0.6	4.8	1.4	6.8	0.2	3.2	2.6	6.0	0.8	5.5	1.8	8.1
350 m	0.7	9.3	2.0	12.0	0.5	7.1	4.3	11.9	0.8	10.4	3.4	14.6
400 m	0.5	7.3	1.3	9.1	0.4	5.4	4.7	10.6	0.6	8.5	2.6	11.7
450 m	57.2	9.6	0	66.8	54.4	4.3	0	58.7	76.6	16.9	0	93.5
500 m	4.4	6.0	0.6	11.0	3.6	4.0	1.5	9.2	6.0	10.2	3.0	19.3
Filtered Control 200 m	61.4	7.7	0.2	69.3	53.8	2.9	0.4	57.1	94.3	6.3	0.6	101.2
Filtered Control 400 m	58.8	6.9	0.1	65.9	54.2	4.9	0.4	59.5	88.3	8.4	0.4	97.1
T0 200 m	51.2	8.4	0	59.6	49.8	6.4	0	56.2	81.1	10.9	0	92.0
T0 400 m	53.1	6.3	0	59.4	53.9	4.4	0	58.3	78.7	7.2	0	85.9

After five days (Tf), the concentration of ^{57}Fe-siderophore were similar in the filtered controls at 200 m and 400 m (61.4 pM and 58.8 pM for peak **a**; 53.8 pM and 54.2 pM for peak **b**; 94.3 pM and 88.3 pM for peak **c**, Table 4.1), therefore we used the average concentrations for each peak from the filtered controls, to represent the filtered control concentrations for all depths. This average represents an expected concentration on Tf if biological processes did not exist. We did not use samples from T0 as the reference, and the reason will be discussed below.

For each of the siderophore peaks **a-c**, the concentration at Tf was equal to or lower in the unfiltered samples than in the filtered controls (Figure 4.6), showing that there are biological processes that draw down of ^{57}Fe-siderophores.

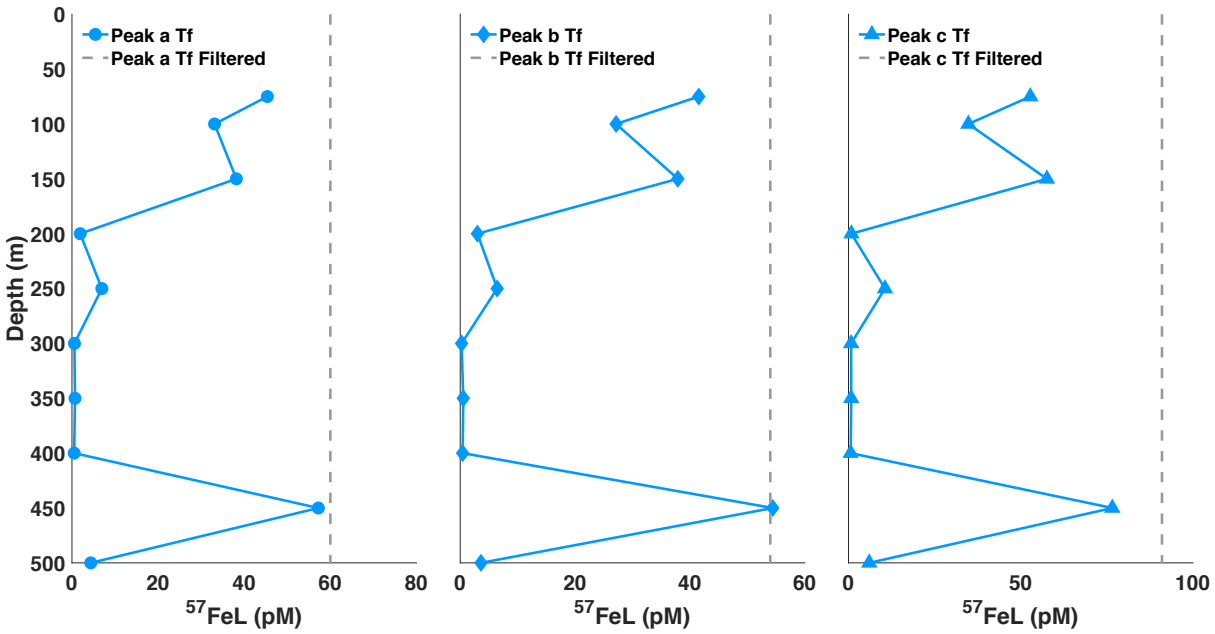

Figure 4.6: The results of incubation in PG2022-S3C2 for peak **a-c**. The solid symbols indicate the concentration in the unfiltered sample on Tf, and the vertical dashed line indicates the concentration in the filtered control on Tf, which was calculated as the average of the two filtered controls at 200 m and 400 m.

Between 200 and 400 m, we found almost complete drawdown of all three siderophores after 5 days (Figure 4.6). When samples from 200 m, 300 m, 350 m and 400 m are averaged, 98%, 98% and 99% of ^{57}Fe-siderophores are consumed for siderophores **a-c**. At 250 m, 88% of the siderophores were consumed. Within any sample, the same percentage of peaks **a-c** was consumed, indicating that the uptake was nonselective. The depth interval of the fast siderophore uptake and the rate of siderophore uptake in PG2022-S3C2, which was performed in dark, are similar to the results of PG2021, which was performed at 50% ambient light. Therefore, the drawdown of ^{57}Fe-siderophores in both PG2021 and PG2022-S3C2 at 200-400 m were both likely mediated by heterotrophic bacteria, not phytoplankton.

4.3.4 Turnover of siderophores suggests the drawdown was largely due to ^{57}Fe uptake

For both ferrioxamines which have a peptidic head group, and amphibactins or marinobactins which have a peptidic head group and fatty acid chain, siderophores are released into seawater to bind metals. In culture of both *Vibrio* (Boiteau et al 2016) and *Marinobacter* (Martinez et al 2000), amphibactins and marinobactins are found in the spent medium. After binding to Fe, the Fe-siderophore complex is transported across the cell membrane by TonB dependent transporters (Moeck and Coulton 1998), which show high affinity and high specificity to siderophores. Once the Fe-siderophore enters the cytoplasm, Fe(III) is reduced to Fe(II), which is incorporated into enzymes, or stored in proteins. The fate of the siderophores after Fe uptake is less understood, due to the challenge in siderophore measurement and in distinguishing potential siderophore release from siderophore production.

Between 200-400 m we found a consistent drawdown of ^{57}Fe-siderophore among peaks **a-c**, and we postulate that the drawdown is due to uptake and acquisition of Fe by heterotrophic bacteria. As shown in Figure 4.7, we expected that siderophore will be released back into seawater after ^{57}Fe uptake, and the siderophore could then bind ^{56}Fe, which is the most abundant Fe isotope in seawater, or ^{27}Al, which has a similar concentration in seawater as dFe. Therefore, on Tf, a lower ^{57}Fe-siderophore concentration than the filtered control would suggests Fe uptake from siderophore, and a higher concentration of ^{56}Fe-siderophore or ^{27}Al-siderophore concentration would suggest the release of apo siderophore after Fe uptake.

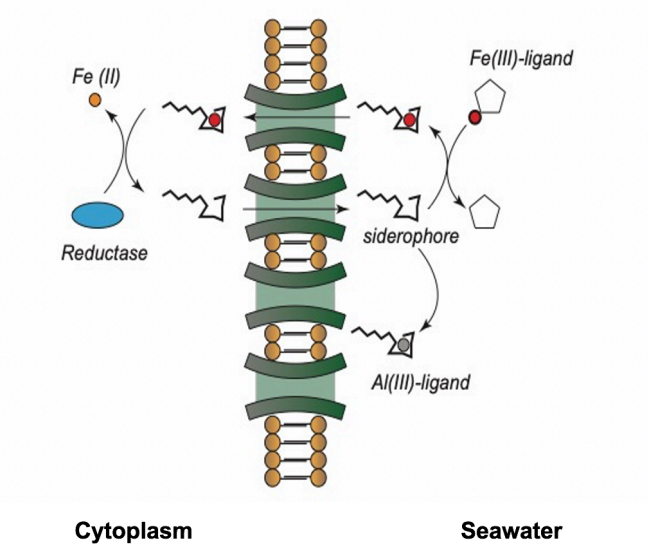

Figure 4.7: Illustration of the cycling of Fe and siderophores by heterotrophic bacteria. Apo siderophore could compete with weaker ligands for Fe. The Fe siderophore complex is transported to the cell, where Fe (III) is reduced to Fe (II). Iron (II) has a lower affinity to siderophores, which results in the dissociation of Fe from the siderophore. Then, the Fe is incorporated into proteins and the siderophore is released into seawater. The apo siderophore could also bind Al, but the bioavailability of Al-siderophore is probably low, because Al has only one oxidation state and therefore could not be reduced.

Indeed, the concentration of ^{27}Al-siderophores is a better proxy for siderophore turnover than ^{56}Fe-siderophores. ^{56}Fe is the most abundant Fe isotope, and it could bind apo siderophores once they are released after Fe uptake. The ^{56}Fe-siderophore could be taken up again and the Fe is removed, a process that could repeat multiple times before the siderophore is ultimately metabolized. Therefore, in the presence of dynamic turnover of siderophores, the concentration of ^{56}Fe-siderophore could be lower in the unfiltered sample than the filtered control, due to a faster ^{56}Fe uptake from siderophores, than the formation of ^{56}Fe-siderophores, which would preclude the discovery of siderophore turnover.

In contrast, Al-siderophores is presumably less bioavailable than Fe-siderophores because Al could not be reduced to the +2 oxidation state, and is therefore possibly not

bioavailable in the timescale of our incubation. Therefore, in the presence of dynamic turnover of siderophores, we would see a higher concentration of ^{27}Al-siderophores in the unfiltered samples than the filtered control, due to the accumulation of ^{27}Al-siderophores.

For peak **c**, the concentration of ^{27}Al-siderophores is higher (268-793%) in all the unfiltered samples at 200-400 m, than in the filtered control (Figure 4.8). For example, for peak **c**, ^{27}Al-siderophore concentration increased from 0.5 pM in filtered controls to 1.8 pM in the unfiltered sample at 200 m (Table 4.1). Therefore, uptake of ^{57}Fe and release of apo-amphibactins and marinobactins back into the environment results in an increase of 1.3 pM ^{27}Al-siderophore for peak **c** over the course of the incubation. Our results are consistent with siderophore uptake and release as shown in Figure 4.7. Therefore, the Al-siderophores we find in GP15 (Chapter 3) are due to the competition between Al and Fe for apo siderophores that are released into seawater, and reflect an inefficiency in the siderophore Fe uptake system.

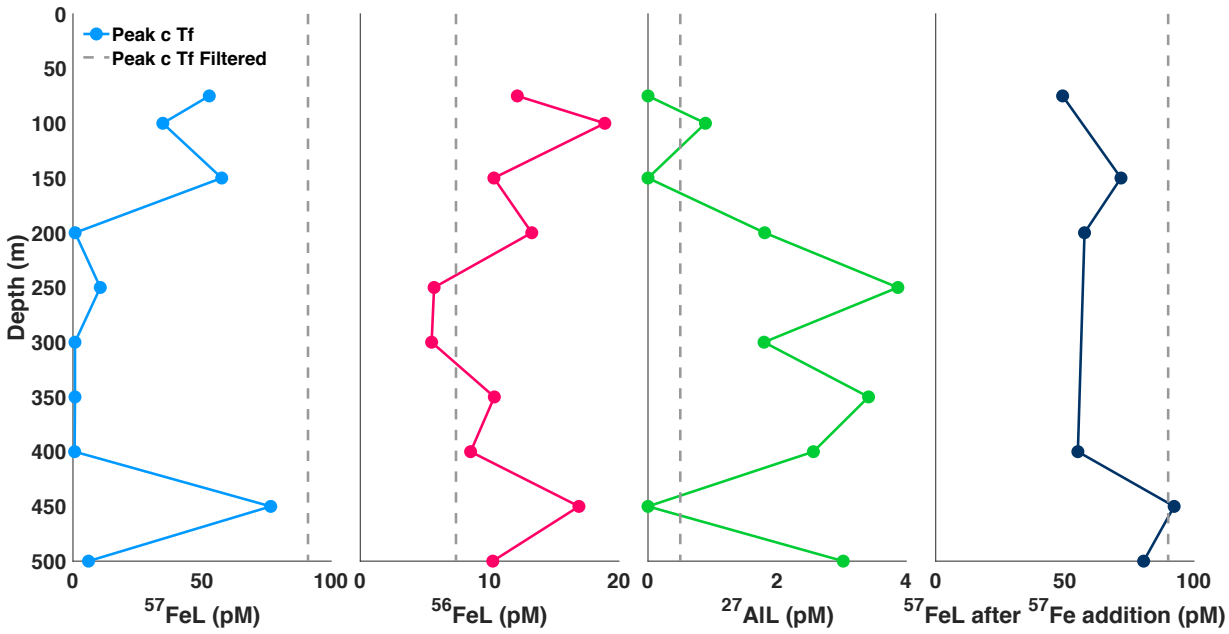

Figure 4.8: The results of incubation in PG2022 for peak **c**. The light blue line indicates the concentration for ^{57}Fe-siderophore on Tf, the red line indicates the concentration for ^{56}Fe-siderophore, the green line indicates the concentration for ^{27}Al-siderophore. The dark blue line represents the concentration for ^{57}Fe-siderophore after ^{57}Fe addition, which resulted in an ^{57}Fe:siderophore ratio of 10:1.

Between 200-400 m, we find parallel losses of ^{57}Fe-siderophores among peaks **a-c**. There seems to be no selectivity of uptake, although we could not rule out selectivity on timescales shorter than our incubations. For peak **c**, the concentration of ^{27}Al-siderophores is consistently higher (268-793%) in all the unfiltered samples at 200-400 m, than in the filtered control (Figure 4.8). However, the behavior of ^{27}Al-siderophore shows some variation among peaks. At 200 m, the concentration of ^{27}Al-siderophore increased by 0.4, 3.4 and 1.3 pM for peaks **a-c** over the course of the incubation (Figure 4.8). Because the total siderophore additions are 67.6, 58.3 and 99.1 pM for peaks **a-c**, the increase of ^{27}Al-siderophore represents 0.6%, 5.8% and 1.3% of the total siderophore addition for peak **a-c** (Table 4.1). The relative stability constant for Fe and Al (K_{FeL}/K_{AlL}) might be different for different siderophores, which could result in the higher relative production of ^{27}Al-siderophores for peak **b**. For example, all three peaks include a marinobactin and an amphibactin, and the contribution by marinobactin is

higher in peak **b**, than peak **a** and peak **c** (Figure 4.1). Therefore, it is possible that marinobactins have lower K_{FeL}/K_{AlL} than amphibactins, and when the apo siderophore is released into seawater, the Fe:Al ratio in peak **b** will be lower than peak **a** and peak **c.**

For peak **c**, the total siderophore addition was 99.1 pM for all depths, including ^{57}Fe-siderophore, ^{56}Fe-siderophore and ^{27}Al-siderophore. There were no apo siderophores in the stock solution. On Tf, only a portion (8.1-20.2 pM) of these siderophores could be accounted for in unfiltered samples at 200-400 m as ^{57}Fe, ^{56}Fe, or ^{27}Al siderophores. For example, at 200 m, 0.8 pM ^{57}Fe-siderophore, 13.3 pM ^{56}Fe-siderophore, 1.8 pM ^{27}Al-siderophore remain in the unfiltered sample on Tf. Therefore, at the end of the incubation, only 15.9 pM of the 99.1 pM siderophore could be accounted for by LC-ICPMS.

This deficiency in total siderophore concentration before and after incubation is also found for peaks **a** and peak **b** (Table 4.1), which led us to suspect there may be other forms of siderophores, most likely apo siderophores, in the unfiltered samples at the end of the incubation, which cannot be quantified directly by ICPMS. Therefore, we took an aliquot which represented 20% of the sample, added 1000 pmoles of ^{57}Fe to these samples, or 10 times the total siderophores addition, to complex any apo siderophores with ^{57}Fe. The samples were allowed to equilibrate for 3 hr, then analyzed again on LC-ICPMS (Table 4.2).

Table 4.2: The concentration of siderophores for peak **a-c** in the experiment of PG2022-S3C2, after ^{57}Fe addition

	Peak **a** (pM)				Peak **b** (pM)				Peak **c** (pM)			
	^{57}FeL	^{56}FeL	^{27}AlL	Total	^{57}FeL	^{56}FeL	^{27}AlL	Total	^{57}FeL	^{56}FeL	^{27}AlL	Total
75 m	42.1	12.6		54.7	50.5	11.9		62.4	49.1	11.6		60.7
150 m	52.3	10.1		62.4	67.6	11.1		78.7	71.7	10.7		82.4
200 m	35.6	7.3	1.0	43.9	40.8	7.6	1.8	50.2	57.6	10.0	1.2	68.8
400 m	39.7	7.5	1.0	48.2	46.5	8.2	1.3	56.0	55.0	8.1		63.1
450 m	64.3	8.2		72.5	82.2	10.0		92.2	92.3	11.8		104.1
500 m	49.2	8.5	1.1	58.8	57.6	8.3	1.2	67.1	80.5	10.9		91.4
T0 200 m	62.5	6.4		68.9	79.4	8.0		87.4	90.0	9.2		99.2
T0 400 m	61.3	5.2		66.5	80.1	6.4		86.5	90.1	7.1		97.2

The difference in ^{57}Fe-siderophore concentration before and after ^{57}Fe addition represents the concentration of apo siderophores in the sample. For peak **c**, we found 56.8 pM apo siderophores in the unfiltered sample from 200 m and an increase of 54.4 pM apo siderophores in the unfiltered sample from 400 m.

The high concentration of apo siderophores on Tf demonstrates that the drawdown of ^{57}Fe-siderophore at 200-400 m was largely due to ^{57}Fe uptake from siderophores. Although there is clearly loss of siderophores in all samples, probably due to the uptake of siderophore as labile N or C, these losses contributed less than Fe uptake to the drawdown of ^{57}Fe-siderophores. In GP15, we found high concentration of siderophores at 200-400 m of the NPSG. In addition, Mazzota et al (2020) found high abundance of *Alteromonas* TonB-dependent Fe transport protein at 200-400 m of the Central Pacific Ocean. The fast Fe uptake from siderophores is in accordance with these results, suggesting that heterotrophic bacteria are Fe limited at 200-400 m of the NPSG.

The concentration of apo siderophore is 14.1 pM at 150 m and 15.7 pM at 450 m on Tf, suggesting that heterotrophic bacteria are acquiring Fe from siderophores at these two depths, but to a lesser extent than in the 200-400 m region.

At 75 m, the ^{57}Fe addition results only a small change in the concentration of ^{57}Fe-siderophore (from 52.8 pM to 49.1 pM), suggesting the absence of apo siderophores at the end of the incubation. Therefore, the drawdown of ^{57}Fe-siderophore in the euphotic zone over the course of the incubation was for the energy and/or nutrient (N or C) content of the siderophore, and heterotrophic bacteria in the euphotic zone are not Fe limited, or do not have siderophore transporters. Our results reveal that the zone of potential Fe limitation in the ocean extends well below the euphotic zone and includes oligotrophic gyres that are not classically Fe limited. Our results substantially expand the volume of the ocean in which microbial communities are likely Fe limited.

We performed two additional uptake experiments near Station ALOHA in 2022 (PG2022-S2TM2 and PG2022-S2TM3), and we found complete consumption of ^{57}Fe-siderophores at mesopelagic depths in both experiments, regardless of the identity and concentration of siderophores added (Figure 4.9). Indeed, the depth interval for fast ^{57}Fe uptake varies among experiments, but they are all confined in the 200-400 m depth. Therefore, iron limitation and siderophore uptake might be a prevalent feature at the upper mesopelagic of the NPSG, which is supported by the prevalent siderophore hotspots in GP15 (Chapter 3).

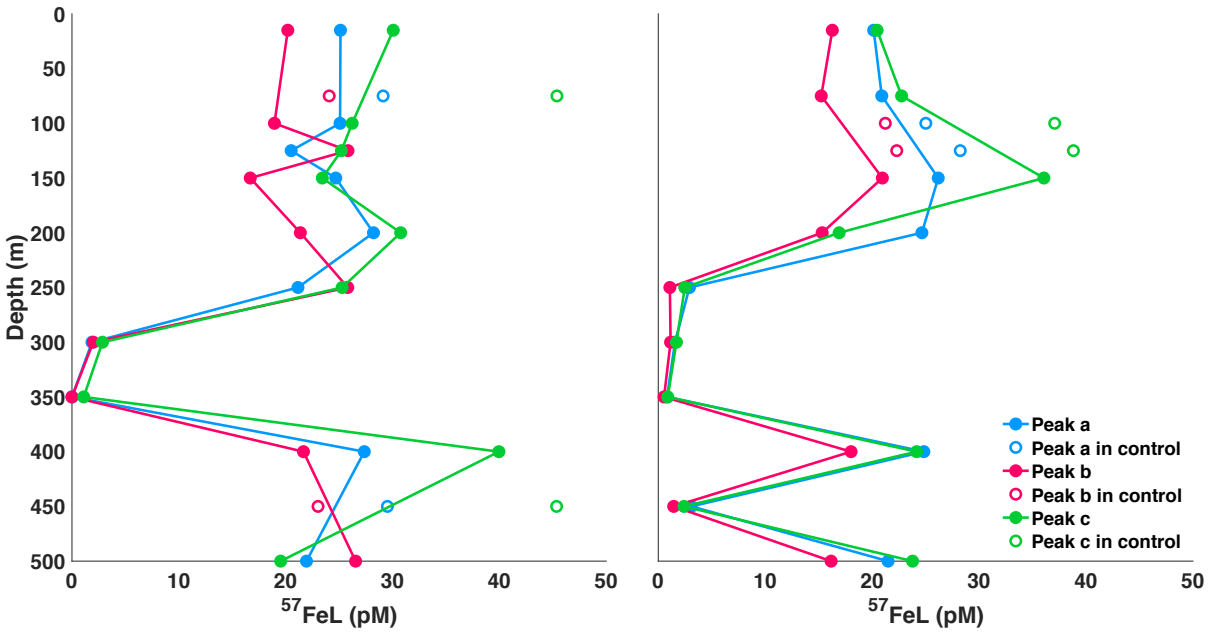

Figure 4.9: The results of incubation in PG2022-S2TM2 and PG2022-S2TM3. The blue line indicates the concentration for peak **a**, the red line indicates the concentration for peak **b**, the green line indicates the concentration for peak **c**. Solid circle indicates the concentration in the unfiltered sample on Tf, and open circle indicates the concentration in the filtered control on Tf, which was prepared at two depths in each experiment.

4.3.5 The rate of Fe uptake from siderophores are fast, on a timescale of days

In addition to unfiltered samples for Tf and filtered sample for Tf, which are both incubated for 5 days, we also collected seawater at 200 m and 400 m that was amended with siderophores then immediately filtered and extracted for an experimental T0. The concentration of ^{57}Fe-siderophores on T0 was compared to the Tf of the two filtered controls from 200 m and 400 m, which were spiked after filtration.

For peak **a-c**, the two filtered controls on Tf have an average concentration of 60.1, 54.0 and 91.3 pM, consistently higher than the average concentration of 52.2, 51.9 and 79.9 pM in the two unfiltered samples on T0 (Figure 4.10). The precision of quantification for Fe ligands in standards and samples by LC-ICPMS is within 5% after normalization to the internal standard of Ga-DFE. Therefore, the higher concentration of ^{57}Fe-siderophores in filtered controls than in T0 samples could not be explained by

instrumental reproducibility, although we could not rule out the possibility of low biological reproducibility.

A higher concentration in filtered controls than in T0 samples was not expected, because there is no production of ^{57}Fe-siderophore in the filtered control. In one aspect, this suggests that abiotic processes do not influence the Fe siderophore complexes under environmental conditions. In another aspect, the most likely explanation for the drawdown in T0 samples is ^{57}Fe uptake during sample processing. Indeed, the seawater with both microbial community and ^{57}Fe-siderophores was incubated for 3 hours as it was pumped through the filter and the SPE cartridge, and ^{57}Fe uptake could have happened. In contrast, ^{57}Fe-siderophore in the filtered control did not interact with the microbial community, and there was no uptake for either ^{57}Fe or siderophore.

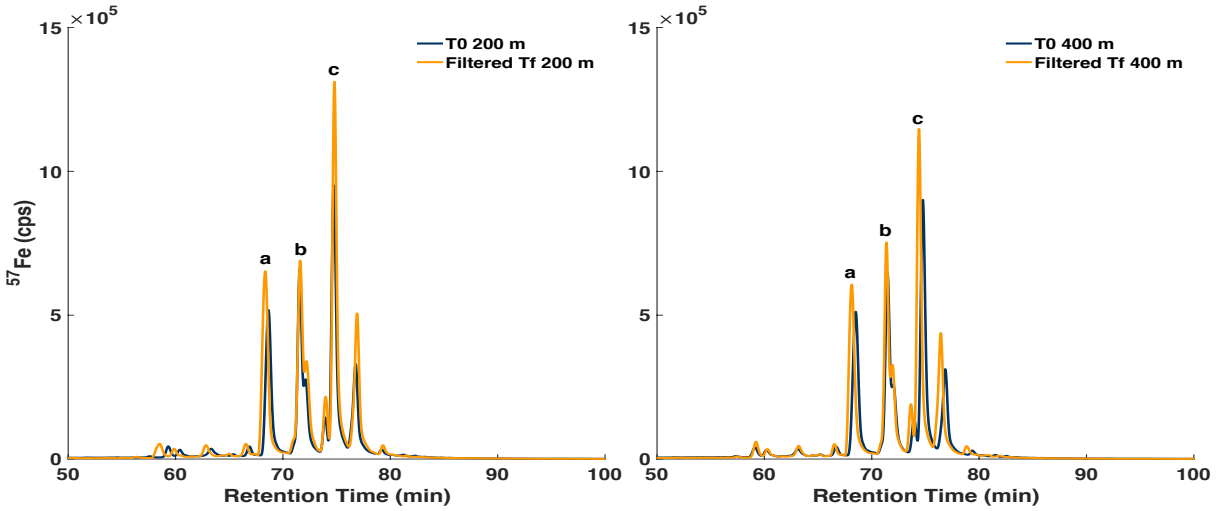

Figure 4.10: The LC-ICPMS chromatograms of the T0 sample and the filtered control at 200 m and 400 m. The dark blue line indicates the counts for ^{57}Fe in the T0 sample, which was extracted immediately after ^{57}Fe-siderophores were added to unfiltered seawater, and the extraction took 3 hours. The orange line indicates the counts for ^{57}Fe in the filtered control, which was extracted after 5 days of incubation of ^{57}Fe-siderophores in filtered seawater. Peak **a-c** are selected as representative siderophores for discussion.

If the 11.4 pM drawdown of peak **c** happens within 3 hrs, it is likely that the complete drawdown of 91.3 pM of peak **c** at 200-400 m happens within a day. The temperature during the incubation was 10-15 °C higher than the temperature in situ, and the siderophore addition may have added small amounts of labile carbon from organic matter that was co-isolated with the siderophores used to amend the incubation samples. This co-isolated SPE extractable organic C could have promoted the growth of heterotrophic bacteria. Therefore, the in situ Fe uptake rates might be lower than those in the incubation bottles. However, the fast uptake in our incubation suggests that the turnover of Fe-siderophores is at least on the order of days at 200-400 m, which could explain the patchiness of siderophore distribution (Figure 3.4). This also shows dynamic turnover of dFe. In GP15, we find prevalent hotspots of siderophores with a concentration higher than 20 pM at 200-400 m of NPSG (Chapter 3). If we assume 200 pM dFe at 200 m of Station ALOHA (Figure 4.4, Fitzsimmons et al 2015), and daily turnover of 20 pM Fe-siderophores (Chapter 3) due to Fe uptake by heterotrophic bacteria, the turnover time for dFe by siderophore complexation and uptake is 10 days.

4.3.6 Siderophore uptake for N or C persists in the upper water column

The total siderophore addition on T0, including ^{57}Fe-siderophore, ^{56}Fe-siderophore and ^{27}Al-siderophore could be represented by the average of the two filtered controls on Tf. The total siderophore concentration in the unfiltered samples on Tf, including ^{57}Fe-siderophore, ^{56}Fe-siderophore, ^{27}Al-siderophore and apo siderophore, could be calculated after ^{57}Fe addition (Table 4.3). Therefore, the difference between the two concentrations represent the drawdown of siderophores over the course of the incubation, possibly due to N or C uptake. For example, for peak **c**, we find N or C uptake at 5 out of 6 depths (Table 4.3) with a slightly higher uptake rate in the upper water column.

At 200 m, there is a production of 56.8 pM apo siderophore and a consumption of 30.4 pM siderophore in the unfiltered sample over the course of the incubation, suggesting that 65% of the consumption was due to Fe uptake, and 35% was due to siderophore

uptake (Figure 4.8). It is possible that a small portion of the apo siderophore on Tf was due to the conversion from ^{56}Fe-siderophore or ^{27}Al-siderophore that was present in the stock solution and was added with ^{57}Fe-siderophore, but this portion is known to be < 10% of the ^{57}Fe-siderophore in the stock solution. At 75 m, there is a drawdown of ^{57}Fe-siderophore without production of apo siderophore over the course of the incubation, and the drawdown was probably due to N or C uptake, which was irrelevant to Fe.

Table 4.3: The concentration of siderophores for peak **c** in the experiment of PG2022-S3C2. The total siderophore addition on T0 is represented by the average of the two filtered controls on Tf, including ^{57}Fe-siderophore, ^{56}Fe-siderophore and ^{27}Al-siderophore. The total siderophore after ^{57}Fe addition includes concentration of ^{57}Fe-siderophore, ^{56}Fe-siderophore and ^{27}Al-siderophore. The N or C uptake is calculated by the difference between total siderophore addition and total siderophore after ^{57}Fe addition, representing drawdown of siderophores during the incubation.

	Total siderophore addition (pM)	Total siderophore after ^{57}Fe addition (pM)	N or C Uptake (pM)
75 m	99.2	60.7	38.5
125 m	99.2	82.4	16.8
200 m	99.2	68.8	30.4
400 m	99.2	63.1	36.1
450 m	99.2	104.1	-4.9
500 m	99.2	91.4	7.8
T0 200 m	99.2	99.2	0
T0 400 m	99.2	97.2	2.0
Tf 200 m Filtered	101.2		
Tf 400 m Filtered	97.1		

4.4 Conclusion

Using ^{57}Fe labeled marinobactins and amphibactins, we measured the Fe uptake from siderophores at Station ALOHA, a representative station for the NPSG. At 200-400 m, there was a fast drawdown in the concentration of ^{57}Fe-siderophore from filtered control for all of the siderophores, suggesting that it was due to biological processes, most

likely by microbial uptake. Furthermore, the drawdown was found in both light and dark incubations, suggesting that it was mediated by heterotrophic bacteria, not phytoplankton. In addition to the decrease in the concentration of Fe-siderophore, we found an increase in the concentration of Al-siderophore, suggesting the release of apo siderophore after Fe uptake. Over the course of the incubation, the production of Al-siderophore could not account for the consumption of Fe-siderophore, which led us to suspect there were apo siderophore at the end of the incubation. With ^{57}Fe addition, we found that apo siderophores on Tf accounted for more than 50% of the siderophore addition on T0, suggesting that the drawdown of ^{57}Fe-siderophore over the course of the incubation was largely due to Fe uptake, not N or C uptake.

At 75 m, there is drawdown of ^{57}Fe-siderophores over the course of the incubation, which is due to the uptake of siderophores. These siderophores were probably used for N or C, and not released back into seawater.

The fast Fe uptake from siderophores suggests that heterotrophic bacteria are Fe limited at 200-400 m, which is in accordance with the hotspots of siderophore concentration at 200-400 m of NPSG (Chapter 3). Our results reveal that the zone of potential Fe limitation in the ocean extends well below the euphotic zone and includes oligotrophic gyres that are not classically Fe limited. Our results substantially expand the volume of the ocean in which microbial communities are likely Fe limited.

4.5 References

Schlitzer, R., Anderson, R. F., Dodas, E. M., Lohan, M., Geibert, W., Tagliabue, A., ... & Lechtenfeld, O. J. (2018). The GEOTRACES intermediate data product 2017. *Chemical Geology*, 493, 210-223.

Ho, T. Y., Quigg, A., Finkel, Z. V., Milligan, A. J., Wyman, K., Falkowski, P. G., & Morel, F. M. (2003). The elemental composition of some marine phytoplankton 1. *Journal of phycology*, *39*(6), 1145-1159.

De Baar, H. J., Boyd, P. W., Coale, K. H., Landry, M. R., Tsuda, A., Assmy, P., ... & Wong, C. S. (2005). Synthesis of iron fertilization experiments: from the iron age in the age of enlightenment. *Journal of Geophysical Research: Oceans*, *110*(C9).

Boyd, P. W., & Ellwood, M. J. (2010). The biogeochemical cycle of iron in the ocean. *Nature Geoscience*, *3*(10), 675-682.

Church, M. J., Hutchins, D. A., & Ducklow, H. W. (2000). Limitation of bacterial growth by dissolved organic matter and iron in the Southern Ocean. *Applied and Environmental Microbiology*, *66*(2), 455-466.

Kirchman, D. L., Meon, B., Cottrell, M. T., Hutchins, D. A., Weeks, D., & Bruland, K. W. (2000). Carbon versus iron limitation of bacterial growth in the California upwelling regime. Limnology and oceanography, 45(8), 1681-1688.

Fourquez, M., Bressac, M., Deppeler, S. L., Ellwood, M., Obernosterer, I., Trull, T. W., & Boyd, P. W. (2020). Microbial competition in the subpolar southern ocean: an Fe–C Co-limitation experiment. Frontiers in Marine Science, 6, 776.

Church, M. J., Ducklow, H. W., & Karl, D. M. (2004). Light dependence of [3H] leucine incorporation in the oligotrophic North Pacific Ocean. Applied and environmental microbiology, 70(7), 4079-4087.

Hutchins, D. A., Witter, A. E., Butler, A., & Luther III, G. W. (1999). Competition among marine phytoplankton for different chelated iron species. *Nature*, *400*(6747), 858-861.

Maldonado, M. T., & Price, N. M. (1999). Utilization of iron bound to strong organic ligands by plankton communities in the subarctic Pacific Ocean. *Deep Sea Research Part II: Topical Studies in Oceanography*, *46*(11-12), 2447-2473.

Lis, H., Shaked, Y., Kranzler, C., Keren, N., & Morel, F. M. (2015). Iron bioavailability to phytoplankton: an empirical approach. *The ISME journal*, *9*(4), 1003-1013.

Boiteau, R. M., Fitzsimmons, J. N., Repeta, D. J., & Boyle, E. A. (2013). Detection of iron ligands in seawater and marine cyanobacteria cultures by high-performance liquid chromatography–inductively coupled plasma-mass spectrometry. *Analytical chemistry*, *85*(9), 4357-4362.

Bundy, R. M., Boiteau, R. M., McLean, C., Turk-Kubo, K. A., McIlvin, M. R., Saito, M. A., ... & Repeta, D. J. (2018). Distinct siderophores contribute to iron cycling in the mesopelagic at station ALOHA. Frontiers in Marine Science, 5, 61.

Li, J., Boiteau, R. M., Babcock-Adams, L., Acker, M., Song, Z., McIlvin, M. R., & Repeta, D. J. (2021). Element-Selective Targeting of Nutrient Metabolites in Environmental Samples by Inductively Coupled Plasma Mass Spectrometry and Electrospray Ionization Mass Spectrometry. *Frontiers in Marine Science*, *8*, 630494.

Boiteau, R. M. (2016). Molecular determination of marine iron ligands by mass spectrometry (Doctoral dissertation, Massachusetts Institute of Technology).

Vraspir, J. M., Holt, P. D., & Butler, A. (2011). Identification of new members within suites of amphiphilic marine siderophores. Biometals, 24, 85-92.

Boiteau, R. M., Mende, D. R., Hawco, N. J., McIlvin, M. R., Fitzsimmons, J. N., Saito, M. A., ... & Repeta, D. J. (2016). Siderophore-based microbial adaptations to iron scarcity across the eastern Pacific Ocean. *Proceedings of the National Academy of Sciences*, *113*(50), 14237-14242.

Kem, M. P., & Butler, A. (2015). Acyl peptidic siderophores: structures, biosyntheses and post-assembly modifications. *Biometals*, *28*, 445-459.

Karl, D. M., & Church, M. J. (2014). Microbial oceanography and the Hawaii Ocean Time-series programme. Nature Reviews Microbiology, 12(10), 699-713.

Karl, D. M., Church, M. J., Dore, J. E., Letelier, R. M., & Mahaffey, C. (2012). Predictable and efficient carbon sequestration in the North Pacific Ocean supported by symbiotic nitrogen fixation. Proceedings of the National Academy of Sciences, 109(6), 1842-1849.

Campbell, L., Liu, H., Nolla, H. A., & Vaulot, D. (1997). Annual variability of phytoplankton and bacteria in the subtropical North Pacific Ocean at Station ALOHA during the 1991–1994 ENSO event. Deep Sea Research Part I: Oceanographic Research Papers, 44(2), 167-192.

Martínez-García, S. (2017). Microbial respiration in the mesopelagic zone at Station ALOHA. Limnology and Oceanography, 62(1), 320-333.

Karl, D. M., Björkman, K. M., Church, M. J., Fujieki, L. A., Grabowski, E. M., & Letelier, R. M. (2022). Temporal dynamics of total microbial biomass and particulate detritus at Station ALOHA. Progress in Oceanography, 205, 102803.

Fitzsimmons, J. N., Hayes, C. T., Al-Subiai, S. N., Zhang, R., Morton, P. L., Weisend, R. E., ... & Boyle, E. A. (2015). Daily to decadal variability of size-fractionated iron and iron-

binding ligands at the Hawaii Ocean Time-series Station ALOHA. Geochimica et Cosmochimica Acta, 171, 303-324.

Boyle, E. A., Bergquist, B. A., Kayser, R. A., & Mahowald, N. (2005). Iron, manganese, and lead at Hawaii Ocean Time-series station ALOHA: Temporal variability and an intermediate water hydrothermal plume. Geochimica et Cosmochimica Acta, 69(4), 933-952.

Hayes, C. T., Fitzsimmons, J. N., Boyle, E. A., McGee, D., Anderson, R. F., Weisend, R., & Morton, P. L. (2015). Thorium isotopes tracing the iron cycle at the Hawaii Ocean Time-series Station ALOHA. Geochimica et Cosmochimica Acta, 169, 1-16.

Hawco, N. J., Barone, B., Church, M. J., Babcock-Adams, L., Repeta, D. J., Wear, E. K., ... & John, S. G. (2021). Iron depletion in the deep chlorophyll maximum: mesoscale eddies as natural iron fertilization experiments. Global Biogeochemical Cycles, 35(12), e2021GB007112.

Tortell, P. D., Maldonado, M. T., & Price, N. M. (1996). The role of heterotrophic bacteria in iron-limited ocean ecosystems. *Nature*, *383*(6598), 330-332.

Casciotti, K. L., Trull, T. W., Glover, D. M., & Davies, D. (2008). Constraints on nitrogen cycling at the subtropical North Pacific Station ALOHA from isotopic measurements of nitrate and particulate nitrogen. *Deep Sea Research Part II: Topical Studies in Oceanography*, *55*(14-15), 1661-1672.

Tortell, P. D., Maldonado, M. T., & Price, N. M. (1996). The role of heterotrophic bacteria in iron-limited ocean ecosystems. *Nature*, *383*(6598), 330-332.

Martinez, J. S., Zhang, G. P., Holt, P. D., Jung, H. T., Carrano, C. J., Haygood, M. G., & Butler, A. (2000). Self-assembling amphiphilic siderophores from marine bacteria. *Science*, *287*(5456), 1245-1247.

Moeck, G. S., & Coulton, J. W. (1998). TonB-dependent iron acquisition: mechanisms of siderophore-mediated active transport. Molecular microbiology, 28(4), 675-681.

Mazzotta, M. G., McIlvin, M. R., & Saito, M. A. (2020). Characterization of the Fe metalloproteome of a ubiquitous marine heterotroph, Pseudoalteromonas (BB2-AT2): multiple bacterioferritin copies enable significant Fe storage. Metallomics, 12(5), 654-667.

Chapter 5 Nutrient limitation on siderophore production by heterotrophic bacteria at 150 m of Station ALOHA

5.1 Introduction

In Chapter 3, we report the distribution of siderophores in the upper 1000 m of the US GEOTRACES GP15 Pacific Meridional Transect. The distribution of siderophores is controlled by the production and the turnover of siderophores. In Chapter 4, we report the measurement of Fe uptake from siderophores by heterotrophic bacteria at 75-500 m of Station ALOHA. In this chapter, we investigate the effect of nutrient limitation on siderophore production at Station ALOHA.

At Station ALOHA, a long-term oceanographic study site representative of the ecology and biogeochemistry of the North Pacific Subtropical Gyre (NPSG), the nitracline starts at 100-150 m (Casciotti et al 2008). Nitrate concentrations are less than 100 nM at 0-100 m, and less than 2 μM at 0-150 m (Figure 4.4). At 0-150 m, the dFe concentrations are greater than 100 pM (Fitzsimmons et al 2015). Therefore, the surface ocean between 0-150 m of Station ALOHA is associated with a $Fe:NO_3^-$ ratio that is greater than 50 μmol/mol. Below 150 m, nitrate concentrations increase with depth at a faster rate than concentrations of dFe, which results in an $Fe:NO_3^-$ ratio that is less than 50 μmol/mol.

Heterotrophic bacteria including *Pseudomonas* spp. grown under low Fe concentrations have an Fe:C ratio of 8 μmol/mol (Tortell et al 1996), or an Fe:N ratio of 50 μmol/mol, assuming Redfield stoichiometry. Assuming that the $Fe:NO_3^-$ ratio of *Pseudomonas* spp. grown under low Fe concentrations is representative of other heterotrophic bacteria, then waters at 0-150 m of Station ALOHA are likely deficient in N, while waters below 150 m are likely deficient in Fe with respect to heterotrophic bacteria cellular Fe and N quotas.

In the NPSG, siderophores concentrations between 0-150 m in our GP-15 samples were low or not detectable (Chapter 3). In addition, we found no measurable Fe uptake from siderophores in experiments performed at 75 m and 100 m at Station ALOHA following incubation of unfiltered seawater that had been amended with ^{57}Fe-siderophores (Chapter 4). Therefore, the low concentration of siderophores, the slow turnover of siderophores and the high Fe:NO_3^- ratio characteristic of the 0-150 m upper ocean of the NPSG suggests that heterotrophic bacteria inhabiting this portion of the upper ocean were not Fe limited. In contrast, between 200-400 m, we found high concentration of siderophores (Chapter 3), and fast turnover of siderophores (Chapter 4), and we postulate that heterotrophic bacteria in the upper mesopelagic of the NPSG were likely Fe limited.

At Station ALOHA, 150 m approximates the top of the nitra- and ferriclines, the transition between waters with Fe:NO_3^- > 50 μmole/mole to waters with Fe:NO_3^- < 50 μmole/mole. In our Fe uptake experiments (Chapter 4), we found that the rate of Fe uptake from siderophores at 150 m was faster than at 75 m but slower than rates measured between 200-400 m, suggesting that heterotrophic bacteria are Fe limited at 150 m, but to a less extent than at 200-400 m. Furthermore, the depth of 150 m denotes a transition zone that separates bacterial C and N limitation in the euphotic zone from an Fe limitation zone in the upper mesopelagic.

In GP15, we expected to find high concentration of siderophores at 150 m of NPSG, where heterotrophic bacteria are Fe limited. However, the concentrations of siderophores at 150 m of NPSG were low, which could be explained by the low populations of siderophore producing bacteria, or nutrient limitation on siderophore production by N or C.

To explore nutrient limitation on siderophore production at 150 m, we performed a suite of incubation experiments with seawater collected at 150 m from Station ALOHA. Samples of seawater were amended with nutrients, including glucose for the investigation of C limitation, and freshly collected particles for N limitation. Each

experiment includes one treatment with no Fe addition and one treatment with Fe addition, to investigate the control of siderophore production by dFe. Samples were incubated for 2-7 days in the dark and the siderophore concentration was monitored. We emphasize that our incubation aims to investigate nutrient limitation on siderophore production, not on bacterial production. ^{3}H leucine uptake measurements were made as part of the experiment, but fall outside of the scope of this discussion.

Our hypothesis was that if siderophore production at 150 m was limited by organic carbon, the addition of a labile carbon substate (glucose) would stimulate siderophore production. However, if siderophore production at this depth were limited by N, the addition of glucose would not be sufficient to stimulate siderophore production, and the addition of POM would promote siderophore production, due to the injection of both labile C and N. In addition, we expected to see low concentration of siderophores in the + Fe treatment, due to the mitigation of Fe limitation.

5.2 Methods

5.2.1 Incubation experiments for siderophore production

The experiments in this chapter were performed by incubating 150 m Station ALOHA seawater amended with glucose or particulate organic matter (POM) as a labile carbon sources, with and without the addition of iron. Seawater was collected for all samples using a powder coated Al framed rosette (Seabird), with external spring sample collection bottles (Ocean Test Equipment) and dispensed directly into 4 L acid washed polycarbonate bottles. Five incubations (Experiments 1-5) were performed during PARAGON I in August 2021, and two incubations (Experiments 6-7) were performed during PARAGON II in August 2022 (Table 5.1). Experiment 1 served as a control, with a companion treatment of only iron (5 nM) added. Experiments 2-5, and 7 had one treatment with labile carbon only, and a companion treatment with labile carbon plus Fe. Experiment 6 had one treatment with POM and one treatment with both POM and glucose, with no addition of iron to either treatment.

Table 5.1: Summary of the conditions of the seven incubation experiments. In some experiments with POM addition, the measurement of POC samples have not been completed.

Expt	Year	Treatment	Glucose (μM)	POC from 150 m (μM)	POC from surface (μM)	T1 (hr)	Tf (hr)
1	2021	Control, Control + Fe				48	72
2	2021	+ Glucose, + Glucose + Fe	10			48	72
3	2022	+ Glucose, + Glucose + Fe				96	168
4	2021	+ POM, + POM + Fe		1.8		48	96
5	2021	+ POM, + POM + Fe		N. D.			48
6	2021	+ POM, + POM + Glucose	10	N. D.			48
7	2022	+ POM, + POM + Fe			3.7	72	120

For each incubation, the seawater for different treatments was collected from the same cast, and one cast was performed for each incubation. For example, for the Experiment 4 in 2021, sinking particles were collected from 150 m using a sediment net trap fitted with a 50 μm mesh net and cod end collection bottle, which had been deployed 24 hours prior. After recovery, the particles in the net were pre-screened through a 335 μm mesh sieve and 9/10ths of the total particulate material (>50 μm and <335 μm) was evenly divided into twenty splits using a McLane wet sample divider (WSD-10). A single particle split (4.5% of the total material) was then added to each of the 14 incubation bottles. In Experiment 4, POC analyses of a replicate sample showed that particle additions increased the particulate carbon concentration in the incubation bottles from 1.2 μM to 3.0 μM (Table 5.1). In 2022 suspended POM were collected near the surface (~3-10 m) via a surface net tow equipped with a 50 μm mesh net and cod end. The particles were pre-screened, divided and added to the incubation bottles in the same approach as in the Experiment 4. Half the incubation bottles were also spiked with 5 nM $FeCl_3$

For the 2021 experiments, Experient 1-3 were performed for 3-4 days and included three time points (initial (T0), intermediate (T1), and final (Tf)). Two incubations (Experiment 4 and 5) were performed for 2 days with only two time points (T0, Tf). The incubations in 2022 were performed for 5-7 days and included three time points (Table 5.1). All T0 samples were immediately pumped at 20 mL/min through 0.2 μm sterivex

filter, and 2 L out of the 4 L filtrate was collected into acid cleaned polycarbonate bottles and stored at 4°C. The remaining incubation bottles were placed in heavy-duty PVC bags to maintain dark conditions and submerged in temperature-controlled on-deck incubator set to 20 °C, the 150 m *in-situ* temperature. Over the course of the incubation, the six samples each for T1 and Tf were filtered as described for the T0 samples, and 2 L of filtrate was collected for siderophore measurement.

In Experiments 2 and 6 glucose was added to each bottle to a final concentration of 10 μM (equivalent to 60 μM total carbon). The stock solution of glucose was passed beforehand through Chelex-100 resin to remove Fe contamination in the glucose. In the 2021Glu/GluFe-Short and 2021POM/POMGlu-Short experiments (Experiments 4 and 5), the sample volume for siderophore measurements was 1 L, lower than the sample volume of 2 L in the other five experiments.

5.2.2 Analysis of siderophores in incubation samples and water column samples

Within 5 days of filtration the samples were pumped at 20 mL/min onto Bond-Elut ENV solid phase extraction (SPE) columns (1 g, 6 mL, Agilent Technologies) that had been previously activated by passing 6 mL each of distilled methanol (MeOH, Optima LCMS grade, Fisher Scientific) and ultrapure water (qH_2O, 18.2 MΩ) through the column. SPE columns were frozen (-20 °C) immediately after sample collection and returned to the laboratory for processing.

Two water column profiles of siderophores were collected on each of the 2021 and 2022 expeditions. Samples were processed as described in detail in Chapter 3. For both incubation samples and water column samples, the LC-ICPMS analysis was described in Chapter 3, except that the post-column addition of 35 μL/min water was not implemented. The LC-ESIMS analysis was also described in detail in Chapter 3.

5.3 Results and Discussion

5.3.1 Experiment 1: No siderophore is produced when no C or N is added

At 150 m of the NPSG, siderophores are low in concentration or absent, according to GP15 (Chapter 3). Prior analyses of water column samples from Station ALOHA by Bundy and colleagues (Bundy et al 2018), and our own analyses of the water column on both PARAGON cruises confirm these results. Bundy and colleagues found only low concentrations of siderophores (0.1 pM of ferrioxamines and 0.2 pM of amphibactins) at 150 m with higher concentrations above and below this depth (2.1 pM of ferrioxamines and 0.3 pM of amphibactins near the surface and 1.2 pM of ferrioxamines and 11.1 pM of amphibactins at 300 m). In both 2021 and 2022 cruises where the incubations were performed, we did not find siderophores at 150 m in any of four depth profiles.

At 150 m of Station ALOHA, we measured Fe uptake from siderophores by heterotrophic bacteria (Chapter 4), suggesting that heterotrophic bacteria were Fe limited. However, the Fe-siderophore uptake rate was 10-20 times slower than at 200-400 m (Chapter 4), suggesting that the low siderophore concentration at 150 m is due to low production, not fast turnover of siderophores. Under Fe limitation, the low production of siderophores could be explained by the absence of siderophore producing bacteria, or nutrient limitation on siderophore production by N or C. To investigate the reason for the low siderophore concentration at 150 m, we performed seven incubations with nutrient amended seawater collected from 150 m, and monitored siderophore production. We emphasize that our incubation aims to investigate nutrient limitation on siderophore production, not on bacterial production.

Experiment 1 was an incubation with unfiltered seawater, including both microbial community and in situ particles, without C or N addition. This experiment would be used as a control for further nutrients amendment. We expected to find no siderophore production in the control, due to the high Fe:NO_3^- ratio and the low concentration of nitrate for siderophore production. In the + Fe treatment, we also expected to find no siderophore production, due to the mitigation of Fe limitation by Fe addition.

Indeed, no siderophore was found in the T0 samples of the Experiment 1 (Figure 5.1), which was extracted immediately after Fe addition. At T1 (48 hrs), only trace amounts of siderophores (< 1 pM; retention time 35-45 min) were found in both control and the + Fe treatment. The retention time of the siderophore peak in our T1 samples was similar to ferrioxamines. At Tf (72 hrs), no siderophore was found in any of the treatments (Figure 5.1). In one aspect, the presence of ferrioxamine-like siderophores on T1 suggests the presence of siderophore producing bacteria at 150 m. In another aspect, there seems to be little siderophore production over the course of the incubation, which is most likely due to C or N limitation of siderophore production at 150 m.

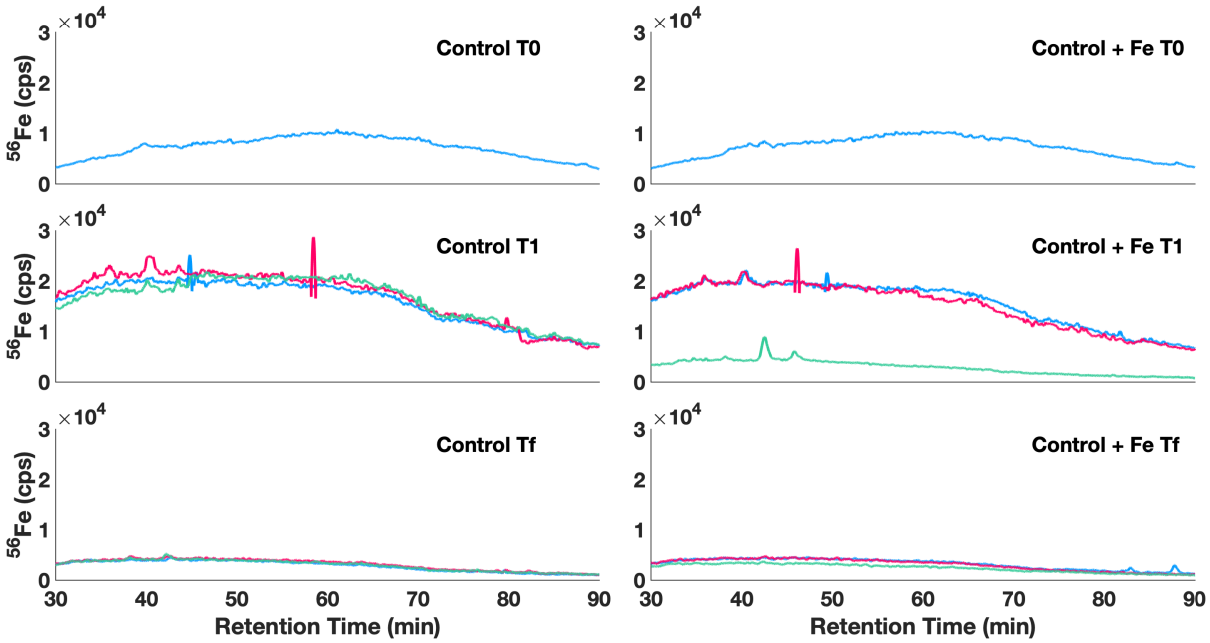

Figure 5.1: LC-ICPMS chromatograms of ^{56}Fe for the Experiment 1. The upper panels have one sample per treatment, and the lower panels have triplicate samples per treatment. The different colors of the Fe chromatograms represent different triplicate bottles.

5.3.2 Experiment 2: No siderophore is produced when glucose was added

Fe limitation of heterotrophic bacteria is supported by Fe uptake from siderophores at 150 m of Station ALOHA (Chapter 4). According to Experiment 1, siderophore production at 150 m is limited by C or N. To explore this further, we performed

Experiment 2 with glucose addition as labile C source. If bacteria are limited by primarily by labile carbon, we expected that the addition of glucose should result in enhanced siderophore production in the + Glucose treatment, but not in the +Glucose + Fe treatment.

On T0, T1 (48 hrs) and Tf (72 hrs), a small siderophore peak (< 1 pM) was found at around 80 min across treatments (Figure 5.2). The retention time of the peak was similar to marinobactins or amphibactins, but we were not able to assign a mass to the peak due to its low concentration.

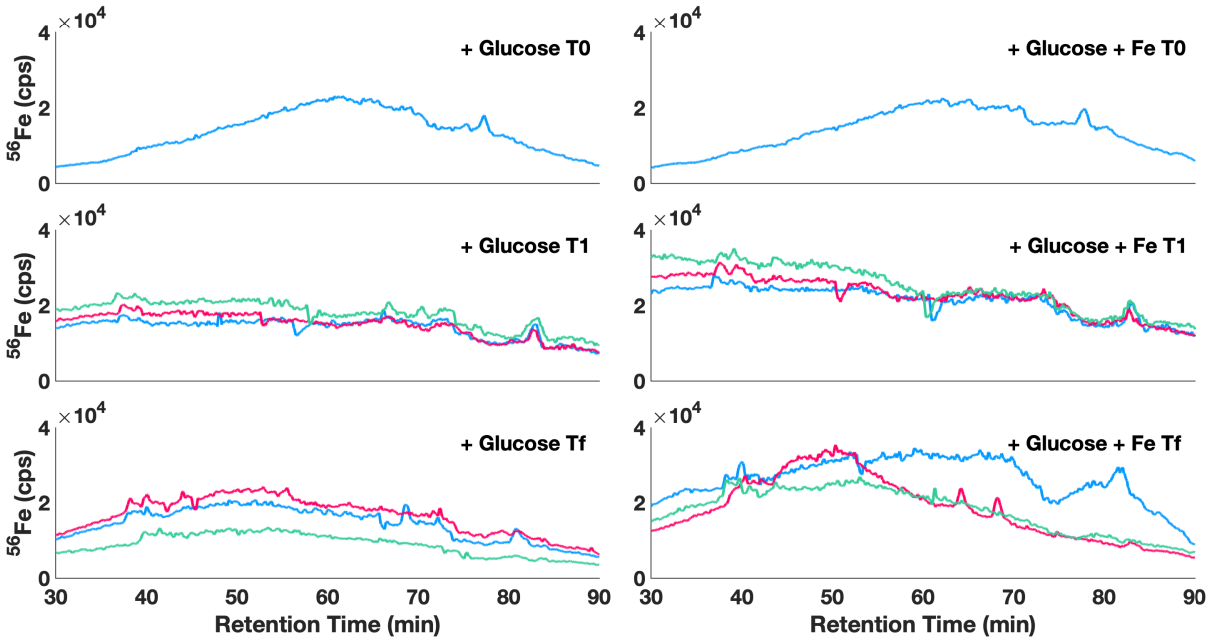

Figure 5.2: LC-ICPMS chromatograms of ^{56}Fe for the Experiment 2.

The observation that addition of labile carbon does not stimulate siderophore production suggests that the most likely explanation for the low siderophore production in the Experiment 2 is a N limitation on siderophore production. During the 2021 cruise for the Experiment 2, the total concentration for nitrate and nitrite is 20 nM at 150 m (Foreman and Karl, personal communication). Post cruise nutrient analyses of the incubation samples showed that over the course of the incubation, the total concentration for nitrate and nitrite was 100 nM in the incubation bottles. The dFe samples have not been

processed for either the water column or incubation samples, but if a dFe concentration of 100 pM at 150 m of Station ALOHA (Fitzsimmons et al 2015) is assumed, and a total concentration for nitrate and nitrite of 100 nM is used, the Fe:N ratio in the incubation bottles without Fe addition would be 1000 μmol/mol. Heterotrophic bacteria including *Pseudomonas* spp. grown under low Fe concentrations have an Fe:C ratio of 8 μmol/mol (Tortell et al 1996), or an Fe:N ratio of 50 μmol/mol assuming Redfield stoichiometry. At 150 m of Station ALOHA, the Fe:N ratio is 20 times higher, suggesting possible N deficiency of siderophore producing heterotrophic bacteria.

Low concentration of N could limit both N metabolism and siderophore production, which are N rich molecules, and therefore limit Fe uptake. Indeed, we find high concentration of siderophores at 200-400 m of the NPSG, and low concentration at 0-200 m (Chapter 3), which might be due to low N at 0-200 m. Therefore, it seems that although glucose addition would increase the extent of Fe deficiency for heterotrophic bacteria, the nitrogen was more deficient, and there was a N limitation of siderophore production in the + Glucose treatment. When both glucose and Fe were added, the Fe:C ratio in seawater is 37 μmol/mol. Therefore, heterotrophic bacteria were not Fe limited, and siderophore production was not found, which was in accordance with the expectation.

When 9 mM glucose, 200 μM ammonium chloride and 20 μM phosphate were added to seawater from English Channel, both ferrioxamines and amphibactins are produced over the course of the incubation, as the microbial community was driven to Fe limitation (Gledhill et al 2004). At 150 m of Station ALOHA, siderophore producing bacteria are present, and Fe limited. However, when 10 μM glucose was added to the incubation bottles, siderophores production is low. This could not be explained by the difference in the glucose concentration between the two experiments, because there is high concentration of siderophore at 200-400 m of NPSG (Chapter 3), where the concentration of organic carbon is even lower than 150 m, and glucose addition is absent. Therefore, we conclude that the most likely explanation for the absence of siderophore production in Experiment 2 is a N limitation on siderophore production.

5.3.3 Experiment 3: High ammonium at 150 m results in siderophore production under glucose addition

To reproduce the results of Experiment 2, we repeated the experiment one year later, again at a site near Station ALOHA (Experiment 3).

In Experiment 3, we have one sample for the + Glucose treatment and one sample for the + Glucose + Fe treatment on T0 (Figure 5.3). However, both of them represent the in situ condition at 150 m, as they were processed immediately after nutrient addition. On T0, the + Glucose + Fe treatment sample had 6.6 pM of a ferrioxamine siderophore (Figure 5.3). This concentration was higher than any of the T0 samples in the 2021 experiments. Indeed, siderophores were not found in the water column samples at 150 m from both 2021 and 2022 cruises, and found only at low concentration (< 0.3 pM) at 150 m at Station ALOHA (Bundy et al 2018).

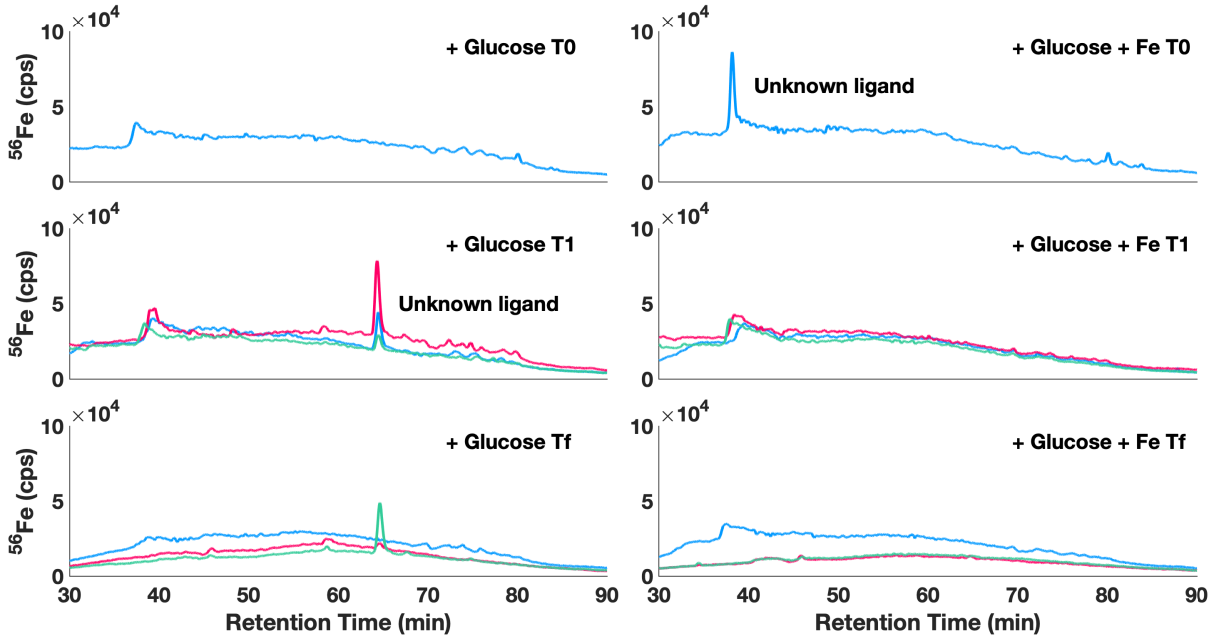

Figure 5.3: LC-ICPMS chromatograms of ^{56}Fe for the Experiment 3.

On both T1 (96 hrs) and Tf (168 hrs), a siderophore peak of 3.3±3.7 pM (1 SD, n=6) was found at ~65 min in the + Glucose treatment (Figure 5.3). This peak was absent in T0 samples (Figure 5.3), and in the + Glucose + Fe treatment. This peak is not a known

ferrioxamine, amphibactin or marinobactin. We are unable to assign masses to these peaks in any of the experiments due to the low concentration.

At the time of the 2022 sample collection, the study site featured an ongoing diatom bloom at the surface. In parallel, there is an ammonium maximum at 140 m and a nitrite maximum at 160 m (Foreman and Karl, personal communication), which are not typical for Station ALOHA. At 150 m, there is 50 nM of ammonium and 109 nM of nitrite, which is higher than the nitrate+nitrite concentration of Experiment 2 in 2021.

For nitrogen, heterotrophic bacteria prefer ammonium over nitrate (Wheeler and Kirchman 1986). Therefore, the presence of siderophore in one of the two samples on T0, and the production of siderophore in the Experiment 3 could be explained by a high concentration of ammonium at 150 m of the station. Ferrioxamines, amphibactins and marinobactins all have 5-10 N per molecule, and 50 nM ammonium could support the production of pM siderophores in the Experiment 3.

When glucose was added to 150 m seawater samples that are typical Station ALOHA's mean state, no siderophores were produced. However, when glucose was added to 150 m seawater samples with elevated N, siderophores are rapidly produced. The presence of siderophore production in the Experiment 3 and the absence of siderophore production in the Experiment 2 suggest the importance of N in siderophore production, although we could not eliminate the possibility of different microbial communities in the two experiments.

The co-limitation of siderophore production by C and N seems less possible, because we found siderophores on T0 in the Experiment 3, which represents the in situ condition at the time of sampling, featuring high concentration of ammonium. The POC sample for T0 in the Experiment 3 has not been processed, and it is possible that the high concentration of siderophores on T0 was due to high concentration of ammonium, not high concentration of both ammonium and POC. In addition, there is high concentration of siderophore at 200-400 m of NPSG (Chapter 3), where the concentration of organic

carbon is even lower than 150 m. Furthermore, the addition of labile carbon does not seem to increase the bioavailability of organic nitrogen, which is another potential source for labile N that could fuel the production of siderophores.

5.3.4 Experiment 4: Siderophores are produced when POM was added

According to these two experiments, siderophore producing bacteria are present at 150 m of Station ALOHA and siderophore production is limited by N. However, these two experiments do not represent the in situ condition, where sinking POM constantly introduces C (Karl et al 1996; Christian et al 1997; Gabrowski et al 2019; Karl et al 2022), N (Karl et al 1996; Christian et al 1997) and Fe (Boyd et al 2010; Hawco et al 2022) to 150 m during particle remineralization. In addition, it is unclear how representative is glucose as a carbon source to heterotrophic bacteria. To represent the in situ condition, and investigate the influence of sinking particles on siderophore production, we performed the Experiment 4, with addition of sinking POM collected by sediment trap as C and N source.

Sinking particles at 150 m of Station ALOHA have an Fe:C ratio of 400 μmol/mol for non lithogenic Fe and total carbon (Hawco et al 2022), or an Fe:N ratio of 2700 μmol/mol if Redfield stoichiometry is assumed. Although this Fe:N ratio is two orders of magnitude higher than dFe:NO_3^- ratio, the bioavailability of Fe is probably lower than N in sinking particles, according to a faster increase in NO_3^- concentration (Casciotti et al 2008) than dFe concentration with depth (Fitzsimmons et al 2015). Therefore, we expected to find siderophore production in the + POM treatment, due to the preferential release of N during particle remineralization, and Fe limitation on heterotrophic bacteria at 150 m. In the + POM + Fe treatment, we expected to find no siderophore production due to the mitigation of Fe limitation by Fe addition.

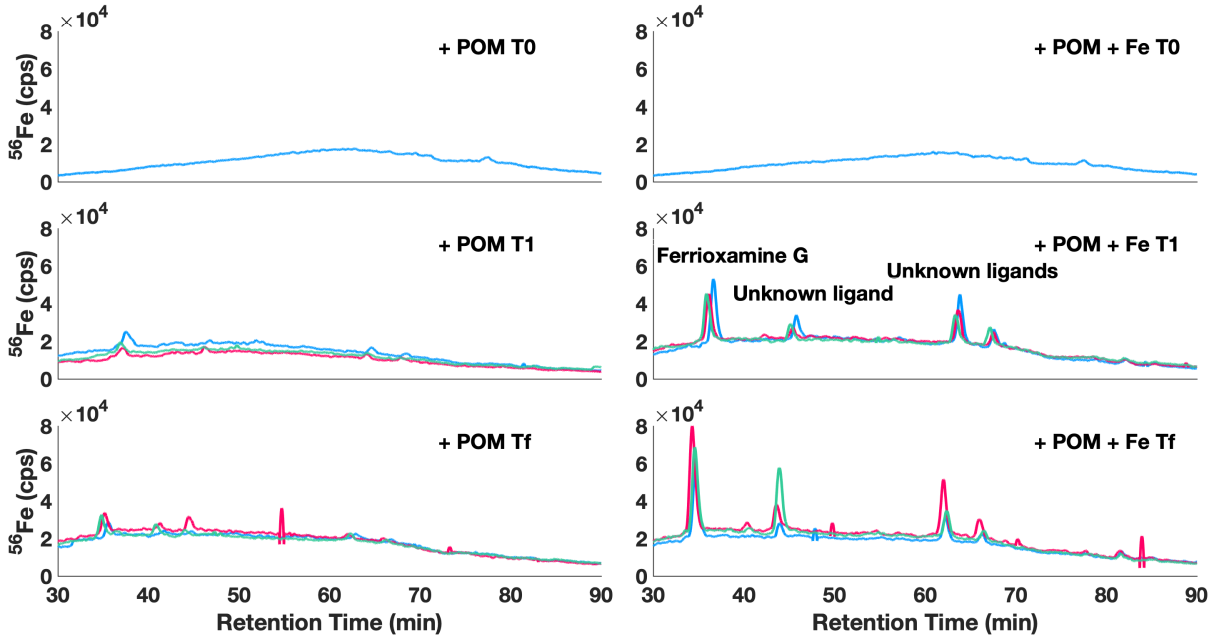

Figure 5.4: LC-ICPMS chromatograms of ^{56}Fe for the Experiment 4.

At T0, a small peak is found at around 78 min (Figure 5.4). At both T1 (48 hrs) and Tf (96 hrs), this peak was absent, but peaks from other siderophores appeared (Figure 5.4). For example, the peak at 35 min was identified as ferrioxmaine G. The peak at 63 min seems to be novel, and we were not able to assign a mass due to its low concentration.

Although we found ferrioxmaine G at the end of incubation with POM, we are unable to conclude whether the ferrioxamine was produced as a response to the particle addition, or released during particle disintegration. We find ferrioxamine G in the suspended particles collected in GP15 (Chapter 3), and we postulate that ferrioxamines should be in the sinking particles at 150 m of Station ALOHA. Therefore, it is likely that ferrioxamines are consistently released in both + POM and + POM + Fe treatments. Because the concentration of ferrioxamine might not reflect siderophore production, we do not attempt to compare the concentration of ferrioxamine between treatments. In any future experiments, a T0 sample is needed for siderophores in the sinking particles, in addition to the seawater for incubation.

Indeed, ferrioxmaine G was the only siderophore we found in suspended particles of the NPSG (Chapter 3). Therefore, the siderophore at 63 min is presumably produced over the course of the incubation, due to nutrients introduced by POM, not released during particle disintegration. One explanation for the production of non polar siderophores in the Experiment 4 is the introduction of labile N by particles. Particle addition increased particulate carbon concentration from a background concentration of 1.2 μM to 3.0 μM in the incubation bottles (Dr. Lauren Manck, personal communication). Therefore, the particle addition results increased POC and PON by ~1.8 μM and ~0.3 μM respectively, if Redfield stoichiometry is assumed. On a global mean, C:N ratios of marine sinking particles from surface water is 7.1, and the C:N ratio increases with depth by 0.2 per 1000 m (Schneider et al 2003). Therefore, Redfield stoichiometry is a reasonable assumption for the sinking particles in the experiment.

Although the bioavailability of the PON to heterotrophic bacteria that could produce siderophores was not previously known, the concentration of potentially labile N added in the experiment was much higher than the total concentration of nitrate and nitrite in the Experiment 1 and Experiment 2, which is 100 nM. Therefore, the addition of PON could have provided labile N for siderophore production, above the concentrations of Experiment 1 and Experiment 2.

The retention time of the non polar peaks in Experiment 4 are similar to the non polar peaks in Experiment 3, where glucose was added without the introduction of particle associated bacteria. Therefore, these non polar siderophores were most likely produced in situ by bacteria, not particle associated bacteria introduced by POM addition.

At both T1 and Tf, the concentrations of siderophores at 63 min were higher in the + POM + Fe treatment, than the + POM treatment. For example, on T1, the concentration for the siderophore at ~63 min was 3.0±0.8 (n=3) pM in the + POM + Fe treatment, and 0.2±0.4 pM (n=3) in the + POM treatment (Figure 5.4). Similarly, on Tf, the concentration for the siderophore at ~63 min was 2.3±0.8 (n=3) pM in the + POM + Fe treatment, and 0.4 pM (n=3) in the + POM treatment (Figure 5.4).

We expected to find lower concentration of siderophores in the + POM + Fe treatment than the + POM treatment, due to the mitigation of Fe limitation by 5 nM $FeCl_3$. We are unable to explain the higher siderophore concentration in the + POM + Fe treatment than the + POM treatment (Figure 5.4). One possible explanation is, POM addition resulted in Fe limitation, the Fe addition resulted in a higher bacterial productivity by mitigating Fe limitation, and siderophore production scaled up with bacterial production. When Fe was added to HNLC surface waters, an increase in bacterial growth has been shown in incubation with light (Cochlan 2001; Oliver et al 2004; Bertrand et al 2011), and no effect in bacterial growth has been shown in incubation in dark (Church et al 2000). Therefore, it is likely that Fe addition promoted bacterial growth by promoting phytoplankton growth and production of organic carbon. If heterotrophic bacteria at 150 m of Station ALOHA were limited by Fe and organic carbon to the same extent, and the bioavailability of Fe was low in POM, siderophore concentration in the + POM + Fe treatment would be higher than the + POM treatment, due to a higher bacterial production.

Another possible explanation is, that siderophores were produced in both treatments, but the siderophores in the + POM only treatment did not bind Fe due to the low dFe concentration in the incubation bottles, and we were not able to detect these apo siderophores on LC-ICPMS.

5.3.5 Experiment 5-6: Siderophore production under particle addition is prevalent across experiments

In addition to the Experiment 4, we performed two shorter incubations with POM addition, Experiment 5 and Experiment 6, to confirm the influence of POM on siderophore production, and to investigate the influence of labile organic carbon and nitrogen on siderophore production. In the Experiment 5, there was a + POM treatment and a + POM + Fe treatment. In the Experiment 6, there was a + POM treatment and a + POM + Glucose treatment. According to Experiments 2-4, POM would provide N for siderophore production. At 150 m of Station ALOHA, siderophore production is presumably limited by N or C. If N limitation is mitigated, siderophore production might be limited by C, although POM also provide labile C. If siderophore production is limited

by C in the presence of POM, due to low bioavailability of C in POM, additional glucose would promote siderophore production. These two experiments were shorter incubations with only a final time point, which represents a snapshot of the incubation, Therefore, we do not attempt to compare the concentration of siderophores between treatments.

We found siderophore production in both Experiment 5 and Experiment 6 (Figure 5.5 and Figure 5.6). For both experiments, the polar siderophore at ~38 min was ferrioxamine G, according to the alignment of isotopologue of ^{56}Fe-siderophore and ^{27}Al-siderophore (Figure 5.7). The polar siderophore at ~48 min was ferrioxamine E, according to the alignment of isotopologue of ^{56}Fe-siderophore and ^{54}Fe-siderophore, the same retention time of authentic standard of ferrioxamine E, and the fragmentation pattern (Figure 5.8). The MS^2 fragmentation spectra of ^{56}Fe-ferrioxamine E (m/z = 654.27) shows major fragments of 471, 573, 554, 591 and 636, which are all characteristic for ferrioxamines in agreement with the fragmentation spectra of authentic ^{56}Fe-ferrioxamine E (Mawji et al 2008).

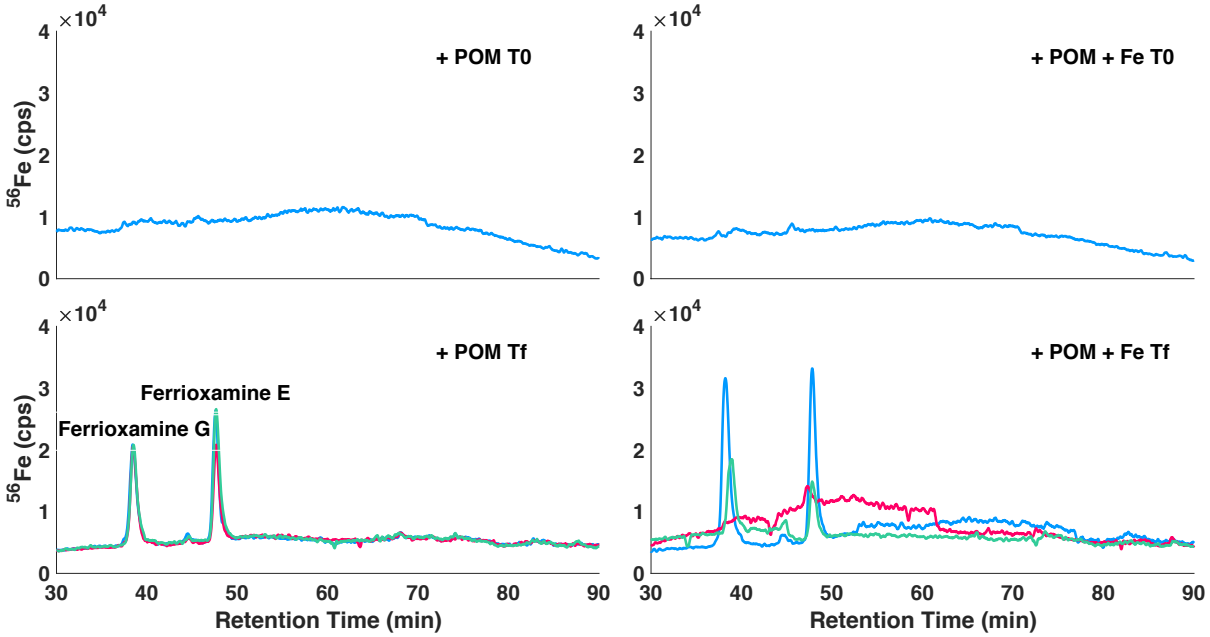

Figure 5.5: LC-ICPMS ^{56}Fe-chromatograms for the Experiment 5.

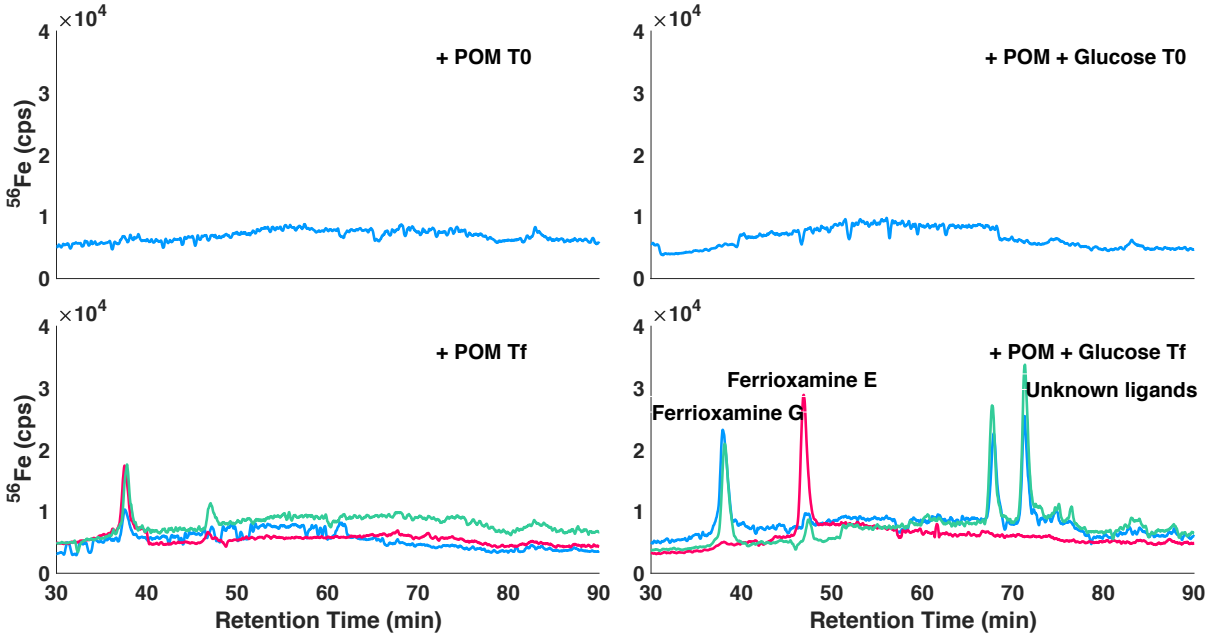

Figure 5.6: LC-ICPMS chromatograms of ^{56}Fe for the Experiment 6.

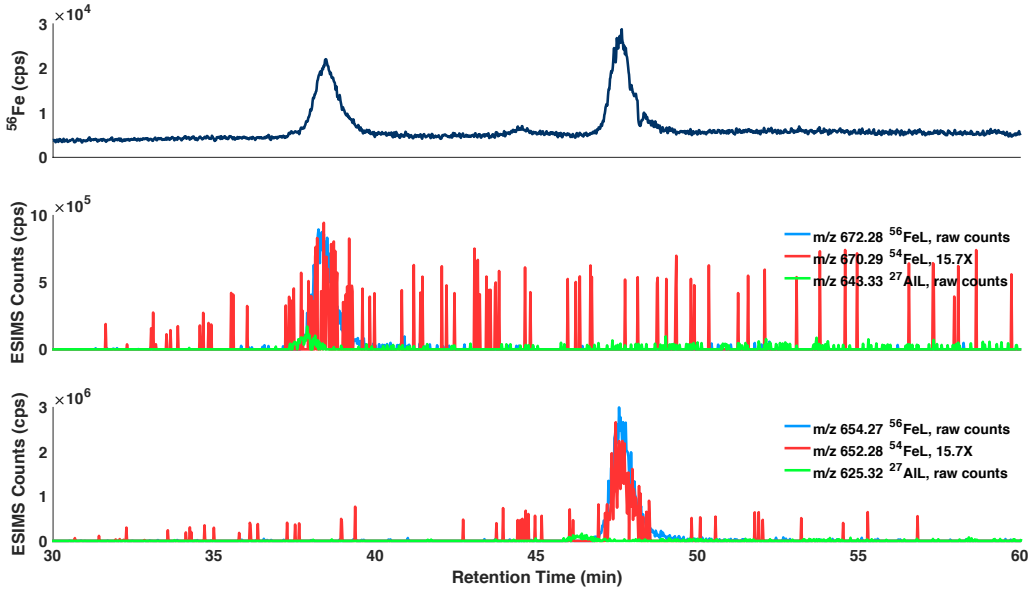

Figure 5.7: Ferrioxamine G and Ferrioxamine E characterization. The top panel is the ^{56}Fe LC-ICPMS chromatogram from the replicate A of the Experiment 4 on T1. The lower panels are the extracted ion chromatograms (EIC) from positive mode LC-ESIMS chromatograms. Blue lines correspond to the ^{56}Fe-siderophore $[M+H]^+$ isotopologue, red lines correspond to the ^{54}Fe-siderophore $[M+H]^+$ isotopologue, and green lines correspond to the ^{27}Al- siderophore $[M+H]^+$ isotopologue. The intensity of the light iron isotopologue has been scaled by the natural abundance ratio of ^{56}Fe/^{54}Fe (scaled up by 15.7) so that the isotopologues overlap.

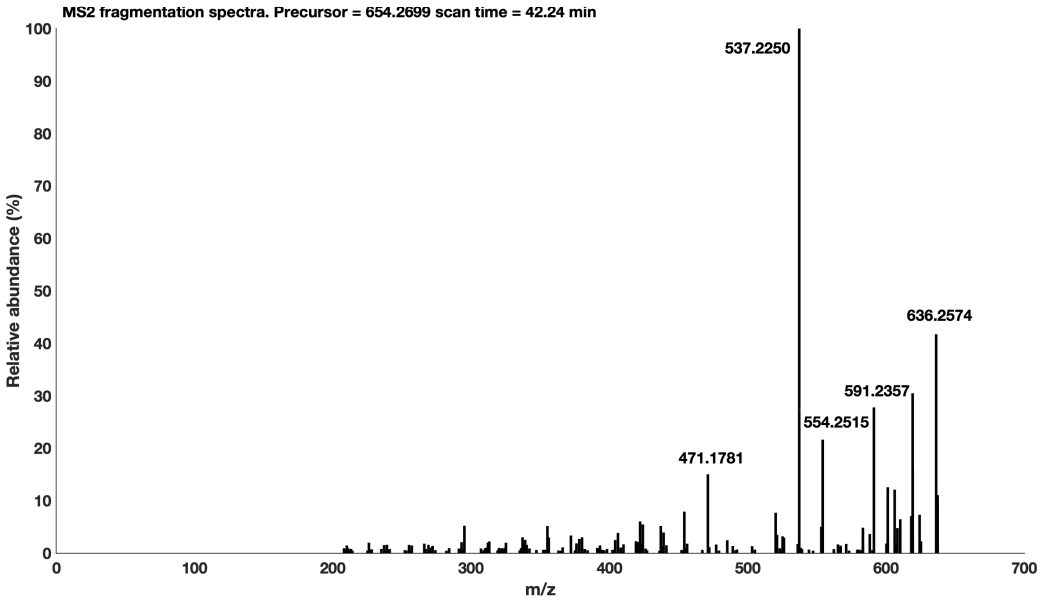

Figure 5.8: MS^2 fragmentation spectra of the ^{56}Fe-Desferrioxamine E.

The consistent production of ferrioxamines under particle addition in our experiments is in accordance with other experiments (Velasquez et al 2016; Bundy et al 2018). Although we consistently find ferrioxamines at the end of + POM treatment, we are unable to conclude whether the ferrioxamines were produced as a response to the particle addition, or released during particle disintegration.

In Experiment 6, we found production of non polar siderophores on Tf at 68-72 min (Figure 5.6). These siderophores have similar retention times to marinobactins and amphibactins, but we did not identify any known marinobactins or amphibactins in the LC-ESIMS data, and we were not able to assign masses to these non polar siderophores, which was unexpected due to their high concentration (8.0-20.6 pM).

These short incubations were performed with 1 L of seawater, which is 25% of a typical sample for siderophores. Therefore, the concentration for these non polar siderophores are equivalent to 2.0-5.2 pM in a typical 4 L sample. For siderophores with concentrations <5 pM in 4 L samples, the mass search algorithms might not be able to assign a mass to the Fe-siderophore complex, because the ^{54}Fe-siderophore is often

below the limit of detection of LC-ESIMS. In addition, these non polar siderophores do not bind Al according to LC-ICPMS, and we could not use Al as a pseudoisotope of Fe in the mass search algorithms.

In our standard protocol, siderophores are extracted from 4 L of seawater by SPE cartridge, which is washed with to 6 ml of qH_2O and eluted with 6 ml of MeOH. The MeOH extract was concentrated to 500 µl, resulting in a concentrating factor of 8000 from seawater to the sample that is measured on LC-MS. In the standard protocol, the MeOH extract is not further concentrated, which could result in precipitation of siderophores due to evaporation of MeOH. In the Experiment 6, siderophores were concentrated from 1 L of seawater to 500 µl of MeOH, resulting in a concentrating factor of 2000. In these samples, we found non polar siderophores, but were not able to assign a mass to them. Therefore, we combined the two 500 µl samples that have the non polar siderophores (Figure 5.6), and concentrated the combined sample from 1000 µl to 100 µl, and measured the sample again on LC-ESIMS. However, we were not able to assign a mass to the non polar siderophores in the combined sample, although the concentration was 10 times higher. Indeed, the counts for the ferrioxamines in the sample and the internal standard of Ga-DFE in the sample are both lower than the sample before further concentration, suggesting that siderophores precipitated during further concentration.

In addition, the absence of mass assignment for these non polar peaks might be explained by a low sensitivity of these non polar siderophore on LC-ESIMS. When an external standard including the same concentration of ferrichrome and ferrioxamine E is measured on LC-ESIMS, the counts are 5-10 times lower for ferrichrome than ferrioxamine E. If the non polar siderophores in the Experiment 6 have a low sensitivity that is similar to ferrichrome, it could also result in the absence of detection for ^{54}Fe-isotopologue.

In the Experiment 6, these non polar siderophores are present in the + POM + Glucose treatment, and absent in the + POM treatment. However, these non polar siderophores

are present in the Experiment 4 under POM addition, and absent in the Experiment 5 under POM addition. Therefore, we are not able to conclude the influence of additional glucose on the production of these non-polar siderophores.

When glucose was added to seawater from 150 m, we found low concentration of siderophores over the course of the incubation. When glucose was added with the POM, we found high concentration of siderophores, which was made possible by the introduction of N during particle remineralization, supporting the N limitation on siderophore production.

5.3.6 Experiment 7: Freshly collected diatom biomass results in production of non polar siderophores

The Experiment 4 and 5 (+ POM; + POM + Fe) was also repeated one year later (Experiment 7). The station of Experiment 7 features an ongoing diatom bloom at the surface, similar to the Experiment 3. In contrast to the Experiment 4 and 5, where the particles were collected using the sediment trap at 150 m, the POM in Experiment 7 were collected using a surface net tow. Therefore, the particles in the Experiment 7 represent fresh diatom biomass.

In Experiment 7, a suite of siderophores were found at 70-80 min across treatments on both T1 (72 hrs) and Tf (120 hrs), with a total concentration of 4.2-16.2 pM (Figure 5.9). These siderophores were also present at T0, at a concentration of 3.2-5.2 pM. According to the retention time, they are likely amphibactins or marinobactins (Chapter 3), which are also likely to be present as a suite of peaks.

On both T1 and Tf, the total concentration of siderophores was higher in the + POM treatment than the + POM + Fe treatment (Figure 5.9). For example, the total concentration was 11.9±0.3 pM (n=3) in the + POM treatment on T1, which was higher than the concentration on T0 (3.2-5.2 pM). The total concentration was 5.8±1.4 pM (n=3) in the + POM + Fe treatment on T1, which was similar to the concentration on T0.

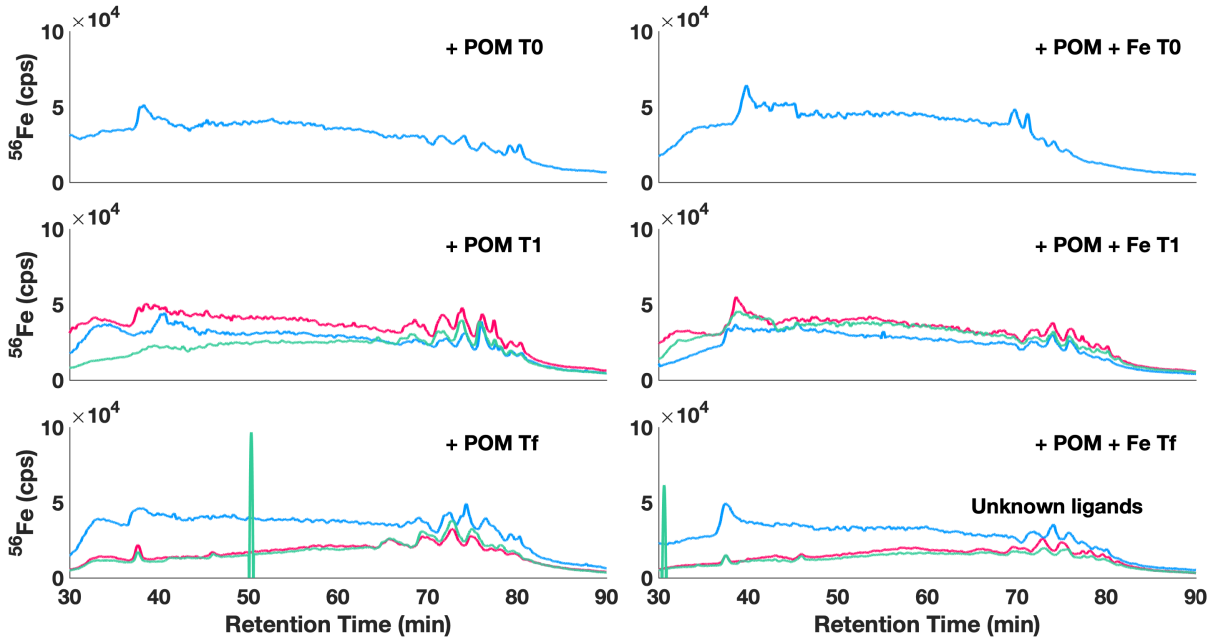

Figure 5.9: LC-ICPMS chromatograms of ^{56}Fe for the Experiment 7.

The similar suite of siderophore between T0, T1 and Tf suggests that sinking particles at 150 m have sufficient bioavailable C to induce Fe limitation in situ, and sufficient bioavailable N to support siderophore production. The higher concentration in the + POM treatment on T1 than T0 suggests that fresh diatom biomass at surface contains more C and N than the processed sinking particles at 150 m, which results in a higher extent of Fe limitation. This Fe limitation could be mitigated by the addition of inorganic Fe, which could explain the lower concentration of siderophores in the + POM + Fe treatment, than the particle alone treatment. Indeed, the concentration in the + POM + Fe treatment is similar to T0, suggesting that there might be no siderophore production over the course of the incubation due to addition of 5 nM inorganic Fe.

5.4 Conclusions

In this chapter, we report the siderophore production in seawater collected at 150 m in the NPSG near Station ALOHA, after nutrient amendment including glucose, POM, and Fe.

The absence of siderophore production in the glucose experiment suggests that siderophore production is limited by N at 150 m of Station ALOHA with a typical nutrient distribution. During some dynamic processes, such as a surface diatom bloom which results in high concentration of ammonium 150 m, siderophores could be produced in situ, due to the presence of highly bioavailable N.

POM addition consistently results in the production of ferrioxamines. However, it remains unclear whether the ferrioxamines were produced as a response of nutrient addition by POM, or released from POM over the course of the incubation. The addition of POM alone could also result in the production of non polar siderophores, which also suggests the importance of PON in siderophore production.

5.5 References

Tortell, P. D., Maldonado, M. T., & Price, N. M. (1996). The role of heterotrophic bacteria in iron-limited ocean ecosystems. Nature, 383(6598), 330-332.

Casciotti, K. L., Trull, T. W., Glover, D. M., & Davies, D. (2008). Constraints on nitrogen cycling at the subtropical North Pacific Station ALOHA from isotopic measurements of nitrate and particulate nitrogen. Deep Sea Research Part II: Topical Studies in Oceanography, 55(14-15), 1661-1672.

Fitzsimmons, J. N., Hayes, C. T., Al-Subiai, S. N., Zhang, R., Morton, P. L., Weisend, R. E., ... & Boyle, E. A. (2015). Daily to decadal variability of size-fractionated iron and iron-binding ligands at the Hawaii Ocean Time-series Station ALOHA. Geochimica et Cosmochimica Acta, 171, 303-324.

Bundy, R. M., Boiteau, R. M., McLean, C., Turk-Kubo, K. A., McIlvin, M. R., Saito, M. A., ... & Repeta, D. J. (2018). Distinct siderophores contribute to iron cycling in the mesopelagic at station ALOHA. Frontiers in Marine Science, 5, 61.

Gledhill, M., McCormack, P., Ussher, S., Achterberg, E. P., Mantoura, R. F. C., & Worsfold, P. J. (2004). Production of siderophore type chelates by mixed bacterioplankton populations in nutrient enriched seawater incubations. Marine Chemistry, 88(1-2), 75-83.

Wheeler, P. A., & Kirchman, D. L. (1986). Utilization of inorganic and organic nitrogen by bacteria in marine systems 1. Limnology and Oceanography, 31(5), 998-1009.

Karl, D. M., Christian, J. R., Dore, J. E., Hebel, D. V., Letelier, R. M., Tupas, L. M., & Winn, C. D. (1996). Seasonal and interannual variability in primary production and particle flux at Station ALOHA. Deep Sea Research Part II: Topical Studies in Oceanography, 43(2-3), 539-568.

Christian, J. R., Lewis, M. R., & Karl, D. M. (1997). Vertical fluxes of carbon, nitrogen, and phosphorus in the North Pacific Subtropical Gyre near Hawaii. Journal of Geophysical Research: Oceans, 102(C7), 15667-15677.

Grabowski, E., Letelier, R. M., Laws, E. A., & Karl, D. M. (2019). Coupling carbon and energy fluxes in the North Pacific Subtropical Gyre. Nature Communications, 10(1), 1895.

Karl, D. M., Björkman, K. M., Church, M. J., Fujieki, L. A., Grabowski, E. M., & Letelier, R. M. (2022). Temporal dynamics of total microbial biomass and particulate detritus at Station ALOHA. Progress in Oceanography, 205, 102803.

Boyd, P. W., Ibisanmi, E., Sander, S. G., Hunter, K. A., & Jackson, G. A. (2010). Remineralization of upper ocean particles: Implications for iron biogeochemistry. Limnology and Oceanography, 55(3), 1271-1288.

Hawco, N. J., Yang, S. C., Pinedo-González, P., Black, E. E., Kenyon, J., Ferrón, S., ... & John, S. G. (2022). Recycling of dissolved iron in the North Pacific Subtropical Gyre. Limnology and Oceanography, 67(11), 2448-2465.

Schneider, B., Schlitzer, R., Fischer, G., & Nöthig, E. M. (2003). Depth-dependent elemental compositions of particulate organic matter (POM) in the ocean. Global Biogeochemical Cycles, 17(2).

Cochlan, W. P. (2001). The heterotrophic bacterial response during a mesoscale iron enrichment experiment (IronEx II) in the eastern equatorial Pacific Ocean. Limnology and Oceanography, 46(2), 428-435.

Oliver, J. L., Barber, R. T., Smith Jr, W. O., & Ducklow, H. W. (2004). The heterotrophic bacterial response during the Southern Ocean iron experiment (SOFeX). Limnology and oceanography, 49(6), 2129-2140.

Church, M. J., Hutchins, D. A., & Ducklow, H. W. (2000). Limitation of bacterial growth by dissolved organic matter and iron in the Southern Ocean. Applied and Environmental Microbiology, 66(2), 455-466.

Mawji, E., Gledhill, M., Milton, J. A., Zubkov, M. V., Thompson, A., Wolff, G. A., & Achterberg, E. P. (2011). Production of siderophore type chelates in Atlantic Ocean waters enriched with different carbon and nitrogen sources. Marine Chemistry, 124(1-4), 90-99.

Velasquez, I. B., Ibisanmi, E., Maas, E. W., Boyd, P. W., Nodder, S., & Sander, S. G. (2016). Ferrioxamine siderophores detected amongst iron binding ligands produced during the remineralization of marine particles. Frontiers in Marine Science, 3, 172.

Appendix 5.1 An Fe ligand produced by axenic culture of *Prochlorococcus*

Culture work by Tyler O'Keefe and Allison Coe

It has been well established that heterotrophic bacteria can produce and use siderophores to facilitate Fe uptake. In eukaryotic phytoplankton, siderophore synthesis has not been demonstrated. However, eukaryotic phytoplankton are able to take Fe bound to exogenous siderophores by cell surface Fe reduction of Fe(III) to Fe(II) (Shaked et al 2005), endocytosis (Kazamia et al 2018), or combination of the two mechanisms (Coale et al 2019).

Siderophore production has been shown in freshwater cyanobacteria (Itou et al 2001; Ito and Butler 2005; Boiteau and Repeta 2015), but not oceanic cyanobacteria including *Prochlorococcus* and *Synechococcus*. Therefore, the Fe uptake mechanism of *Prochlorococcus*, which is the numerically dominant phototroph in the ocean, remains unknown. In this chapter, the Fe ligand production by axenic culture of *Prochlorococcus* was investigated.

By searching known genes responsible for siderophore synthesis in heterotrophic bacteria in the genome of *Prochlorococcus*, Hopkinson and Morel (2009) concluded that *Prochlorococcus* (AS9601, CCMP1375, CCMP1986, MIT9211, MIT9215, MIT9301, MIT9303, MIT9312, MIT9313, MIT9515, NATL1A, NATL2A) appear to not produce siderophores. However, Boiteau (2016) analyzed the supernatant of different *Prochlorococcus* strains (AS9601ax, Natl2Aax, Med4ax, MIT9202ax, MIT9301ax, MIT9303ax), and found Fe ligand complexes (Fe-Ls) in all strains, however the molecular weight of the ligand could not be determined, due to degradation of the ligands during analyses.

To further investigate the Fe ligands by *Prochlorococcus*, we analyzed the supernatant of 3 axenic *Prochlorococcus* culture, including *Prochlorococcus* SBax, *Prochlorococcus* MIT1214ax and *Prochlorococcus* MIT0917ax, and found Fe-Ls in all of them (Figure A.1). These ligands were not in the media blank, suggesting that the ligands are

produced by multiple strains of *Prochlorococcus*. In addition, *Prochlorococcus* SBax produce Fe ligands with both NO_3^- and NH_4^+ as N sources (Figure A.1).

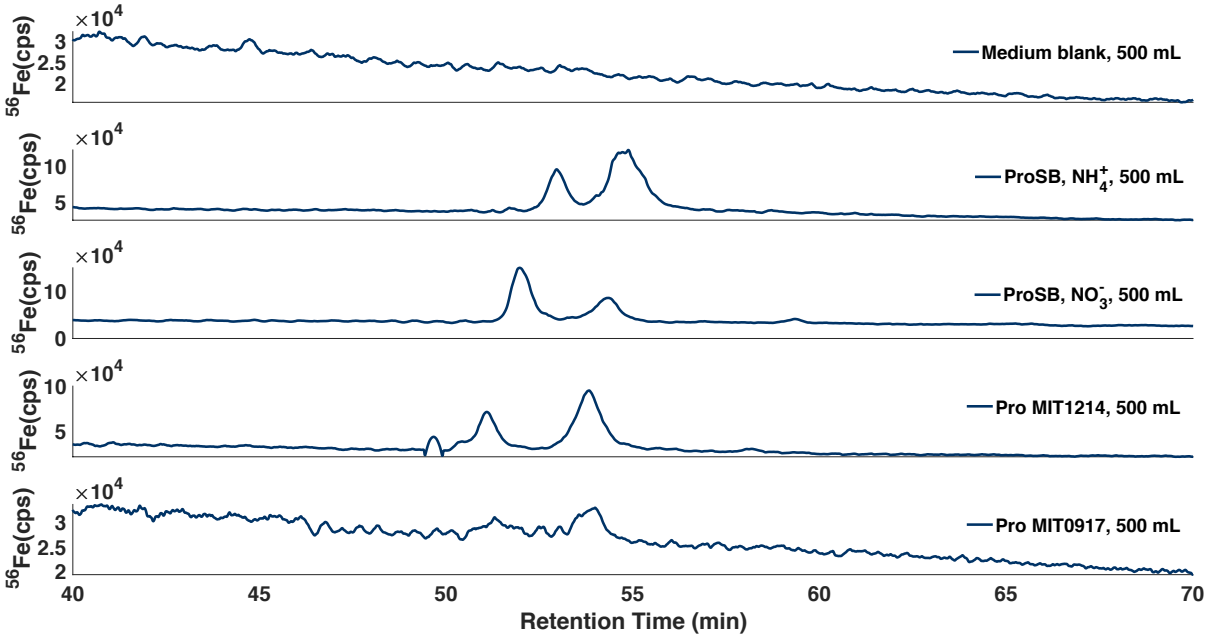

Figure A5.1: LC-ICPMS chromatograms of samples for the supernatant of cultures of *Prochlorococcus* SBax, MIT1212ax, and MIT 0917ax and the media blank for the cultures. *Prochlorococcus* SBax were grown with both NO_3^- and NH_4^+ as N source.

These samples were analyzed with a different LC gradient than used by Boiteau (2016). However, after normalization to the internal standard (Vitamin B_{12}) the Fe-L peaks in our samples show similar retention time as those reported by Boiteau (2016). To acquire sufficient material for LC-ESIMS measurement, we scaled up the culture from 500 mL to 10 L. In the LC-ICPMS measurement, we found Fe-Ls at similar retention times as the peaks in the 500 mL culture (Figure A.2), and the peaks again were not in the media blank. In addition, the peaks were absent in the cell pellet, which was extracted with MeOH under ultrasonication (Chapter 3).

In the LC-ESIMS measurement, we were able to assign an m/z of 908.16 to the most abundant Fe-L complex, according to the presence of the pair of isotopologue representing ^{56}FeL and ^{54}FeL (Figure A.2). In addition, we found the non-metallated apo ligand at the same retention time, and the retention time for both Fe-ligand complex and apo ligand LC-ESIMS are the same as the retention time in LC-ICPMS, confirming the

mass assignment. The difference in m/z between the ^{56}FeL and the apo ligand is 52.91, suggesting that the oxidation state of Fe in the ligand is +3.

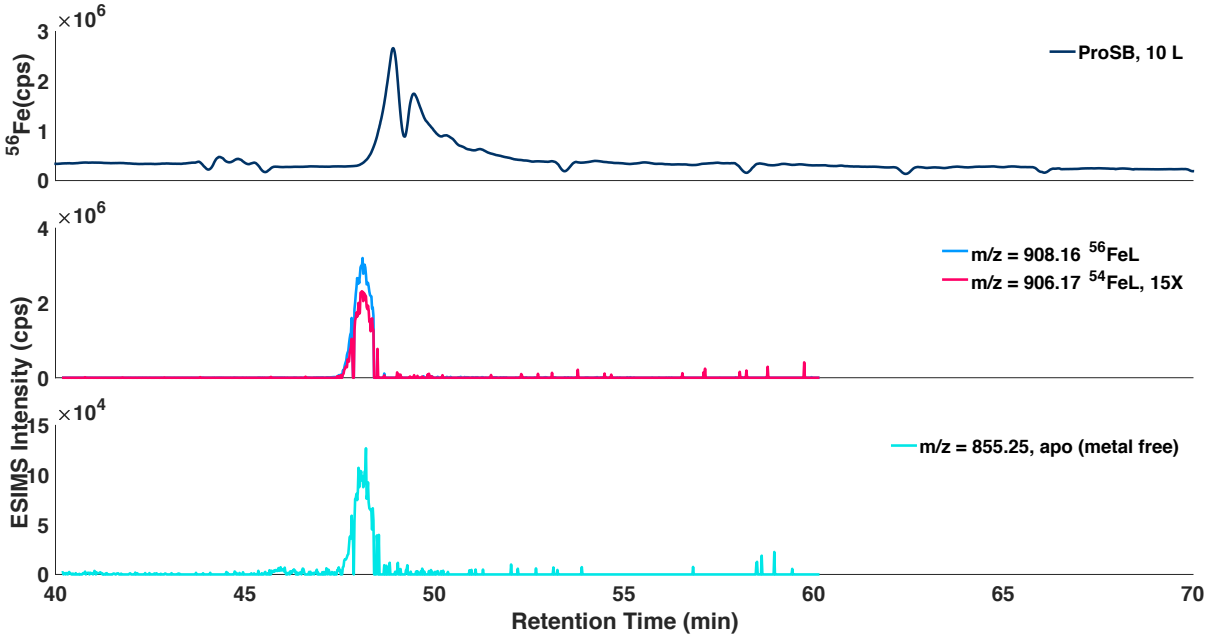

Figure A5.2: Characterization of the Fe ligand complex produced by *Prochlorococcus*. The top panel is the ^{56}Fe LC-ICPMS chromatogram for the supernatant of the culture. The lower panels are the extracted ion chromatograms (EIC) from positive mode LC-ESIMS of the same sample. The blue line corresponds to the ^{56}Fe-siderophore $[M+H]^+$ isotopologue and the red line corresponds to the ^{54}Fe-siderophore $[M+H]^+$ isotopologue. The intensity of the ^{54}Fe-isotopologue has been scaled by the natural (crustal) abundance ratio of ^{56}Fe/^{54}Fe (15.7) so that the isotopologues overlap. The cyan line corresponds to the apo siderophore $[M+H]^+$.

The m/z of 908.16 is not found in the database of 366 known siderophores (Hider and Kong 2010), suggesting that this ligand is novel to the database. Using the natural abundance of stable isotopes, we can estimate the elemental composition of the molecule. For example, the natural abundance of ^{13}C is 1.1%, and the M+1:M ratio is 0.48 for the peak of 908.16, suggesting that there are about 44 carbon atoms in the ligand. In addition, the mass difference between ^{32}S and ^{34}S is 1.996, and the natural abundance of ^{34}S is 4.3%. For the peak of 908.16, the M+2:M (M+1.996:M) ratio is 0.07, suggesting that there are 2 sulfur atoms in the molecule.

For oxygen, the mass difference between ^{16}O and ^{18}O is 2.004 and the natural abundance of ^{18}O is 0.2%. The mass resolution of LC-ESIMS allows us to distinguish the ^{18}O isotopologues from the ^{34}S isotopologues based on their mass differences, but does not allow us to distinguish this M+2 peak from the M+2 peak due to the presence of two ^{13}C atoms (2.007) in the ligand. The ratio of M+2:M (M+2.004:M) is 0.09, which is due to the combination of a M+2 peak for one ^{18}O atom and a M+2 peak for two ^{13}C atoms. For a compound that has 44 carbon atoms, the M+2 peak for two ^{13}C atoms account for 11% of the M peak. Therefore, we are not able to estimate the number of oxygen atoms in the molecule due to the interference of ^{13}C.

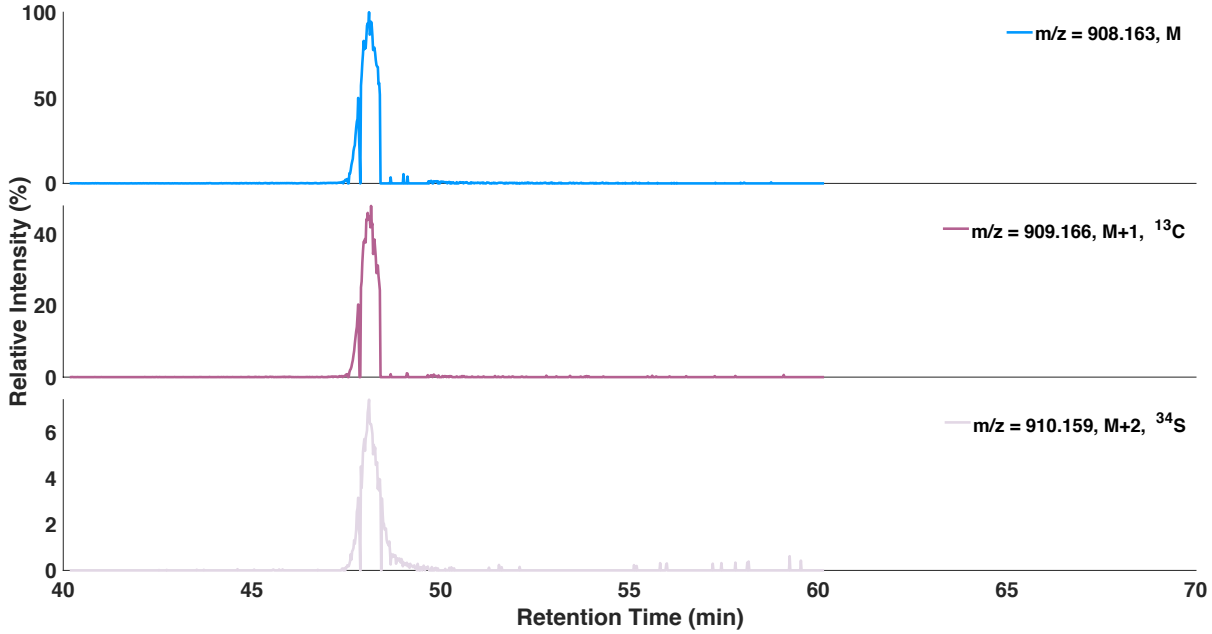

Figure A5.3: The isotope peaks in the LC-ESIMS for the Fe ligand complex produced by *Prochlorococcus* SBax. The top panel is the ^{56}Fe-siderophore without rare isotope in the molecule (^{54}Fe, ^{13}C, ^{18}O, ^{34}S). The second panel is the ^{56}Fe-siderophore with one ^{13}C atom in the molecule. The third panel is the ^{56}Fe-siderophore with one ^{34}S atom in the molecule.

The Fe-ligand complex has one Fe atom, two S atoms. The LC-ESIMS measurement has a mass resolution of 500000 at m/z of 200, and 200000 at a m/z of 1000. Therefore, the accuracy in the molecular weight is ~0.005 amu. Using these conditions, we found 48 possible formula, and we were not able to assign a unique formula to the compound.

To investigate the structure of the ligand, we acquired the MS^2 spectra of the Fe-ligand complex (Figure A.4). One major fragment of 603.097 represents a neutral loss of 305.068 from 908.165, corresponding to the molecular formula of $C_{10}H_{15}N_3O_6S$ (Table A.1). The presence of S in the neutral loss, and therefore in the molecule, is in accordance with the presence of the M+2 peak for S in the LC-ESIMS data. The neutral loss has a similar formula to glutathione, which is $C_{10}H_{17}N_3O_6S$. Indeed, Fe(II)-glutathione is the dominant component of the cytoplasmic labile iron pool (Hider and Kong 2011).

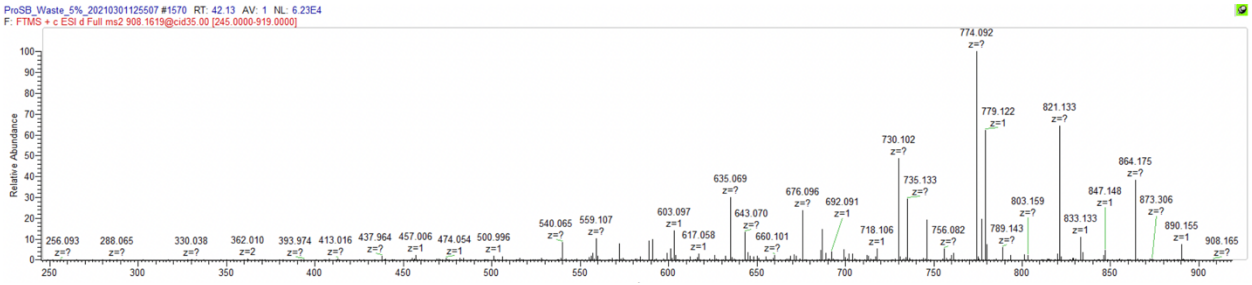

Figure A5.4: MS^2 fragmentation spectra of the ^{56}Fe-complex from *Prochlorococcus* SBax with a m/z of 908.165.

Table A5.1: Neutral losses from the ^{56}Fe-complex with a m/z of 908.165.

Precursor m/z	Fragment m/z	Neutral loss m/z	Neutral loss formula
908.165	864.175	43.990	CO_2
908.165	821.133	87.032	$C_3H_5NO_2$
908.165	779.122	129.043	$C_5H_7NO_3$
908.165	774.092	134.073	$C_9H_{10}O$
908.165	735.133	173.032	$C_5H_7NO_3$, CO_2
908.165	730.102	178.063	$C_9H_{10}O$, CO_2
908.165	676.096	232.069	$C_8H_{12}N_2O_6$
908.165	643.070	265.095	$C_3H_5NO_2$, CO_2, $C_9H_{10}O$
908.165	635.069	273.096	$C_{10}H_{15}N_3O_6$
908.165	603.097	305.068	$C_{10}H_{15}N_3O_6S$
908.165	559.107	349.058	$C_{10}H_{15}N_3O_6S$, CO_2
908.165	540.065	368.100	$C_{10}H_{15}N_3O_6S$, NH_3, CH_2O_2

For example, iron(II) accounts for higher than 80% of the cell labile Fe pool for erythroid (Egyed and Saltman 1984), K562 cells (Breuer et al 1995), and hepatocytes (Petrat et al 2002). This is because Fe(III) is rapidly reduced to Fe(II) in the presence of glutathione at pH of 7-8 (Hamed et al 1983). Then, glutathione binds Fe(II) through the thiol group to a considerable extent at pH 7.0, due to the high stability constant which is similar to H_2S, and a high cytoplasmic concentration which is two orders of magnitude higher than H_2S (Hider and Kong 2011). Therefore, the neutral loss of 305.068 is related to glutathione, with one additional degree of unsaturation, possibly due to the oxidation of glutathione by Fe(III).

In addition, the major fragment of 774.092 represents a neutral loss of 134.073 from 908.165, corresponding to the molecular formula of $C_9H_{10}O$. In the MS^2 of tyrosine, both amine group and carboxyl group are lost, resulting in a fragment ion of $C_8H_7O^-$ that has an m/z of 119 (Syslova et al 2014). The molecular formula of the neutral compound would be C_8H_8O, which differs from $C_9H_{10}O$ by a CH_2. Therefore, the neutral loss of

$C_9H_{10}O$ from the Fe ligand complex might be related to tyrosine. Although we could not assign a unique molecular formula to the ligand, most of the candidate formula have a high degree of unsaturation, which could be explained by the presence of an aromatic functional group in the ligand.

The major fragment of 821.133 represents a neutral loss of 87.032 from 908.165, corresponding to the neutral loss of $C_3H_5NO_2$, consistent with the presence of serine ($C_3H_7NO_3$) in the ligand. The major fragment of 779.122 represents a neutral loss of 129.043 from 908.165, corresponding to the neutral loss of $C_5H_7NO_3$, consistent with the presence of glutamic acid ($C_5H_9NO_4$) in the ligand.

In summary, three axenic strains of *Prochlorococcus* produces an Fe ligand with m/z of 908.16. This ligand is present in the supernatant, but not in the cell pellet. The ligand has two sulfur atoms, and probably two glutathione related groups. The oxidation state of Fe in the ligand is +3.

However, we are not able to confirm the molecular structure of the Fe ligand complex. First, the accuracy in molecular weight does not allow us to assign a unique molecular formula to the Fe ligand complex, which could be addressed by measurement on mass spectrometry of higher resolution. In addition, Furthermore, the Fe binding group in the ligand other than thiol group remains unknown. In the fragmentation pattern, we did not find evidence for the presence of hydroxamate group, catecholate group, or α-hydroxy-carboxylic group, which are the only three Fe binding groups for known siderophores.

Methods

Prochlorococcus culture were grown in AMP1 media at 24 °C and 30 μE light, and harvested at late exponential phase. To confirm samples were axenic (free of heterotrophic contamination), samples were stained with DNA stain Sybr green (Invitrogen, USA) at a 1x final concentration for 60min. Following this, the samples were excited with a 488 nm blue laser on a Guava 12HT flow cytometer (Cytek, USA) and

analyzed for chlorophyll fluorescence (692/40 nm) and DNA content (525/30 nm). The axenicity of the culture was confirmed before inoculation and before harvest.

The cells were pelleted by centrifuge at 7078 rpm for 80 min, and the supernatant including remaining cells were passed through 0.2 μm PES capsule filter (MilliporeSigma) and Bond-Elut ENV solid phase extraction (SPE) columns (1 g, 6 mL, P/N 12255012, Agilent Technologies) at 20 mL/min. The solid phase extraction and LC-MS measurement were performed according to the protocol in Chapter 3.

References

Shaked, Y., Kustka, A. B., & Morel, F. M. (2005). A general kinetic model for iron acquisition by eukaryotic phytoplankton. *Limnology and Oceanography*, *50*(3), 872-882.

Kazamia, E., Sutak, R., Paz-Yepes, J., Dorrell, R. G., Vieira, F. R. J., Mach, J., ... & Lesuisse, E. (2018). Endocytosis-mediated siderophore uptake as a strategy for Fe acquisition in diatoms. *Science Advances*, *4*(5), eaar4536.

Coale, T. H., Moosburner, M., Horák, A., Oborník, M., Barbeau, K. A., & Allen, A. E. (2019). Reduction-dependent siderophore assimilation in a model pennate diatom. *Proceedings of the National Academy of Sciences*, *116*(47), 23609-23617.

Itou, Y., Okada, S., & Murakami, M. (2001). Two structural isomeric siderophores from the freshwater cyanobacterium Anabaena cylindrica (NIES-19). Tetrahedron, 57(44), 9093-9099.

Ito, Y., & Butler, A. (2005). Structure of synechobactins, new siderophores of the marine cyanobacterium Synechococcus sp. PCC 7002. Limnology and Oceanography, 50(6), 1918-1923.

Boiteau, R. M., & Repeta, D. J. (2015). An extended siderophore suite from Synechococcus sp. PCC 7002 revealed by LC-ICPMS-ESIMS. Metallomics, 7(5), 877-884.

Hopkinson, B. M., & Morel, F. M. (2009). The role of siderophores in iron acquisition by photosynthetic marine microorganisms. Biometals, 22, 659-669.

Boiteau, R. M. (2016). Molecular determination of marine iron ligands by mass spectrometry (Doctoral dissertation, Massachusetts Institute of Technology).

Hider, R. C., & Kong, X. (2010). Chemistry and biology of siderophores. Natural product reports, 27(5), 637-657.

Hider, R. C., & Kong, X. L. (2011). Glutathione: a key component of the cytoplasmic labile iron pool. Biometals, 24, 1179-1187.

Syslová, K., Böhmová, A., Mikoška, M., Kuzma, M., Pelclová, D., & Kačer, P. (2014). Multimarker screening of oxidative stress in aging. Oxidative medicine and cellular longevity, 2014.

Egyed', A., & Saltman, P. (1984). Iron is maintained as Fe (II) under aerobic conditions in erythroid cells. Biological Trace Element Research, 6, 357-364.

Breuer, W., Epsztejn, S., & Cabantchik, Z. I. (1995). Iron Acquired from Transferrin by K562 Cells Is Delivered into a Cytoplasmic Pool of Chelatable Iron (II)(∗). Journal of Biological Chemistry, 270(41), 24209-24215.

Petrat, F., Groot, H. D., Sustmann, R., & Rauen, U. (2002). The chelatable iron pool in living cells: a methodically defined quantity.

Hamed, M. Y., Silver, J., & Wilsonx, M. T. (1983). Studies of the reactions of ferric iron with glutathione and some related thiols. Inorganica Chimica Acta, 78, 1-11.

Chapter 6 Conclusions and future work

6.1 Summary

In Chapter 2, we report a revised LC-ICPMS/ESIMS method that incorporates a number of changes, including the configuration of instrument hardware and the development of an internal standard, that improves sensitivity of the method by a factor of 5, and allows for more accurate quantitation of siderophores. We also describe a new suite of mass search algorithms that do not rely on the presence or detection of a pair of isotopologues with difference of 1.995 in m/z and ratio of 15.7 in abundance, representing ^{56}Fe-siderophore and ^{54}Fe siderophore. Therefore, the new algorithms can find and characterize siderophores at lower concentration, or siderophores with unknown extent of isotope fractionation from natural abundances.

In Chapter 3, we report the distribution of siderophores in the upper 1000 m of the US GEOTRACES GP15 Pacific Meridional Transect. Siderophore concentration ranges from 0-70 pM. The distribution of siderophores features prevalent hotspots across the entire transect, suggesting that the siderophore mediated Fe transport is common in the Pacific Ocean. Most hotspots are found in the nitracline. In the NPSG and SPSG, the hotspots are found at mesopelagic depths between 200-400 m. In the upwelling regions where nitracline is lifted to shallower depths, the hotspots are also lifted, to up to 20 m. The transect is dominated by marinobactins. In addition to Fe-siderophores, we also find Al-siderophores, which is the first time they are reported in seawater samples.

In addition to siderophores in dissolved samples, we also measured siderophores in 14 suspended POM samples at hotspots of dissolved siderophores, which is the first time siderophores are measured in POM. We found no marinobactins or amphibactins in any of the 14 samples of suspended POM, suggesting that the marinobactins and amphibactins in dissolved samples are not due to contribution of siderophores in POM. However, we found a polar siderophores in 12 out of the 14 POM samples, and we were able to identify the peak as Ferrioxamine G.

In Chapter 4, we report the measurement of Fe uptake from siderophores by heterotrophic bacteria at 75-500 m of Station ALOHA. Samples of unfiltered seawater were amended with a mixture of ^{57}Fe-labeled amphibactins and marinobactins and incubated in the dark for five days. Between 200 and 400 m, we found almost complete consumption of ^{57}Fe-siderophores for all of the siderophores. Approximately 60% of the added siderophores were present as non-metallated apo siderophores at the end of the incubation. The presence of apo siderophores demonstrates that the drawdown of ^{57}Fe-siderophore was largely due to Fe uptake from siderophores. Therefore, heterotrophic bacteria are Fe limited at this depth, which is in accordance with the high concentration of siderophores in NPSG (Chapter 3).

In Chapter 5, we investigated the siderophore production in seawater collected at 150 m in the NPSG near Station ALOHA, by dark incubation with nutrient amended seawater. C or N limitation on siderophore production was investigated by 3 types of experiments, including one with no nutrient addition, one with glucose addition, and one with addition of sinking POM. In each experiment, there is a Fe treatment and a no Fe treatment, for the investigation of the influence of Fe on siderophore production. The absence of siderophore production in the glucose experiment suggests that siderophore production is limited by N at 150 m of Station ALOHA with a typical nutrient distribution. During some dynamic processes, such as a surface diatom bloom which results in high concentration of ammonium 150 m, siderophores could be produced in situ, due to the presence of highly bioavailable N.

POM addition consistently results in the production of ferrioxamines. However, it remains unclear whether these ferrioxamines were produced over the course of the incubation, or released from POM. The POM addition could also result in the production of non polar siderophores, suggesting the importance of PON in siderophore production.

6.2 Siderophore cycling at Station ALOHA

In the NPSG, the surface ocean at 0-150 m features a dFe:NO_3^- ratio that is higher than 50 μmol/mol, which is the threshold of Fe limitation for heterotrophic bacteria (Tortell et al 1996). In the NPSG, we found siderophores only occasionally and only at low concentrations between 0-150 m in GP15 (Chapter 3), which could be explained by the deficiency of N for siderophore production. In addition, we find no Fe uptake from siderophores (Chapter 4). Indeed, there is a drawdown of ^{57}Fe-siderophore, but this drawdown was exclusively due to C or N uptake, most likely N uptake from siderophores, which also reflects N limitation at 0-150 m. Therefore, the high dFe:NO_3^- ratio, low concentration of siderophores, and slow Fe uptake from siderophores suggest that heterotrophic bacteria are not Fe limited between 0-150 m.

Below 150 m, the concentration for dFe and nitrate both increase with depth, but the increase for nitrate is faster than dFe, which results in an dFe:NO_3^- ratio that is lower than 50 μmol/mol between 200-400 m, the depth interval where we found high concentration of siderophores (Chapter 3), and fast Fe uptake from siderophores (Chapter 4). Therefore, we conclude that heterotrophic bacteria are Fe limited at 200-400 m of NPSG. Below 400 m, we find low concentration of siderophores. Although dFe:NO_3^-- ratio is below 50 μmol/mol, the absence of siderophores in the deep ocean is probably a result of carbon limitation and low iron demand from heterotrophic bacteria.

6.3 New understanding on siderophore cycling

Before this thesis, we expected to find high concentration of siderophores in seawater associated with low dFe, including surface waters of HNLC regions. However, the data from GP15 show that there is no simple relationship between siderophore concentration and dFe. Indeed, high concentration of siderophores are found in seawater associated with a dFe:NO_3^- ratio that is lower than 50 μmol/mol. The low ratio is due to either low dFe, which is the motivation for siderophore production, or high nitrate, which is a necessary resource for siderophore production. The low dFe:NO_3^- ratio seems to be a

necessary but not sufficient condition for high concentration of siderophores. Another necessary condition is labile carbon substrate.

Before GP15, we expected to find ferrioxamines in coastal regions and in the oligotrophic gyres, and amphibactins in the HNLC regions, according to the results from GP16 (Boiteau et al 2016). In GP15 samples, we found ferrioxamines in coastal regions as expected. However, the open ocean portion of the transect is dominated by marinobactins, which is the first time these siderophores are found in the open ocean. The prevalence of marinobactins in the transect suggests they are one type of dominant siderophores in seawater, similar to ferrioxamines and amphibactins.

Before GP15, siderophores have not been measured in suspended or sinking particles. According to their molecular structure and behavior on LC, the polar ferrioxamines were expected to partition into seawater, and the non polar amphibactins and marinobactins were expected to partition into particles. However, we measured siderophores in suspended particles at hotspots of siderophores that were dominated by marinobactins, and did not find marinobactin or amphibactin in any of the sample, suggesting that these non polar siderophores are likely absent in particles. In contrast, we found ferrioxamine G to be common in samples of particles, although it was absent in seawater, and expected to be in seawater.

Most prior studies on Fe limitation focused on phytoplankton, and before Chapter 4, it was assumed that the upper mesopelagic was not Fe limited due to the low rates of organic matter cycling and higher concentrations of dFe that characterize this region of the water column. However, the results of the Fe uptake experiments reveal that the zone of potential Fe limitation in the ocean extends well below the euphotic zone and includes oligotrophic gyres that are not classically Fe limited. Our results substantially expand the volume of the ocean in which microbial communities are likely Fe limited.

6.4 Future work

In Chapter 3, we found high concentration of siderophores at 200-400 m of NPSG in September-October during GP15. In addition, Bundy et al (2018) found siderophores at the surface and at 300-400 m of Station ALOHA, which is a representative station for the NPSG. However, we did not find siderophores at Station ALOHA in any of the four depth profiles over the course of two years during PARAGON 1 and PARAGON 2 cruises.

This difference could not be explained by seasonal variability in siderophore concentration, because the samples in Bundy et al (2018) and PARAGON 1 and PARAGON 2 were all collected in July-August. NPSG is an oligotrophic gyre with little seasonal or interannual changes in nutrient distribution, chlorophyll a distribution and euphotic zone integrated primary production (Karl et al 2021). Therefore, we do not expect daily or seasonal variability in siderophore distribution. However, according to Chapter 4, the dynamic turnover of siderophores at 200-400 m, with a turnover time that is possibly less than a day suggests the possibility of daily variation in siderophore concentration.

Indeed, the data on the time series of siderophore distribution are rare, and the daily variability of siderophore distribution remains unknown. Therefore, the difference in siderophore distribution among cruises suggests the importance of siderophore sampling in time series, which would explain whether siderophore distribution is in steady state.

In Chapter 4, we found the release of apo siderophores and accumulation of Al-siderophores in seawater after ^{57}Fe uptake. This is in accordance with the presence Al-siderophores in GP15 samples. The presence of Al-siderophore was not expected, because the stability constant of ferrioxamine B is six orders of magnitude stronger than Al-Desferrioxamine B (Martell and Smith 2004), and the Al-siderophore would convert to Fe-siderophore when dFe and dAl are similar in concentration.

The accumulation of Al-siderophore suggest that the bioavailability of Al-siderophore is probably low. In contrast to Fe, Al does not have an oxidation state of +2. Therefore, it is likely that Al could not be reduced or used in the cytoplasm, so that Al siderophore complexes may be released into seawater. Therefore, the low bioavailability and slow metal exchange result in a sink of Al-siderophore for siderophores, and decrease the efficiency of siderophore production for Fe uptake. The bioavailability of Al-siderophore could be investigated by ^{27}Al uptake experiment similar to the ^{57}Fe uptake experiment. If ^{27}Al is consumed, the apo siderophore would be released into seawater, and remain apo or bind ^{56}Fe, due to the higher stability constant for Fe than for Al. The apo siderophore could also bind Al, but the concentration should be lower than Fe-siderophore, and lower than the ^{27}Al-siderophore addition, allowing ^{27}Al to be used as a tracer for uptake. Therefore, at the end of the experiment, there would be a large drawdown in the concentration of ^{27}Al-siderophores.

In the Appendix, we found an Fe ligand in axenic culture of *Prochlorococcus*. We were able to assign a molecular weight to the ligand, and our result shows that it has two S atoms in the molecule. However, this compound is novel to the database, and we were not able to determine the structure of the Fe ligand. This could be addressed by a combination of MS measurement of higher resolution, which would provide the exact molecular weight and molecular formula, and MS^2 measurement of higher fragmentation energy, which would provide more details in the building blocks of the ligand.

6.5 References

Fitzsimmons, J. N., Hayes, C. T., Al-Subiai, S. N., Zhang, R., Morton, P. L., Weisend, R. E., ... & Boyle, E. A. (2015). Daily to decadal variability of size-fractionated iron and iron-binding ligands at the Hawaii Ocean Time-series Station ALOHA. Geochimica et Cosmochimica Acta, 171, 303-324.

Tortell, P. D., Maldonado, M. T., & Price, N. M. (1996). The role of heterotrophic bacteria in iron-limited ocean ecosystems. Nature, 383(6598), 330-332.

Boiteau, R. M., Mende, D. R., Hawco, N. J., McIlvin, M. R., Fitzsimmons, J. N., Saito, M. A., ... & Repeta, D. J. (2016). Siderophore-based microbial adaptations to iron scarcity across the eastern Pacific Ocean. Proceedings of the National Academy of Sciences, 113(50), 14237-14242.

Bundy, R. M., Boiteau, R. M., McLean, C., Turk-Kubo, K. A., McIlvin, M. R., Saito, M. A., ... & Repeta, D. J. (2018). Distinct siderophores contribute to iron cycling in the mesopelagic at station ALOHA. Frontiers in Marine Science, 5, 61.

Karl, D. M., Letelier, R. M., Bidigare, R. R., Björkman, K. M., Church, M. J., Dore, J. E., & White, A. E. (2021). Seasonal-to-decadal scale variability in primary production and particulate matter export at Station ALOHA. Progress in Oceanography, 195, 102563.

Martell, A. E., Smith, R. M., & Motekaitis, R. J. (2004). Critically Selected Stability Constants of Metal Complexes: Version 8.0. *National Insitutue of Standards and Technology, Gainesburg*.